JOURNAL OF APPLIED PHYSICS

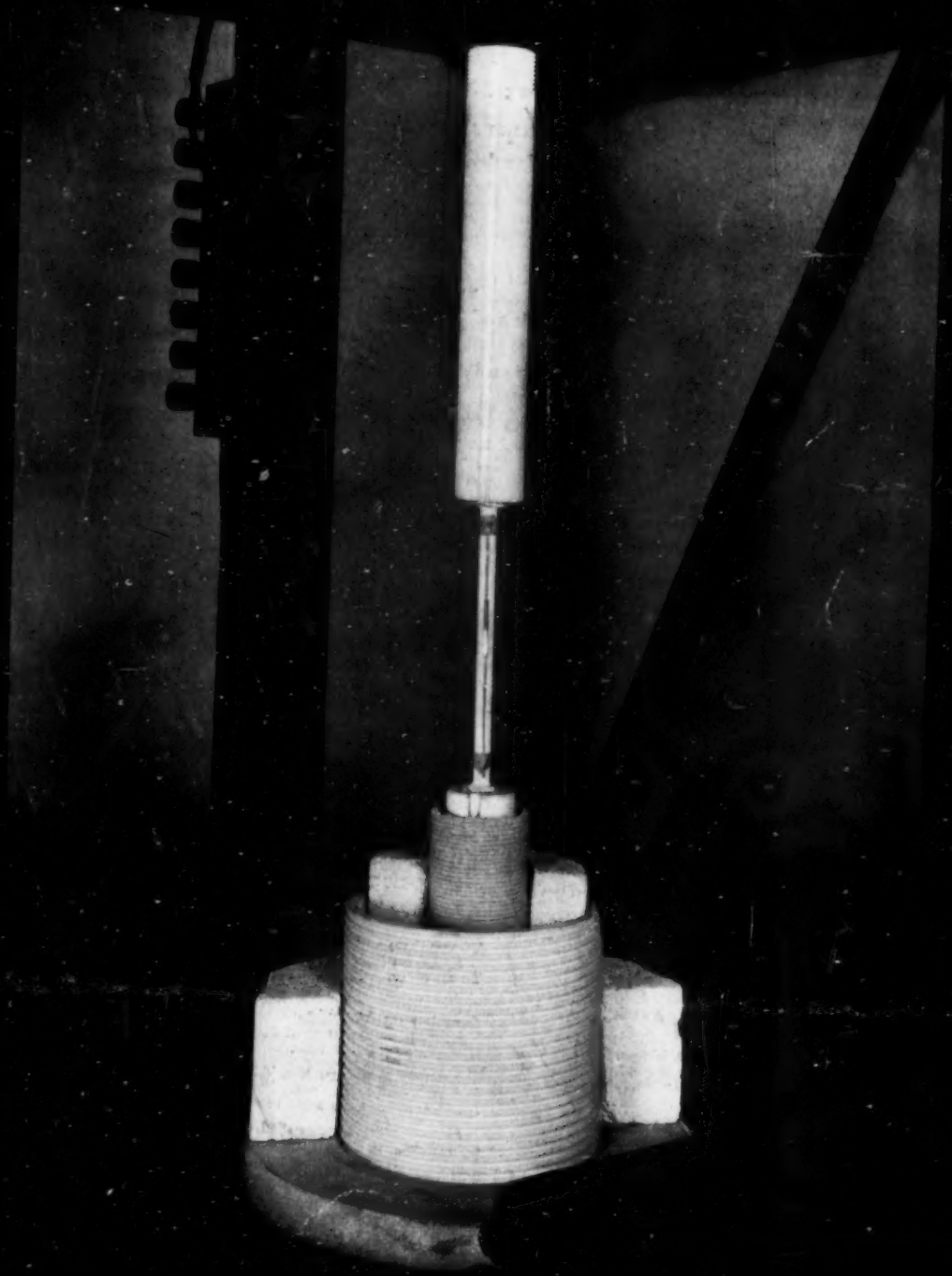

JOURNAL OF APPLIED PHYSICS

Vol. 21, No. 1 JANUARY, 1950

In This Issue

	Page
Thermionic Work Function of the (100) Face of a Tungsten Single Crystal A. A. Brown, L. J. Neelands, and H. E. Farnsworth	1
Interference of Growing Spherical Precipitate Particles C. Wert and C. Zener	5
Response Characteristics of Linear Systems Marcello Cini	8
Use of Spraying Methods and of Volatile Suspending Media in the Preparation of Specimens for Electron Microscopy Robert C. Backus and Robley C. Williams	11
On the Diffraction of Radar Waves by a Semi-Infinite Conducting Screen C. W. Horton and R. B. Watson	16
Measurement of the Surface Temperature of Evaporating Water Drops John C. Johnson	22
X-Ray Measurement of Order in Single Crystals of Cu_3Au J. M. Cowley	24
Integrating Crystal Detectors for High Energy Photons and Particles R. S. Alger	30
Thermionic Emission from Oxide Cathodes: Retarding and Accelerating Fields C. S. Hung	37
Augmented Flames in Half-Open Tubes Marjorie W. Evans, Milton D. Scheer, Louis J. Schoen, and Emmy L. Miller	44
Static Magnetic Storage and Delay Line An Wang and Way Dong Woo	49
General Solution for the Bending of Beams on an Elastic Foundation of Arbitrary Continuity M. Hetényi	55
Letters to the Editor:	
Microwave Frequency Dividers Harold Lyons	59
Particle Size of Evaporated Gold P. G. Wilkinson and L. S. Birks	60
Energy Partition in Isothermal Fracture Marguerite M. Rogers and F. T. Rogers, Jr.	60
Low Temperature Replica Method for Electron Microscopy C. E. Hall	61
Plasma Oscillator Gottfried Wehner	62
Wave-Lengths Suitable for X-Ray Microscopy of Biological Specimens J. L. Farrant	63
Thin Films Peeled from Teflon C. K Jones	64
High Strength Ceramics for High Temperature Use	65
Proceedings of the Electron Microscope Society of America	66
Index to Advertisers	XXII

BOARD OF EDITORS
Elmer Hutchisson, *Editor*

Associate Editors
Howard H. Aiken
Otto Beeck
James Hillier
W. James Lyons
Philip Morrison
Eric Reissner
Raymond J. Seeger
Frederick Seitz
Charles S. Smith

Publication of the American Institute of Physics

OFFICERS
George R. Harrison, *Chairman*
George B. Pegram, *Treasurer*
John T. Tate, *Adviser on Publications*

GOVERNING BOARD
Luis W. Alvarez
J. W. Beams
Wallace R. Brode
E. U. Condon
W. F. Fair, Jr.
Harvey Fletcher
George R. Harrison
W. V. Houston
Paul Kirkpatrick
Paul E. Klopsteg
F. W. Loomis
Philip M. Morse
J. R. Oppenheimer
George B. Pegram
Harold K. Schilling
John T. Tate
Wallace Waterfall
M. W. White

Consultant on Printing
Melvin Loos

ADMINISTRATIVE STAFF
Henry A. Barton, *Director*
Wallace Waterfall, *Executive Secretary*
Theodore Vorburger, *Assistant Treasurer and Comptroller*
Ruth F. Bryans, *Publication Manager*
Betty Hofstadter, *Assistant Secretary*
Eileen B. Neuberger, *Circulation Manager*

The Journal of Applied Physics, published monthly at Prince and Lemon Sts., Lancaster, Pa., is devoted to physics in its role as the science basic to other natural sciences and to the arts and industries. Previous to 1937 this publication was known as Physics. The Journal of Applied Physics publishes editorials and reviews, as well as technical papers of applied physics. Articles appearing in it are indexed regularly, according to their field, by Physics Abstracts, Chemical Abstracts, Engineering Index, Inc., Industrial Arts Index, etc.

Manuscripts should be submitted to Elmer Hutchisson, Editor, Case Institute of Technology, Cleveland 6, Ohio. The authors' institutions are requested to pay a **publication charge** of $8 per page which, if honored, entitles them to 100 free reprints. Instructions will be sent with galley proofs.

Subscriptions and orders for back numbers should be addressed to Prince and Lemon Streets, Lancaster, Pa. or to the American Institute of Physics, 57 East 55 Street, New York 22, N. Y.

Subscription Price	U.S. and Canada	Elsewhere
To members and associate members of the American Institute of Physics	$7.00	$ 8.00
To all others	9.00	10.00

Back Number Prices
Complete set: Vol. 1, July, 1931–Vol. 19, 1949—$148.00
Yearly back number rate: $10.00
Single copies: $1.00 each.

Changes of address should be sent to the Business Manager, American Institute of Physics; **corrected proofs** should be sent to the Publication Manager, American Institute of Physics.

Advertising rates supplied on request. Orders, advertising copy, and cuts should be sent to the American Institute of Physics.

Entered as second class matter January 22, 1937, at the Post Office at Lancaster, Pennsylvania, under the Act of March 3, 1879.
Accepted for mailing at the special rate of postage provided for in the Act of February 28, 1925, authorized May 2, 1932.

Copyright 1950, by the American Institute of Physics. Permission is hereby given to reproduce freely author abstracts in abstract journals.

Journal
of
Applied Physics

Volume 21, Number 1 January, 1950

Thermionic Work Function of the (100) Face of a Tungsten Single Crystal

A. A. Brown,* L. J. Neelands,** and H. E. Farnsworth
Department of Physics, Brown University, Providence, Rhode Island
(Received July 5, 1949)

A slab with one surface cut and etched parallel to (100) crystallographic planes formed the cathode in a low power electron microscope. The electron image of the cathode was formed on a fluorescent screen with a small hole at the center. An electron collector placed behind the hole permitted a measure of the electron current passing through the hole as a function of the temperature of the cathode as measured with an optical pyrometer.

The most probable value of the work function, φ, obtained after 2400 hours of outgassing in a sealed-off, gettered tube is 4.59 ± 0.02 ev. This may be compared with 4.56 ev obtained previously by Nichols for the work function in the [100] direction of a tungsten single crystal wire.

INTRODUCTION

IT is now quite well established experimentally that the work function of a metal single crystal is a function of the crystallographic plane which forms the surface boundary, although the amount of reliable experimental data is still very small. Some theoretical treatments[1] have been published but more experimental data are needed to check the validity of any satisfactory theory. Most of the previous measurements have been made photoelectrically or by means of contact potential differences, although Nichols[2] has obtained thermionic values for tungsten characteristic of certain crystal directions from measurements on a single crystal filament. Because these values may differ from those characteristic of the crystallographic planes of the same Miller indices, we have made measurements which are characteristic of the crystal planes. The (100) and (110) faces were chosen since they are the ones which appear most readily as a result of the heat treatment that tungsten filaments receive in use.

PREPARATION OF THE CRYSTAL

The crystal[3] was cut parallel to a specified set of crystal planes with an error of less than 0.05°, using a diamond wheel, and optical arrangement for alignment. The cutting marks left in the crystal surface by this method were removed by hand grinding. The resulting surface was substantially free of voids.

Attempts to remove the disturbed surface layer were made by (1) chemical etching with a number of different reagents and various conditions of temperature and concentration, (2) electrolytic etching, and (3) heat treatment. No single reagent or etching condition was found to expose smooth plane surfaces parallel to only one set of crystallographic planes. A (110) surface was prepared by first obtaining a good electrolytically polished surface,[4,5] and then heating the crystal, by electron bombardment of the back surface, at 2600°K. The resulting single crystal surface was quite smooth except for a few small pits corresponding to the natural voids of the crystal. A (100) surface was similarly prepared and heated to 2600°K for 100 hours. The resulting surface, although as smooth as the prepared (110) surface, was slightly more pitted. However, even in

* Now with Pratt and Whitney Aircraft, Inc., East Hartford, Connecticut.

** Now with General Electric Company, Electronics Park, Syracuse, New York.

*** Based on dissertations presented for the degree of Doctor of Philosophy in Brown University.

[1] R. Smoluchowski, Phys. Rev. **60**, 661 (1941). I. N. Stranski and R. Suhrmann, Ann. d. Physik **6**, **1**, 153 (1947). C. Herring and M. H. Nichols, Rev. Mod. Phys. **21**, 185 (1949).

[2] M. H. Nichols, Phys. Rev. **57**, 297 (1940).

[3] The crystal was obtained from Professor A. Geotz of the California Institute of Technology. It had been obtained previously from the Lamp Department of the General Electric Company, Cleveland, Ohio. Analyses of similar ingots indicated that there was less than 0.05 percent of extraneous material present.

[4] W. C. Elmore, J. App. Phys. **10**, 724 (1939).

[5] J. M. Hughes and E. A. Coomes, Phys. Rev. **55**, 1138A (1939).

this case the pits covered only a very small fraction of the total area.

Two slabs with sides parallel to the (100) and (110) crystallographic planes respectively were cut from a large single crystal; these were cut to a size of 8×5×1 and 8×4×1 mm, respectively. One edge of each was beveled at an angle of 45° so that when the two were placed with the beveled edges together there resulted a slab 8 mm square and 1 mm thick with a division line between the (110) and (100) faces across the front. These were then ground and polished as described above.

The advantage of studying the two faces chosen is due to the fact that while the (110) surface appears most readily upon heat treatment,[6,7] the (100) face appears to have the lower work function[2,8] so that small pits showing other faces will not affect appreciably any observed current readings.

APPARATUS

A schematic diagram of the experimental tube is shown in Fig. 1. The crystals formed the cathode, Q, of a low power electron microscope. They were heated by electron bombardment from the filaments at P. The electrons emitted from the front surface were focused by means of the electrostatic lenses, L, M, and N, on the fluorescent screen and collector system, F. The temperatures of the crystals were measured by means of an optical pyrometer sighted through the side tube, B. In this tube a magnetically controlled shutter, C, prevented tungsten from depositing on the window at high crystal temperatures when readings were not being taken. The image could be deflected on the screen by a magnetic field and the emission current measured from any portion of either face by means of a Faraday collector placed behind a small aperture in the screen. R and S were guard rings used to prevent the passage of electrons from the bombarding filaments to the collector.

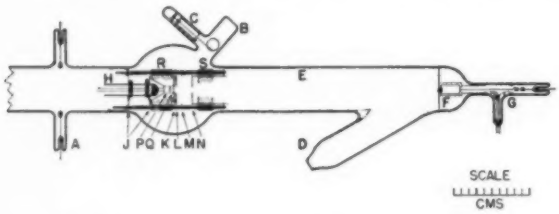

FIG. 1. Schematic diagram of experimental tube.

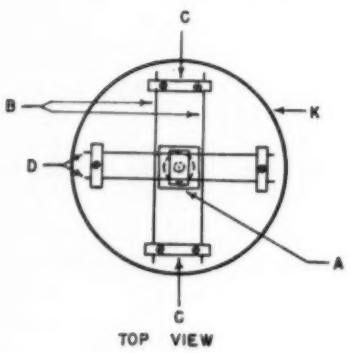

FIG. 2. Diagram of crystal mounting.

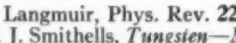

The crystals were attached to the diaphragm, K, by means of 0.5-mm tungsten wires passing through grooves in the backs of the crystals. A piece of 5-mil tungsten wire bent to form a 7-mm square was placed between the crystals and the diaphragm to decrease the heating of the diaphragm. During the later part of the work only one crystal was used. Consequently, the crystal mounting was changed to that shown in Fig. 2. In this mounting the heating of the diaphragm, K, was further decreased by interposing the small tungsten square A between the crystal and the diaphragm. This square was separated from both the crystal and the diaphragm by rectangles formed of 5-mil tungsten wire. The magnification produced by the electrostatic lenses was about ten.

The major part of the glass envelope is shown in Fig. 1. All glass and metal parts were thoroughly cleaned, in boiling dilute sodium hydroxide, in chromic acid, and rinsed in distilled water. The entire assembly was carried out using clean tools and sterile cotton gauze. No part was touched by the hands after being cleaned and a gauze mask was worn to prevent breathing on the parts.

Between the pumps and the experimental tube, and between the diffusion pumps and the fore pump, were traps cooled by dry ice and acetone. The tube, after being evacuated, was baked for two 24-hour periods. Between these bakings the crystals were heated 170 hours at a temperature of 1500°C. Just before the second baking, the trap between the pumps and the experimental tube was warmed to room temperature to remove any condensed vapors. After the second baking the ionization gauge indicated a pressure of 1.5×10^{-8} mm of Hg with the crystals cool and 6×10^{-8} mm of Hg with the crystals at a temperature of 1750°C. After an additional 380 hours of outgassing with the crystals at 1750°C, the first getter was flashed and the tube sealed off. Following this the pressure did not rise above 4×10^{-8} mm of Hg with the crystals at 1750°C and after 1500 hours of outgassing at this temperature it did not rise higher than 1.5×10^{-8} mm of Hg. The flashing of the second getter at this time did not cause any detectable change in the vacuum conditions.

[6] I. Langmuir, Phys. Rev. **22**, 357 (1923).
[7] C. J. Smithells, *Tungsten—Metallurgy, Properties, and Applications* (D. Van Nostrand Company, Inc., New York, 1936).
[8] S. T. Martin, Phys. Rev. **56**, 947 (1939).

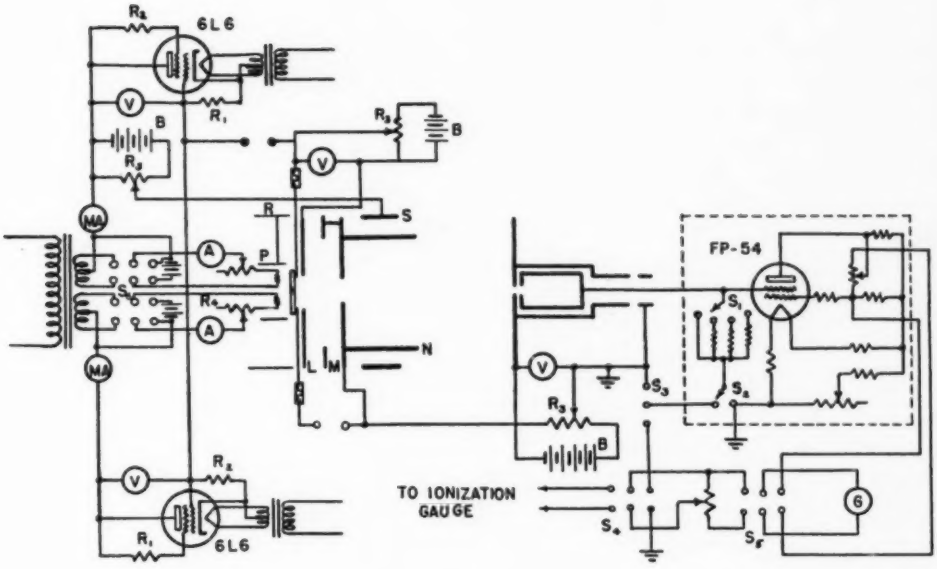

FIG. 3. Wiring diagram of the electrical circuit.

An optical pyrometer of the disappearing filament type was used to measure the temperature of the crystal surfaces. Experience indicated that even at temperatures as high as 2300°C, settings by different operators could be made as close as 2°C. The pyrometer was calibrated against a standard lamp obtained from the Bureau of Standards. The true temperature of the crystals was obtained from the brightness temperature by using the Wien equation and the value of the emissivity of tungsten obtained by Wahlin and Whitney[9] who found it constant and equal to 0.46 in the temperature range from 1200 to 2200°C at a wave-length of 6900A. Another correction was necessary due to reflection at the Pyrex window through which readings were taken. This correction was based on the work of Benford.[10]

A wiring diagram for the complete electrical circuit is shown in Fig. 3. The measuring system consisted of a d.c. amplifier and a galvanometer. This permitted the measurement of currents from 10^{-4} to 10^{-14} ampere.

PROCEDURE AND RESULTS

Measurements were started after 75 hours of heating and continued until the crystal had been degassed 2400 hours. All of the degassing except the first 240 hours was carried out at a temperature of 1750°C. The image was in focus when an accelerating potential of 2500 volts and a focusing potential of −200 volts with respect to the crystal were used. A retarding potential of 230 volts on the collector was sufficient to keep out the secondary electrons.

After the tube had been in operation for some time, evidence was obtained that some of the bombarding electrons were passing between the crystals and into the collector. This made measurements below 1300°C impossible. When a short circuit developed in the tube and made a reassembly necessary, the crystal mounting was redesigned and only one crystal with the (100) face was used. Consequently the measurements on the (110) face are of qualitative significance only, since they were taken before the most favorable conditions were obtained. The discussion which follows pertains only to the later work on the (100) face.

The measurements of the emission current and temperature were fitted to the formula

$$i = AT^2 \exp[-(\varphi/kT)]. \qquad (1)$$

The value of φ was determined from the slope of the experimental curve obtained by plotting $\log i/T^2$ against $1/T$. It was not possible to calculate A since it was not ascertained that all of the electrons from the crystal passed through the various apertures.

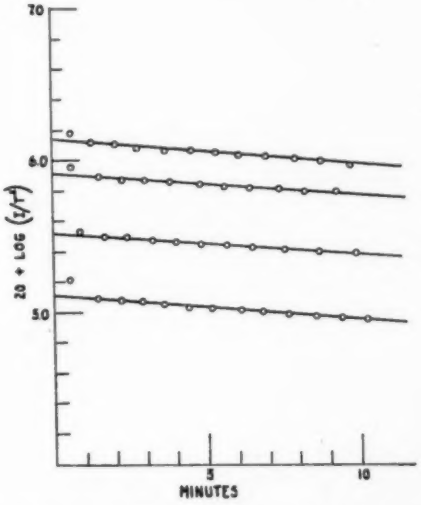

FIG. 4. Plot of $\log(i/T^2)$ against time elapsed after flashing the crystal at 2650°K for 15 seconds.

[9] Wahlin and Whitney, Phys. Rev. **50**, 735 (1936).
[10] F. Benford, J. Opt. Soc. Am. **29**, 162 (1939).

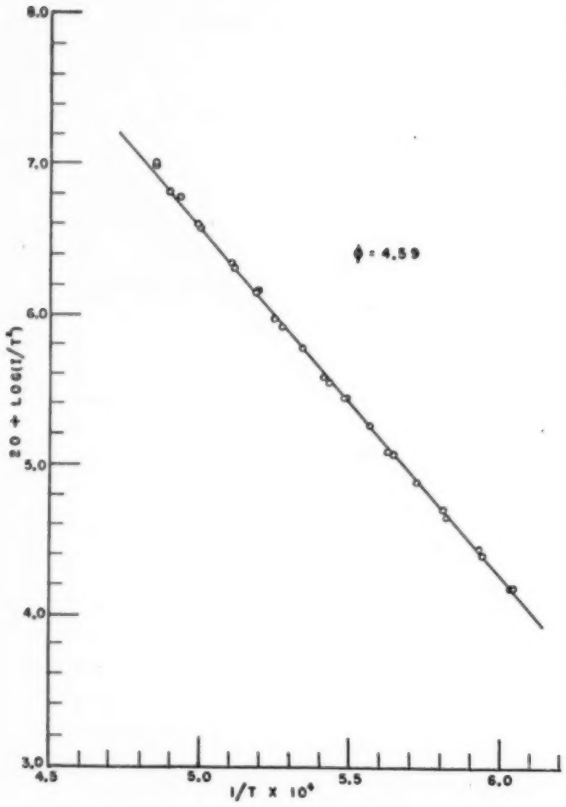

FIG. 5. A typical Richardson graph after 2000 hours of outgassing.

After about 900 hours of heating, the gas pressure as indicated by the ionization gauge did not continue to decrease with outgassing time and the procedure was adopted of flashing the crystal a short time at a temperature of 2650°K to obtain an uncontaminated surface. It was found that a flashing time of 5 sec. or longer resulted in a maximum emission current, and that a flashing time of 30 seconds did not increase the gas pressure over 4×10^{-8} mm of Hg. Consequently a flashing time of 15 seconds was used. Since the crystal surface became contaminated again in less time than was needed to complete a set of measurements, it was necessary to flash the crystal and then follow the emission current as a function of time and extrapolate back to zero time to obtain the values corresponding to the uncontaminated surface. The $\log i/T^2$ was plotted which resulted in a set of straight parallel lines as shown in Fig. 4. The first one or two points are high in each case, since the measurements were made before the crystal had cooled to the desired temperature. This procedure was adopted after about 1000 hours of outgassing. The value of φ was then 4.77 ev. During the next 1000 hours of heating, the value decreased to 4.59 ev. It remained constant at this value until the work was ceased after a total outgassing time of 2400 hours. A typical plot, taken during the last 400 hours, is shown in Fig. 5.

For greatest accuracy, account should have been taken of the effect of the electric field at the crystal surface on the value of the work function. That is, every value of the current should have been corrected to the corresponding zero field value by using the relation

$$i_v = i_0 \exp(SV^{\frac{1}{2}}/T), \tag{2}$$

where i_v is the high field current; i_0 is the zero field current; V is the accelerating potential; and S is a constant which depends on the geometry of the apparatus. Equations (1) and (2) may be combined to give

$$i_v = AT^2 \exp[(\varphi-\Delta\varphi)/kT], \tag{3}$$

where $\Delta\varphi$, the correction due to the field, is given by

$$\Delta\varphi = KSV^{\frac{1}{2}}. \tag{4}$$

The configuration of the electric field in the microscope was such that the field was very low at the crystal surface and it was believed that no correction would be necessary. To confirm this, measurements of φ were made with the accelerating (and focusing) voltage varied by a factor of two. The values checked within the experimental error. It was found impractical to measure S by measuring i_v as a function of the accelerating potential at a constant crystal temperature, since this temperature could not be held constant for the length of time needed to complete a set of measurements.

CONCLUSIONS

The most probable value of φ for the (100) surface, obtained after 2400 hours of outgassing, was found to be 4.59 ± 0.02 ev. This is believed to be characteristic of the uncontaminated crystal surface. This checks well with the value of 4.56 ev obtained by Nichols[11] for the [100] direction. No definite value was obtained for the (110) face but the early results indicate that φ for this face is higher than φ for the (100) face. This is also true of Nichols' results for the [110] direction.

[11] The values of φ first published by Nichols are 0.03 ev to low due to a numerical error. Corrected values are given in Rev. Mod. Phys. **21**, 202 (1949).

Interference of Growing Spherical Precipitate Particles*

C. WERT AND C. ZENER
Institute for the Study of Metals, University of Chicago, Chicago, Illinois
(Received June 27, 1949)

The exact theory of the rate of growth of spherical precipitate particles has previously been developed for the initial stage where the individual precipitate particles do not interfere with one another. In the present paper this theory is carried one stage further to include their mutual interference. It is found that in the particular case of a very dilute solution this interference may be accounted for in a relatively simple manner. The applicability of the theory has been tested by new observations upon the precipitation of carbon from α-iron. Good agreement is found up to 95 percent completion of precipitation.

A. INTRODUCTION AND RESULTS

ONE of the authors (C. W.) has recently studied the rate of precipitation of carbon from freshly quenched α-iron.[1] From the observation that during the initial stage of precipitation the fraction of precipitation completed, W, obeys the equation

$$\tau dW/dt=(\tfrac{3}{2})(t/\tau)^{\frac{1}{2}}, \tag{1}$$

where τ is a constant, he concluded (a) that the growth nuclei were already present when the material was first quenched; (b) that the precipitate particles started as small spheres and remained spherical in shape throughout their growth. During the later stages of precipitation the growth of each precipitate particle is impeded by the general depletion of carbon in the surrounding matrix. An attempt was made to take account of this mutual interference of precipitate particles by the arbitrary introduction into the right side of Eq. (1) of an "interference factor" $(1-W)$. The observations were found to be in fairly good agreement with the resulting equation, namely,

$$\tau dW/dt=\tfrac{3}{2}(1-W)(t/\tau)^{\frac{1}{2}}, \tag{2}$$

which, when integrated, becomes

$$W=1-e^{-(t/\tau)^{\frac{1}{2}}}. \tag{3}$$

In spite of the fair success of this formula, the authors were unsatisfied with its heuristic derivation, and have since placed the theory of interference upon a firmer foundation. This new theory is developed in Section B. Experiments have been made to test the applicability of this theory to the particular system of carbon precipitating from solid solution in α-iron. These experiments are presented in Section C.

The results of the analysis of Section B may be presented in a simple form. Toward this end we rewrite Eq. (1) in the equivalent form

$$\tau dW/dt=\tfrac{3}{2}W^{\frac{1}{2}}. \tag{4}$$

It is then found that in the particular case of a very dilute solution the mutual interference of growing precipitate particles is properly taken into account by multiplying the right side of Eq. (4) by the interference factor $(1-W)$. The governing equation is, therefore, found to be

$$\tau dW/dt=(\tfrac{3}{2})(1-W)W^{\frac{1}{2}}. \tag{5}$$

While the original Eq. (2) can be directly integrated, the authors have been unable to integrate Eq. (5) analytically. However, W is a unique function of t/τ, and this function may be found by numerical integration. The results of such an integration are presented in Figs. 1 and 2. In these same figures a comparison is made with the solution of the original Eq. (2). It is seen that while both methods of taking interference into account lead to essentially the same results during the early stages of precipitation, they lead to markedly different results during the later stages. The very close agreement of the present theory with the observed precipitation is shown in Fig. 3. Tentative reasons for the deviations in the very last stages of precipitation are discussed in Section C.

B. ANALYSIS

The rate of growth of a spherical precipitate particle is completely determined by the gradient in concentra-

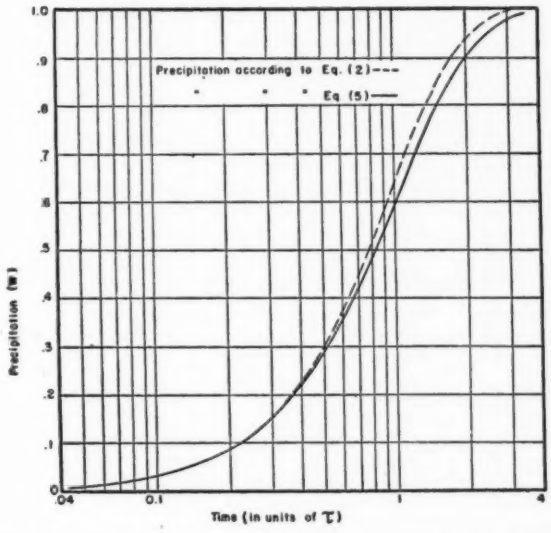

FIG. 1. Comparison of two methods of taking interference into account, standard coordinates being used.

* This research has been partially supported by the Office of Naval Research, U.S.N. (Contract No. N-6ori-20-IV, NR 019 302).

[1] C. Wert, J. App. Phys. **20**, 943 (1949).

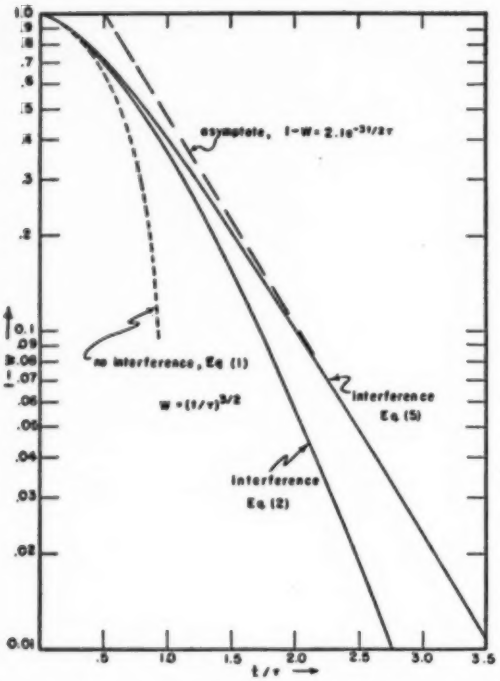

FIG. 2. Comparison of two methods of taking interference into account, coordinates being used which emphasize later stages of precipitation.

tion in the matrix adjacent to the particle. We shall let $n(r, t)$ denote the concentration of solute atoms in terms of number of atoms per unit volume. The value of n in the precipitate will be denoted by n_0, and the boundary value of n in the matrix at the precipitate-matrix interface will be denoted by n_1. The rate of growth is then given by

$$(n_0-n_1)(dV/dt)=4\pi R^2 D(\partial n/\partial r)_{r=R}, \tag{6}$$

where V and R are the volume and radius of the particle, respectively, and D is the diffusion coefficient of the solute atoms. In the particular case of a very dilute solution the particle grows so slowly that the growth rate itself has a negligible effect[2] upon the gradient $(\partial n/\partial r)_{r=R}$. We may thus assign this gradient the steady-state value it would approach if the radius were to remain constant. The steady-state solution of the diffusion equation in the case of a fixed radius R is

$$n(r)=n_\infty-(n_\infty-n_1)(R/r),$$

and hence we shall equate the concentration gradient at the boundary to

$$(\partial n/\partial r)_{r=R}=(n_\infty-n_1)/R. \tag{7}$$

This gradient is fortunately quite insensitive to the precise manner in which we specify the boundary conditions far away from the particle. The gradient is, e.g., not appreciably altered if we specify that the concentration be n_∞ at some radius R_∞ very large compared to R, or if we specify that $\partial n/\partial r$ vanish at some radius R_∞ large compared to R. In the later case n_∞ will be the concentration at R_∞, and will gradually decrease with time.

The assumption of a very dilute solution enables us to make one further simplification. In this case the precipitate particles will be relatively far apart, so that essentially each precipitate particle is surrounded by a concentration field which approaches the average concentration $n_\infty(t)$ as we go away from the particle in any direction. In the case of a dilute solution this average concentration is related to the fraction W of the precipitation which has already occurred by the equation

$$\{n_\infty(t)-n_1\}/\{n_\infty(0)-n_1\}=1-W. \tag{8}$$

If we now let R_0 denote the final radius of the precipitate particles, corresponding to complete precipitation, and observe that

$$W=(R/R_0)^3, \tag{9}$$

we find that substitution of Eqs. (7) and (8) into Eq. (6) leads to Eq. (5) of Section A, with the time of relaxation τ given by

$$\tau=[\{n_0-n_1\}/\{n_\infty(0)-n_1\}]R_0^2/2D. \tag{10}$$

This time of relaxation may be expressed in alternative forms through the introduction of the density of precipitate particles, N, i.e., their number per unit volume, which satisfies the relation

$$(4\pi/3)R_0^3N(n_0-n_1)=n_\infty(0)-n_1. \tag{11}$$

We have implicitly assumed that all the precipitate particles attain the same final radius. In accordance with the empirical observations of one of the authors,[1] it is legitimate, at least in the case of carbon in α-iron, to assume that all the precipitate particles start growing at the same time, namely, at the instant of quenching. It might appear, however, as if fluctuations in the density N would be reflected as fluctuations in the final radii. In order to demonstrate the invalidity of this objection in the case of very dilute solutions we shall eliminate the concentration from Eq. (10) by use of the relation (11), thereby obtaining

$$\tau=3/(8\pi NR_0D).$$

If we now introduce a measure λ of the mean distance apart of the precipitate particles by the definition

$$N=\lambda^{-3},$$

we obtain

$$\tau=(3\pi\lambda/8R_0)(\lambda^2/\pi^2D).$$

The second factor is seen to be the time of relaxation τ_λ for the smoothing out of fluctuations in concentration over a distance λ. Under our assumption of a very dilute solution the first factor is a very large number, and hence τ is very long compared to τ_λ. Thus although those regions in which N is unusually large will suffer an unusually rapid rate of precipitation, the excess

[2] C. Zener, J. App. Phys. **20**, 962 (1949).

rate of depletion of the solute atoms will, to a large extent, be compensated by the long range diffusion of solute atoms from surrounding regions. The average concentration $n_\infty(t)$ will thus remain almost constant in spite of possible fluctuations in N.

In order to have a formula whereby we may calculate N from an empirical value of τ, we eliminate R_0 from Eqs. (10) and (11), therby obtaining

$$N=(\tfrac{3}{4}\pi)2^{-\frac{3}{2}}[(n_0-n_1)/\{n_\infty(0)-n_1\}]^{\frac{3}{2}}(D\tau)^{-\frac{3}{2}}. \quad (12)$$

C. EXPERIMENT

The experiments made to test the validity of the foregoing analysis were carried out in a manner nearly the same as that described in an earlier paper by one of the authors.[1] The apparatus for preparing the specimens and making the internal friction measurements was that used previously. The only real difference between the past and present work is that the earlier work placed emphasis on the initial part of the precipitation process, whereas the present experiments emphasize the latter part of the process.

Precipitation measurements were carried out in the temperature range 85°C to 210°C. These measurements are compared with the theoretical curves in Fig. 3. In this figure the times τ' and τ (which differ only slightly) refer to the time constants of Eqs. (2) and (5) respectively. These constants τ' and τ were so chosen for each temperature that the experimental points coincided with the theoretical curves when the precipitation was about 60 percent complete. In order that simultaneous comparison could be made between experiment and the two theoretical curves, the scale factors for the two equations were so chosen as to make the curves coincide at 60 percent precipitation. It is clear from these plots that the theory deduced in the preceding section fits the experimental facts much better than the treatment expressed by Eq. (2). The experimental points show good agreement with Eq. (5) up to about 90 percent to 95 percent of the total precipitate.

The reason for the discrepancy during the last 5 percent of the precipitation is not known definitely. A possible reason is lack of homogeneity of the initial

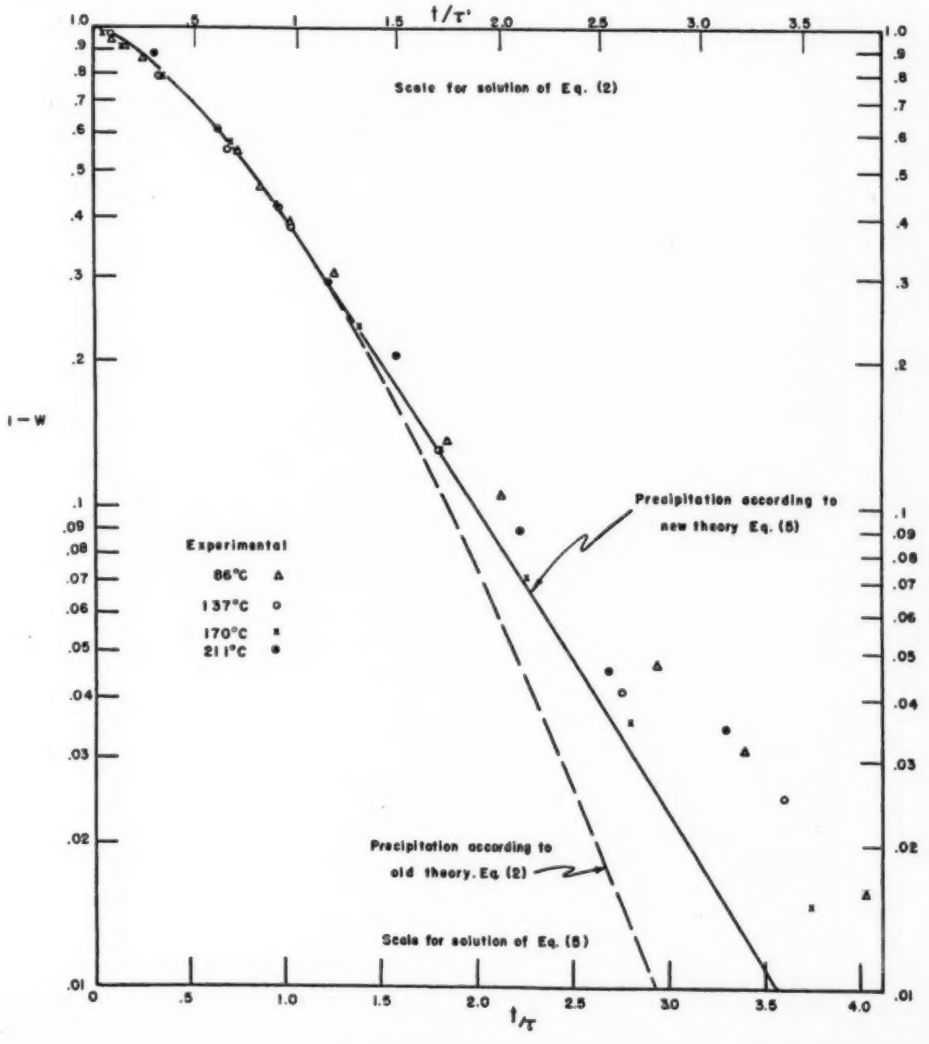

FIG. 3. Comparison of experiments with theory.

TABLE I.

Temp. °C	$n_\infty(0)$ (wt. percent)	τ(sec.)	N/cc
86	0.016	79000	39×10^{12}
137	0.013	3500	26×10^{12}
170	0.018	700	17×10^{12}
211	0.012	190	9×10^{12}

solid solution of carbon, which results in a range of values for τ. It was observed that specimens which were carburized without a long homogenization anneal gave very erratic and nonreproducible data. Further, the data on such specimens deviated from Eq. (4) as early as the 75 percent point of the total precipitation. When such a specimen was homogenized by an anneal of several hours at 720°, much more reproducible data were obtained. All the data shown in Fig. 3 were made on specimens which had been given such an anneal, and still longer anneals gave no improvement in the fit of the data to Eq. (4). However, it seems possible that slight inhomogeneities might still exist which would be large enough to account for at least a part of the discrepancies observed. A second possibility is the binding of dissolved carbon atoms to each other, to other dissolved impurity atoms or to lattice imperfections. That this binding may occur was observed experimentally earlier by the authors.[3]

Through the use of Eq. (12) and the experimentally determined values of τ, one can calculate the number of particles of precipitate per unit volume formed at a given temperature. Table I shows the result of such calculations. The values of N computed in this way are roughly the same as those computed earlier by the authors.[1,2]

[3] C. Wert and C. Zener, Phys. Rev. **76**, 1169 (1949).

The Response Characteristics of Linear Systems

MARCELLO CINI
Riv, Officine di Villar Perosa, Turin, Italy
(Received May 26, 1949)

For a linear system, steady-state response to sinusoidal stress cannot have a unique dynamic modulus and phase shift, but these quantities must be related to rate of creep; particularly they cannot be independent of external frequency.

A proof is given that such linear system is always equivalent to a viscoelastic system. Finally the discrepancy between the relations deduced and experimental results of various authors is pointed out and discussed.

ALTHOUGH hysteretic and elastic properties of rubber-like materials have been thoroughly investigated in the last years, no theory in good agreement with experimental results has been developed, at least as far as the author knows.

On one hand, very general and important results have been reached in the study of viscoelastic systems,[1–6] pointing out the various relationships which allow prediction of their behavior under given conditions of stress or strain; on the other hand many reports[7–14] have been published illustrating tests carried out on different stocks of natural and synthetic rubbers, and giving the derived values of dynamic modulus, loss factor, rate of creep and relaxation and similar quantities. In the present paper linear systems* will be examined from a very general point of view, and some fundamental properties of the response will be established, by means of which it is easy to prove that the most general linear system is equivalent to a viscoelastic model.**

Finally some experimental results of the above-mentioned papers are discussed using the derived relations and pointing out some reasons for the observed contradictions.

1. LINEAR SYSTEMS

We will assume as a fundamental property of a linear system that the steady-state response to a sinusoidal stress

$$P(t)=P_0e^{i\omega t}$$

[1] Fuoss and J. G. Kirkwood, J. Am. Chem. Soc. **63**, 385 (1941).
[2] Robert Simha, J. App. Phys. **13**, 201 (1942).
[3] T. Alfrey and P. Doty, J. App. Phys. **16**, 700 (1945).
[4] John G. Kirkwood, J. Chem. Phys. **14**, 180 (1946).
[5] B. Gross, J. App. Phys. **18**, 212 (1947).
[6] B. Gross, J. App. Phys. **19**, 257 (1948).
[7] Sack, Motz, and Work, J. App. Phys. **15**, 396 (1944).
[8] H. S. Sack and J. Motz, J. App. Phys. **18**, 450 (1947).
[9] Dillon, Prettyman, and Hall, J. App. Phys. **15**, 309 (1944).
[10] Kosten, Rubber Chem. Tech. **13**, 381 (1939).
[11] Stambaugh, Rubber Chem. Tech. **14**, 382 (1941).
[12] Oberto and Palandri, Rubber Age **63**, 725 (1948).
[13] Tobolsky, Prettyman, and Dillon, J. App. Phys. **15**, 380 (1944).
[14] Mooney, Wolstenholme, and Villars, J. App. Phys. **15**, 394 (1944).

* All the following considerations hold as well for electric, acoustic or dielectric systems.
** This identity is also implicitly proved in the papers of Alfrey and Doty (reference 3) and Gross (references 5 and 6.)

be still sinusoidal and given by

$$y(t)=[P_0/E(\omega)]e^{i(\omega t-\varphi(\omega))}.$$

If the sinusoidal stress is given in real form

$$P(t)=a\cos\omega t+b\sin\omega t$$

the response will be

$$y(t)=[a/E(\omega)]\cos(\omega t-\varphi(\omega))+[b/E(\omega)]\sin(\omega t-\varphi(\omega)).$$

As is well known $E(\omega)$ is the dynamic modulus, and $\varphi(\omega)$ the phase shift, both functions of the external frequency ω: $E(\omega)$ and $\varphi(\omega)$ are related to the mechanical impedance, or its reciprocal the mechanical admittance, by simple relations, that we need not report here.

This assumption follows directly from the principle of superposition, and is quite as general. Furthermore, many tests developed to investigate dynamic properties of rubberlike materials are based upon the analysis of steady-state response to sinusoidal stress,*** so that a rather accurate check of its shape is often possible.

Let us impose on such a system an external stress defined as follows:

$$\begin{aligned} P(t)&=0 \quad \text{for } t<0\\ P(t)&=P_0 \quad \text{for } 0<t<\theta\\ P(t)&=0 \quad \text{for } t>\theta. \end{aligned}$$

This function can be developed in Fourier's integral in a well-known way:

$$P(t)=\frac{P_0}{\pi}\int_0^\infty\left(\frac{\sin\omega\theta}{\omega}\cos\omega t+\frac{1-\cos\omega\theta}{\omega}\sin\omega t\right)d\omega.$$

Each infinitesimal harmonic of the stress, divided by the dynamic modulus $E(\omega)$ and shifted by the angle $\varphi(\omega)$, gives the corresponding infinitesimal harmonic of the response: integration from 0 to ∞ gives:†

$$y(t)=\frac{P_0}{\pi}\int_0^\infty\left[\left(\frac{\sin\omega\theta\cos\varphi}{E}-\frac{(1-\cos\omega\theta)\sin\varphi}{E}\right)\cos\omega t+\left(\frac{(1-\cos\omega\theta)\cos\varphi}{E}+\frac{\sin\omega\theta\sin\varphi}{E}\right)\sin\omega t\right]d\omega. \quad (1)$$

In order that Eq. (1) have a physical meaning two conditions must be satisfied:

(a) the response $y(t)$ must be independent of θ, i.e. from the time of application of external load, for $t<\theta$;

(b) the response $y(t)$ must be 0 for $t<0$, i.e. before the application of external load.

*** The presence of an inertial mass does not alter the shape of the response.

† In the following $E(\omega)$ and $\varphi(\omega)$ will be handled as E and φ, it being understood that they are functions of ω.

The first condition means that

$$\frac{\partial y}{\partial\theta}=0 \quad \text{for} \quad t<\theta; \quad \frac{\partial y}{\partial\theta}\neq 0 \quad \text{for} \quad t>\theta. \quad (2)$$

The derivative of Eq. (1) with respect to θ is:

$$\frac{\partial y}{\partial\theta}=\frac{P_0}{\pi}\int_0^\infty\left[\frac{\cos\varphi}{E}\cos\omega(\theta-t)-\frac{\sin\varphi}{E}\sin\omega(\theta-t)\right]d\omega.$$

Then, setting

$$\begin{aligned} \theta-t&=\tau \quad \text{when } t<\theta\\ t-\theta&=\tau \quad \text{when } t>\theta \end{aligned}$$

$$\int_0^\infty\frac{\cos\varphi}{E}\cos\omega\tau d\omega=\frac{\pi}{2}f_1(\tau)$$

$$\int_0^\infty\frac{\sin\varphi}{E}\sin\omega\tau d\omega=\frac{\pi}{2}f_2(\tau),$$

condition (a) is fulfilled if

$$f_1(\tau)=f_2(\tau)=f_1(-\tau)=-f_2(-\tau)=f(\tau),$$

i.e. if $f_1(\tau)$ is an even function, $f_2(\tau)$ an odd function, which are identical for positive values of the variable, being $f(\tau)$ their common value.

Inversion of Fourier transform gives

$$\frac{\cos\varphi}{E}=\int_0^\infty f(\tau)\cos\omega\tau d\tau \quad (3a)$$

$$\frac{\sin\varphi}{E}=\int_0^\infty f(\tau)\sin\omega\tau d\tau. \quad (3b)$$

It is easy to demonstrate that if Eqs. (3) hold, condition (b) is also satisfied. Indeed, introducing Eqs. (3) in Eq. (1), and inverting the order of integrations, we have

$$y(t)=\frac{P_0}{\pi}\int_0^\infty f(\tau)d\tau\int_0^\infty\left(\frac{\sin\omega(\theta-t+\tau)}{\omega}+\frac{\sin\omega(t-\tau)}{\omega}\right)d\omega. \quad (4)$$

Remembering that

$$\int_0^\infty\frac{\sin kx}{x}dx=\begin{cases}\dfrac{\pi}{2} & \text{for } k>0\\ -\dfrac{\pi}{2} & \text{for } k<0\end{cases}$$

we obtain

$$\int_0^\infty\left(\frac{\sin\omega(\theta-t+\tau)}{\omega}+\frac{\sin\omega(t-\tau)}{\omega}\right)d\omega=\begin{cases}0 & \text{for } t<0\\ \pi & \text{for } 0<\tau<t<\theta\\ 0 & \text{for } 0<t<\tau<\theta.\end{cases}$$

Then Eq. (4) can be written

$$y(t)=P_0\int_0^t f(\tau)d\tau \quad \text{for } 0<t<\theta$$
$$y(t)=0 \qquad\qquad \text{for } t<0. \tag{5}$$

The derivative of (5) with respect to time gives

$$dy/dt=P_0f(t), \tag{6}$$

which shows that $f(t)$ is the rate of creep under unit stress.

Equations (3) and (5) do not depend on the magnitude of θ and therefore hold as general laws that must necessarily be fulfilled correlating dynamic modulus and phase shift (or real and imaginary part of mechanical impedance or admittance) with rate of creep. In identical way analogous relations between dynamic modulus, phase shift and rate of relaxation could be developed.

From Eqs. (3) it follows immediately that

$$\lim_{t\to\infty} f(t)=0 \tag{7}$$

$$\lim_{t\to 0} tg\varphi=0. \tag{8}$$

2. CORRELATION WITH VISCOELASTIC SYSTEMS

Identity of the given system with a convenient viscoelastic model, is also proved by means of Eqs. (3). Indeed it is not *a priori* quite plain that all systems whose response to stress obeys the superposition principle can be represented by a model constructed from a discrete set, or a continuous distribution, of elements which obey Hooke's law, and elements which obey Newton's viscosity law.

Remembering that creep under a constant stress P_0 of a viscoelastic system having a distribution function of retardation times $F(\tau)$ is

$$y(t)=P_0\beta\left(1-\int_0^\infty F(\tau)e^{-t/\tau}d\tau\right)$$

with

$$\int_0^\infty F(\tau)d\tau=1,$$

we have

$$\frac{dy}{dt}=P_0\beta\int_0^\infty \frac{F(\tau)}{\tau}e^{-t/\tau}d\tau.$$

As Eq. (6) gives the rate of creep for the linear system, the condition for identity of this one and the former one is

$$f(t)=\int_0^\infty \rho(s)e^{-ts}ds, \tag{9}$$

where

$$s=\frac{1}{\tau}-\beta\frac{F(1/s)}{s}=\rho(s).$$

This means that $f(t)$ is the Laplace transform of the auxiliary distribution function $\rho(s)$.

The determination of $\rho(s)$ is always possible because $f(t)$ must obey the conditions that assure evaluation of integrals in Eqs. (3) which are sufficient to allow the inversion of the Laplace transform.

As Eqs. (3) and (9) are identical to Eqs. (6) and (25) in Gross paper,[6] all further developments such as methods of evaluation of distribution functions, are omitted here, having already been published there.

3. DISCUSSION OF EXPERIMENTAL RESULTS

Many of the above mentioned reports agree in the statement that the elastic modulus $E(\omega)$ and the phase shift $\varphi(\omega)$ are with good approximation, independent of frequency ω in the range from a few cycles per sec. to about 1300 c.p.s. This property has also been assumed as a general law of internal friction replacing Newton's viscosity law, not only to take account of experimental results, but also because calculations can be carried out in a very simple way.[15, 16]

As Eqs. (3) and (8) show that this deduction is not compatible with the assumption of linearity, we must conclude as follows:

(a) Experimental results are not sufficiently extended and a different behavior of E and φ is to be expected in the ranges of extremely low and very high frequencies.‡

(b) Tested materials do not give a linear response; in this case E and φ would no longer have a meaning, but energy loss per cycle could still be measured.

(c) The presence of plastic deformations may alter the results in a considerable way independently of frequency.

These reasons may also coexist together, and, more or less, explain the observed results, but further tests should be undertaken to check them.

---

[15] Krall, Tech. Ital. **I**, 2 (1946).

[16] Cattaneo, Acta Pont. Acad. Sci. **IX**, 14 (1946).

‡ *Note added in proof.*—It has already been pointed out that E varies appreciably over a sufficiently large frequency range. See, for example, A. W. Nolle, J. App. Phys. **19**, 753 (1948).

The Use of Spraying Methods and of Volatile Suspending Media in the Preparation of Specimens for Electron Microscopy*

ROBERT C. BACKUS AND ROBLEY C. WILLIAMS
Department of Physics, University of Michigan, Ann Arbor, Michigan
(Received June 16, 1949)

Developments have been made in the use of spraying methods in the preparation of specimens for examination in the electron microscope. At the same time, two wholly volatile diluents, containing electrolytes and adjusted to normal *p*H, have been developed for use in forming the spray drops. The use of volatile electrolytes makes it unnecessary to wash the specimen after the droplet patterns have been formed on the specimen screens.

There are several qualitative and quantitative uses and advantages of the spray technique as described. The qualitative ones are these: (1) the brief drying time of the droplets helps to preserve the shapes of particles upon drying, and also allows studies to be made of rapidly reacting systems; (2) since the drop patterns are reproducibly representative samples of the suspension under investigation, qualitative assays of the particulate composition of the suspension can be made, and a comparison of the particulate composition of two closely similar suspensions can be made under ideal control conditions; (3) the droplet patterns are discretely bounded by blank areas of substrate film, and this fact makes practicable the detection of small and subtle differences between the fine structure of the specimen material and that of the substrate.

The quantitative uses of the spray technique are: (1) by use of reference particles of known numbers in a suspension it is readily possible to determine the volumes of droplets issuing from a spray-making device; (2) by use of reference particles it is also possible to make an assay of the number of other particles, such as a virus, per unit volume of mixed suspension; (3) if a suspension is highly purified, the particle weight of the material in suspension can be determined. Experiments involving the counting of about 10,000 particles show that the quantitative precision is as good as would be expected from the statistics of random sampling.

The construction and use of a spray gun are described, as well as the characteristics of two volatile diluents: ammonium acetate and ammonium carbonate.

I. INTRODUCTION

SPECIMENS for electron microscopy are commonly prepared by placing a drop of liquid containing some suspended material upon the film-covered specimen screen, and allowing the drop to dry either unassisted or hastened by the withdrawal of some of the liquid on a piece of filter paper. If the material is suspended in a non-volatile medium, such as one of the usual diluents containing salts, it is necessary to wash the microscope screen in distilled water subsequent to the initial drying of the suspension. It is generally agreed that this technique is unsatisfactory, owing to the chemical and physical changes that may occur during the drying period of several seconds to a few minutes, and to the inevitable non-uniform distribution of the suspended material as it dries on the screen. The exposure of biological materials of even moderate lability to an environment of high ionic strength, followed by immersion in distilled water, is a procedure likely to cause changes in the shapes and sizes of the specimen materials. Attempts have been made to alleviate some of these unfavorable conditions; notably by freeze-drying the specimen drop, and by treatment of the suspended material with a fixative such as formalin.

A method occasionally used since the earliest days of electron microscopy can be used to reduce many of the drawbacks of the usual procedure described above. This is a method by which the suspension is either allowed to settle on the specimen screen as tiny droplets, or is sprayed directly and forcibly upon the screen. As a result of this procedure, the screen is partially covered with discrete, roughly circular, droplet patterns from about 5 to 20 microns in diameter.

Spray methods have been described by Riedel and Ruska,[1] Haardick, Kausche and Ruska,[2] and by Cravath, Smith, Vinograd, and Wilson.[3] They appear not to have been put to any general use, however, probably because their advantages largely disappear when the specimen material is suspended in the non-volatile diluents commonly used. We have made developments in the spray technique with the primary purpose of applying it to the preparation of specimens of biological material, and have at the same time developed aqueous suspending media which are wholly volatile. The method now appears to be highly useful for both qualitative and quantitative electron microscopy. Its

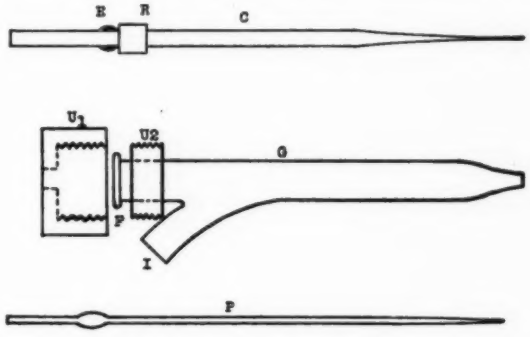

FIG. 1. Sketch of glass spray gun.

* This research has been supported in large part by a grant from the American Cancer Society upon recommendation of the Committee on Growth of the National Research Council, and by a research grant from the Division of Research Grants and Fellowships of the National Institute of Health, U. S. Public Health Service.

[1] G. Riedel and H. Ruska, Kolloid-Zeits. **96**, 86 (1941).
[2] Haardick, Kausche, and Ruska, Naturwiss. **27/39**, 226 (1944).
[3] Cravath, Smith, Vinograd, and Wilson, J. App. Phys. **17**, 309 (1946).

advantages and uses will be detailed below, following a description of a spray gun and a discussion of volatile suspending media.

II. CONSTRUCTION AND USE OF A SPRAY GUN

A spray gun should be capable of depositing upon the specimen screens a pattern of discrete droplets of approximate uniformity of size, reproducibly representative of the suspension, without the presence of contaminants originating in the gun, and devoid of any sprayed material in the regions between the droplet patterns. The simple glass gun to be described has been found adequate to meet these requirements, although it is realized that other gun designs might be found to be equally adequate. Figure 1 is a schematic drawing of the gun in which the parts are shown unassembled.

The outer envelope G is made of apparatus-weight, 7 mm glass, and is provided with an air inlet I and a means for securing the insert tube C. Tube G is provided with a threaded Lucite union U_1 and U_2, with U_2 of an internal diameter less than the diameter of the enlarged flange at F. U_1 threads over U_2, but also has an unthreaded base section with a hole just large enough to fit over tube C. The tube C is provided with a rubber sleeve R and a retaining bulge at E, and upon assembly an air-tight seal is made by compressing R between the flange F and the base of U_1. The purpose of E is to ensure that the tube C will not be violently forced out of the end of G when the compressed air is admitted. Tube C is of uniform diameter except for the bulge at E and the finely drawn portion at the tip.

It has been found convenient to make a number of small pipettes P whenever a series of samples is to be sprayed. The use of these pipettes minimizes the chances of sample-to-sample contamination by restricting the area of contact between fluid and glass to the small region at the tip of C. The pipettes are inserted into C sufficiently far to cause their ends to wedge lightly into the capillary constriction in C. Each pipette is discarded after having been used with one sample of a series.

Extended trial has shown that the dimensions of the orifices are fairly critical. The I.D. of tube C should be about 0.1 mm, and the O.D. about 0.3 mm. The I.D. of the tip of tube G should be about 0.75 mm. A spraying pressure of 20 to 30 p.s.i. is satisfactory, with the gun some 15 to 20 inches from the filmed microscope screens. The screens can be mounted to a supporting surface with Scotch tape, or can be held in position magnetically. Very clean air must be used for spraying, and it appears that tank-compressed air, reduced with a suitable valve, is satisfactorily clean. The gun should be carefully aligned to cause the central region of the spray to intersect the screens; the alignment and other spray characteristics can conveniently be observed with the aid of a beam of light in a darkened room. The gun as described will deposit a convenient number of droplets from about 0.2 ml of sprayed material. A smaller orifice can be used at the tip of tube C (with higher air pressure and diminished distance from gun to screens), when the use of a smaller volume of suspension is necessary.

One of the commercially available all-glass nebulizers has been experimented with, but it has not been found to be as satisfactory for the production of representative drop patterns as is the high air-velocity gun just described. The nebulizer is not as conveniently kept free of contamination, and it does not produce drop patterns that are both discretely bounded and reproducibly representative of the specimen. We believe that the reason for the difference in the performance of the two kinds of spraying devices is that, in the case of the low air-velocity nebulizer, some material from droplets which have completely dried in transit is left in varying amounts and places upon the microscope screens.

III. VOLATILE SUSPENDING MEDIA

The preparation of materials in the form of spray-drop patterns loses most of its unique value when the suspending medium is non-volatile, since the dried salts must be rinsed off the specimen screens with consequent disturbance of the drop patterns. For many substances a satisfactory volatile medium is distilled water, but for others, particularly of a biological nature, a medium containing electrolytes is demanded. The requirements to be met by volatile electrolytes when used in electron microscopy can be stated only after consideration of the type of observation to be made. A minimum requirement would be that the chemical and physical properties of the substance, when suspended in one of the conventional diluents, should be maintained when the substance is suspended in the volatile diluent.

It is clearly necessary that the preparation of a volatile electrolyte be done in a manner calculated to avoid any chance of contamination with non-volatile material. If a non-volatile component is present as much as 1 part in 10^7 in an average spray droplet of 500 microns^3 volume, there will be 5×10^7 A^3 of residual material in the drop pattern. This amount is clearly visible in the electron microscope if it dries on the screen in a form other than a rather uniform film. Such a high degree of freedom from non-volatile contamination requires that only gaseous or freshly redistilled liquid components be used in the chemical preparation.

We have found a 2 percent solution of freshly made ammonium acetate at *p*H 7.0 to be a satisfactory suspending medium for use with several biological materials (for example: fibrinogen, serum globulins, plant viruses, and homogenized tissue suspensions). Ammonium carbonate at a similar ionic strength and *p*H has also been found to be useful. It is advantageous to consider spraying the same material suspended in both of these volatile electrolytes in turn, on account of the changes in *p*H that occur during the brief drying time

of the droplets. The ammonium acetate system will approach a *p*H of about 4.0 as it dries, while ammonium carbonate approaches a *p*H of 10. If differences of form observable in the electron microscope are believed likely to take place in a drying time of about 0.1 sec., their magnitude can be checked by spraying with each volatile system separately, or with the two systems used together in varying concentrations.

IV. USES AND ADVANTAGES OF THE SPRAY METHOD

The consequences of the use of droplets sprayed in a volatile suspending medium may be generally described thus: (1) the time taken for the specimen material to change from its free liquid environment to complete dryness is very short, (2) the droplet patterns are individually and reproducibly representative of the composition of the sprayed material, and (3) the droplet patterns are discretely bounded by areas of blank specimen film. The uses and advantages accruing from these consequences will now be described in detail.

A. Qualitative

1. *Short drying time*—The total time elapsed between the emergence of an aqueous drop of about 500 microns[3] volume from a high air-velocity spray gun and the state of complete dryness on the specimen screen is estimated to be somewhat less than 0.1 sec. The estimate is based upon the known rate of evaporation of water droplets in relatively dry air, and disregards any possible effect of the suspended material in slowing or accelerating the drying process. This drying time is to be compared with a time of several seconds to a minute or so taken by an ordinary, gross drop to dry when placed directly upon the filmed specimen screen.

The advantage of the short drying time is that the suspended material, such as a virus, for example, is exposed only very briefly to an unfavorable electrolytic and osmotic environment and has little time to be morphologically changed. There is also little time for the occurrence of gross aggregation or other particle interactions which must take place during the concentration of the solute materials during the long drying time of a large drop. A further advantage is that very small particles do not imbed themselves in the plastic film as much as they do when the film is softened and swollen by prolonged contact with a large drop of water. An important use of the fact of quick drying is in observations of interparticle reactions, where it is desirable to stop the reaction quickly and at a known instant. In this type of experiment the particulate components are mixed prior to, or during, their introduction into the gun, and the reaction is manifestly stopped within a fraction of a second after the spray drops leave the gun.

2. *Reproducibly representative fields*—It is difficult to overestimate the usefulness of a technique whereby well-defined areas of the microscope screen contain representative and complete samples of all the non-volatile material in the original suspension. This is particularly true when the suspending diluent is in itself free of non-volatile components. The common experience of microscopists is that searching for and photographing "typical" fields is time-consuming, frustrating, and is open to the dangers of subjective judgment. This difficulty has made comparisons between two samples of material, such as normal and infected biological material, relatively uncertain, with the result that the electron microscope has failed to be used to its fullest as an analytical tool. The use of drop patterns eliminates a fundamental difficulty in electron microscopy; namely, the small totally available field of search of about 0.25 mm^2. This restricted field leads to uncertainty as to whether or not the portion of the specimen of great significance lies outside the field, or is obscured by the wires of the specimen grid.

A few qualitative uses of observations on small, representative drop patterns are immediately apparent. The first use lies in making reliable assays of the particulate composition of a given suspension by photographing a few drop patterns. Assays can be made by even an inexperienced person, since the choice of what is typical is independent of his judgment. If the suspension is believed to be a fairly homogeneous one, such as a suspension of a purified plant virus, the microscope can also be used to assay sensitively the amount of particulate impurities present.[4]

The spray method allows a precise comparison to be made of the electron microscopic appearance of two different, but similarly prepared, suspensions. The comparison can be conveniently made in this way: Suspension *A* is sprayed upon a few filmed specimen screens. Suspension *B* is adjusted to have about the same concentration of suspended material as *A*, but to it is added a trace amount of an indicator substance of recognizable shape, such as tobacco mosaic virus. Suspension *B* is then sprayed upon the screens already containing the dried droplets of suspension *A*. The screens are shadowed and examined for regions where discrete, closely adjacent drop patterns of both *A* and *B* can be photographed. This technique seems to embrace all the requirements of controlled electron microscopy, since the methods of mounting the specimen materials are closely identical, even to the details of drying time and surface character of the substrate film, as well as film thickness, shadowing conditions, and circumstances of exposure in the microscope.

3. *Discretely bounded drop patterns*—A constant source of uncertainty in the examination of shadowed electron micrographs of inhomogeneous particulate material is the difficulty of distinguishing between the fine-structure of the specimen material itself and the fine-structure of the substrate film. A similar difficulty

[4] R. C. Williams and R. C. Backus, J. Am. Chem. Soc. (in press).

is present even when preshadowed replicas[5] are used, except that the source of uncertainty is not in the structure of the collodion surface but instead resides in the uncertain degree of cleanliness and discontinuities of the glass surface. When drop patterns are examined, the uncertainty largely disappears, since the patterns occupy discrete areas surrounded by areas of film whose undisturbed structure can be gauged. This separation of regions provides one with a sensitive internal control on the character and cleanliness of the surface of the substrate, and hence enhances the possibility of

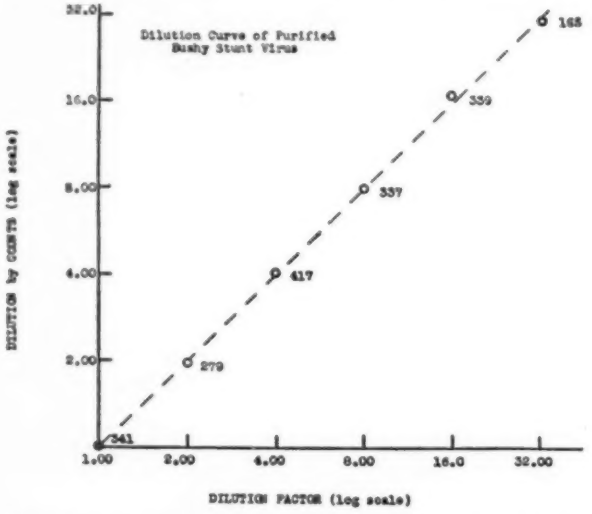

FIG. 2. Determination of the dilution of a suspension of purified bushy stunt virus by spraying and counting. Abscissae are the known dilution factors, obtained by pipetting; ordinates are the dilution factors calculated from the virus counts. The point at the origin has been arbitrarily called a relative dilution of unity. The diameter of the circles represents a 3 percent variation, while the numbers accompanying each circle are the numbers of reference particles counted in the establishment of each point.

making unequivocal observations of the presence or absence of very small particles.

B. Quantitative

The attainment of representative sample fields makes electron microscopy increasingly applicable to certain kinds of quantitative determinations. A technique to provide such fields by centrifugal deposition has been suggested by Crane.[6] A quantitative application of this technique has been made by Sharp[7] who obtained representative fields of swine influenza virus by sedimenting the particles on to a collodion surface. By counting the number of particles per unit area of the film he obtained a satisfactory correlation between counts and known dilution factors, although his results were rendered somewhat uncertain by the necessity of washing the dried buffer salts from the sedimented preparations.

[5] R. C. Williams and R. W. G. Wyckoff, J. App. Phys. **17**, 23 (1946).
[6] H. R. Crane, Rev. Sci. Inst. **15**, 253 (1944).
[7] D. G. Sharp, Proc. Soc. Exp. Biol. Med. **70**, 54 (1949).

1. *Determination of droplet volumes*—If reference particles[8] are present in a known concentration in the suspension being sprayed, a given droplet pattern will contain a number of these particles proportional to the volume of the droplet as it left the spray gun. It has been found that Dow latex particles[9] are particularly useful as reference particles, since they are obtainable in quite pure aqueous suspension, and remain intact and in uniform suspension in ammonium acetate and ammonium carbonate. The particles do not seem to interact with the biological materials we have handled, at least during the brief periods of contact necessary for their use, and their concentration in numbers per unit volume of suspension is readily determinable.[4] It is evident that one can use the latex reference particles directly in a determination of volumes of droplets as they issue from any spray-making device.

2. *Absolute virus assays*—When latex particles are mixed with some other particulate material, such as a virus, simple counts made on the droplet patterns will determine the ratio of the number of latex to the number of virus particles. If the concentration of latex is known, this ratio provides an absolute assay of the number of virus particles per unit volume of the mixed suspension. It is to be noted that this method can be used even though the suspension is not highly purified; as long as one species of particle can be recognized, it can be counted and assayed.

3. *Determination of particle weights*—The technique just described can be used to determine the particle weight of a homogeneous substance, such as a purified virus. The particle counts yield the number of particles per unit volume, and if the material is in highly purified form, this information can be combined with the value of the dry weight of material in an aliquot volume of suspension to allow the weight of an average particle to be computed. This weight in grams, multiplied by Avogadro's number, is the particle weight in molecular weight units. The advantage of this method of determining particle or macromolecular weights lies primarily in its directness, and also in the low concentration of material which can be sprayed and counted.* A satisfactory concentration is 0.0001 percent, and the total weight of material to be diluted and sprayed need be no more than 0.1 microgram.

4. *Assessment of quantitative precision*—Determinations have been made of the quantitative reliability and precision of the method of particle counts by the use of

[8] E. Chamot and C. W. Mason, *Handbook of Chemical Microscopy* (John Wiley and Sons, Inc., New York, 1938), Vol. I, p. 441.
[9] R. C. Backus and R. C. Williams, J. App. Phys. **20**, 224 (1949).
* When very dilute material consisting of small sized particles is sprayed, it is difficult to recognize the confines of the drop patterns in the electron microscope. The admixture of a small amount of highly purified tobacco mosaic virus to the suspension causes the drops to be nicely bounded by easily observed rod-like forms.

reference particles in the spray drops. Two sources of uncertainty might be anticipated: the mixing of the two kinds of particles may not be perfect, and there may be dislodgments of either species of particle from the microscope screens prior to shadowing.

The sources of uncertainty have been checked by measuring the statistical fluctuations of the counts, in a trial where particles of latex and of the bushy stunt virus were mixed in approximately equal numbers. It is found from counts of about 10,000 particles that the standard deviation of the mean ratio of particle numbers lies between 2 and 4 percent when 1000 pairs of particles are counted in 20 or more droplet patterns. Inasmuch as the statistically anticipated standard deviation of the mean ratio should be close to 3 percent, it is believed that the mixing of the particles is nearly perfect, and that they do not become randomly dislodged.

The adequacy of the entire method of quantitative assay of virus particles by electron microscopy has been checked by counts made on mixtures of reference and virus particles of greatly varying relative concentrations. Figure 2 shows the results of an experiment in which the concentration of latex particles was held constant, while the concentration of purified bushy stunt virus was varied through a dilution factor of 32. The evident agreement between the known dilution factors and the dilutions as calculated from the counts of virus and latex particles is very satisfactory, and implies that a quantitative assay of a purified, dilute virus suspension can be made as precise as the statistics of random sampling would indicate.

On the Diffraction of Radar Waves by a Semi-Infinite Conducting Screen*

C. W. Horton and R. B. Watson
Defense Research Laboratory, The University of Texas, Austin, Texas
(Received May 27, 1949)

The diffraction patterns of radar waves about a semi-infinite copper screen have been measured. The measurements were made by revolving a bisectoral horn in a circle of radius 15″ or 30″ about the diffracting edge. Measurements were made at three positions along the edge, one of which coincided with the corner of the screen so that the pattern obtained was actually that of a quarter-infinite plane. Measurements were made for two orientations of the screen corresponding to angles of incidence of 0° and −22½°. Theoretical patterns have been calculated for the entire 360° of rotation and these agree well with the experimental patterns. A comparison is made between the theory, measurements, and the equivalent optical measurements.

I. INTRODUCTION

A RIGOROUS solution of the problem of the diffraction of an electromagnetic wave by a semi-infinite perfectly-conducting screen has been obtained by Sommerfeld.[1,2] Optical measurements have shown deviations from the theory[3] which have usually been attributed to the finite thickness and conductivity of the screen and the irregularities of the edge of the screen.[4] All three of these difficulties are greatly reduced when the experiments are repeated at radar frequencies. A further advantage of the use of radar frequencies is that the smallness of the detector enables one to make significant measurements throughout nearly a full circle. Thus the theoretical results may be checked not only in the shadow region but also in the illuminated regions and especially in the region of geometric reflection. The disadvantages of the change in scale are (1) that a screen of manageable size is not large enough to eliminate diffraction around the other three edges and (2) that the effective aperture of the receiver is of appreciable area, though of the same order as the wave-length squared.

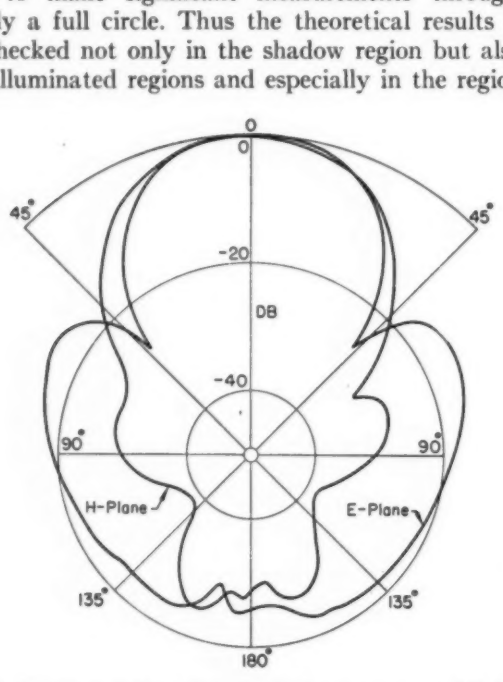

FIG. 1. Experimental patterns for receiving horn type AT-48/UP.

II. EXPERIMENTAL ARRANGEMENT

The experimental arrangement used in this work has been described previously.[5] A modification of this method has been made in which the receiving horn was mounted on a long arm so that it moved on a circle whose center coincided with the edge of the diffracting screen and which lay in a plane normal to the screen. The screen consisted of a single sheet of copper 30″×60″ and $\frac{1}{16}$″ thick which was mounted 30″ above the experimental bench with the long dimension horizontal. One of the 30″ vertical edges was the diffracting edge. The screen was supported by two U-shaped dural channels 2″×1$\frac{3}{8}$″ which were placed symmetrically about the vertical centerline. The channel nearer to the diffracting edge was 18″ from it. Small dural angles $\frac{3}{4}$″×$\frac{3}{8}$″ were required in order to stiffen the copper sheet and prevent vibrations since the sheet was mounted in the open air; however a space of 4$\frac{1}{2}$″ was left completely clear next to the diffracting edge. Some of these stiffeners were placed along the upper and lower edges of the screen.

The receiving horn was a bisectoral horn of the Type AT-48/UP manufactured for the armed services. The aperture of this horn is 1.9″×2.4″ or 1.47λ×1.82λ for a free space wave-length of 3.2 cm. Figure 1 shows the patterns of this horn in the *E*- and *H*-planes.

In order to observe the influence of the upper and lower reinforced edges, the free edge on the far end of the sheet, and the various supporting members, measurements were made with the receiving horn at two radii, 15″ (*ca.* 12 wave-lengths) and 30″ (*ca.* 24 wave-lengths), and at three positions along the diffracting edge. One position was at the midpoint, or 15″ from the upper or lower edges, a second position was 9″ from the upper edge, while the third position was at the upper edge of the screen. This last position really gives

* The work described in this paper was done at the Defense Research Laboratory under the sponsorship of the Bureau of Ordnance, Navy Department, Contract NOrd-9195.

[1] G. Wolfsohn, *Handbuch der Physik* (Julius Springer, Berlin, 1928), Vol. 20, pp. 266–277.

[2] B. B. Baker and E. T. Copson, *The Mathematical Theory of Huygen's Principle* (Oxford University Press, London, 1939), pp. 124–149.

[3] See reference 1, Figs. 6a and 6b, p. 275.

[4] See reference 1, p. 275.

[5] R. B. Watson and C. W. Horton, J. App. Phys. **19**, 661–70 (1948).

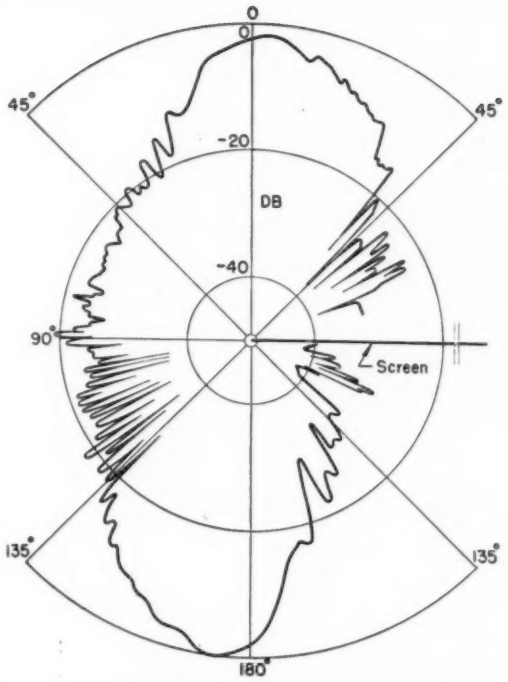

FIG. 2. Experimental diffraction pattern for semi-infinite screen for normal incidence, with incident wave from 0° direction. Receiving horn rotated in 30″ circle about center of diffracting edge. Electric vector parallel to diffracting edge.

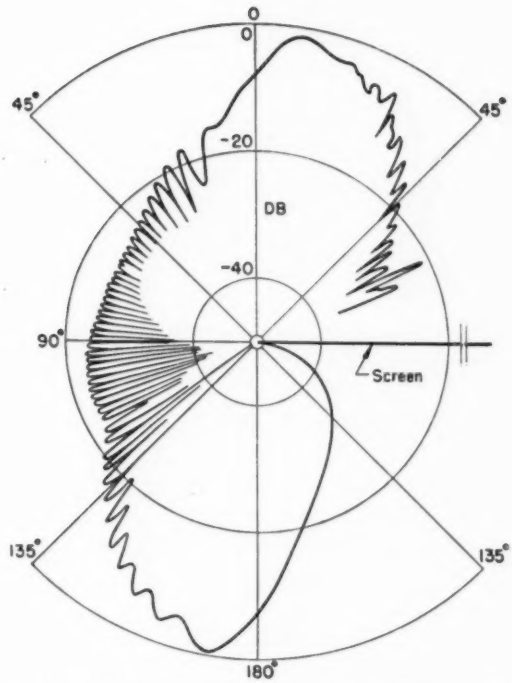

FIG. 3. Theoretical diffraction pattern for the conditions of Fig. 2.

patterns for a quarter-infinite screen. The agreement between the patterns measured about the center of the diffracting edge and the position 9″ from the upper edge is good. However, the presence of an interference pattern in the shadow region behind the screen for both of these positions shows that the screen was only a moderately good approximation to a semi-infinite screen.

Measurements were made for angles of incidence of 0° and of $-22\frac{1}{2}°$.

III. NORMAL INCIDENCE

Figure 2 is a polar plot of the received signal in db *versus* the angle about the edge of the semi-infinite screen for the case of an incident wave polarized with the electric vector parallel to the diffracting edge. The horn was always turned so that it faced the edge of the screen. Thus the diffracted wave was detected at maximum sensitivity and the directionality of the horn was used to discriminate against the incident and reflected waves. Figure 3 is a plot of the theoretical pattern for the same conditions. In computing the theoretical pattern the wave field was resolved into plane and cylindrical waves in accordance with the description of Baker and Copson.[6] The pattern of the horn was applied separately to each wave component in accordance with its orientation with respect to the horn. In the regions that are very near the line of propagation, the approximate expressions for the diffracted field recently developed by Horton[7] have been used.

Figure 4 is a polar plot of the received signal in db *versus* the angle about the edge of the semi-infinite screen for the case of an incident wave polarized with

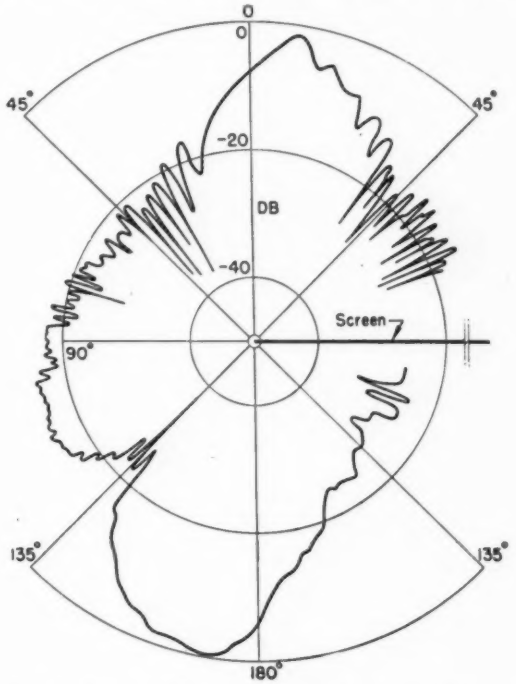

FIG. 4. Experimental diffraction pattern for the conditions of Fig. 2, except electric vector perpendicular to diffracting edge.

[6] See reference 2, p. 146.

[7] C. W. Horton, Phys. Rev. **75**, 1263 (1949).

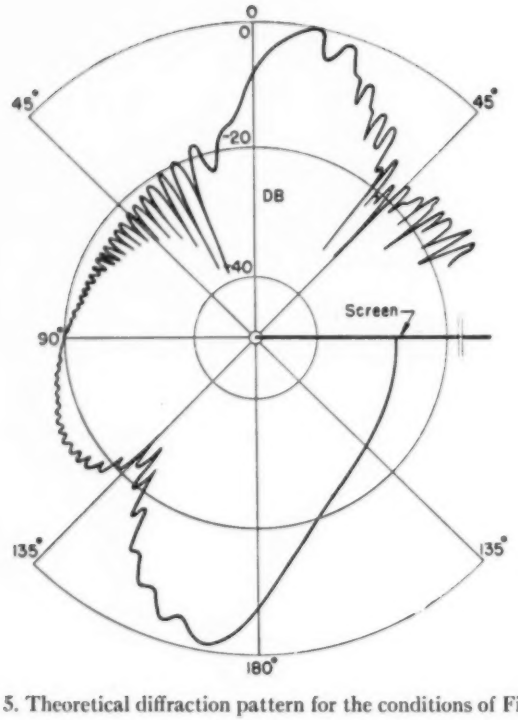

FIG. 5. Theoretical diffraction pattern for the conditions of Fig. 4.

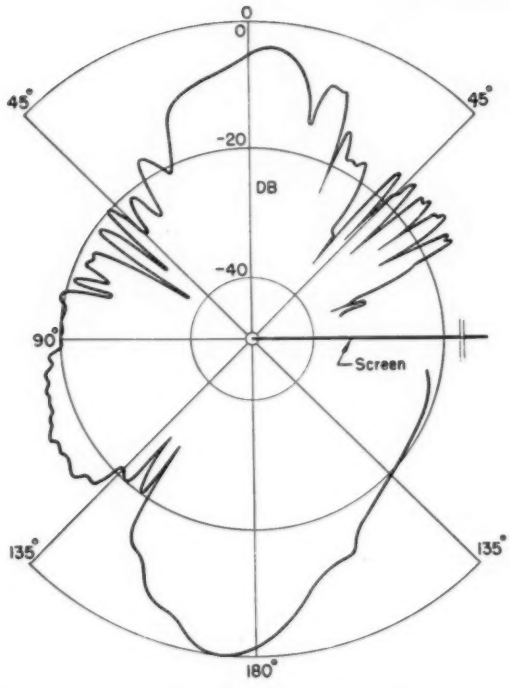

FIG. 7. Experimental diffraction pattern for the conditions of Fig. 6, except electric vector perpendicular to diffracting edge.

the electric vector perpendicular to the diffracting edge of the screen. Again the horn was always turned so that it faced the edge of the screen. The theoretical pattern for the same conditions is shown in Fig. 5.

The process of resolving the total wave field into component fields has received a striking verification from these patterns. In the region of geometric reflection, the field can be resolved into three components; the incident plane wave, the reflected plane wave and a cylindrical wave diverging from the edge. To each of these the horn has a different response. Yet when the contributions of the three components are added, very good agreement with experimental patterns is obtained.

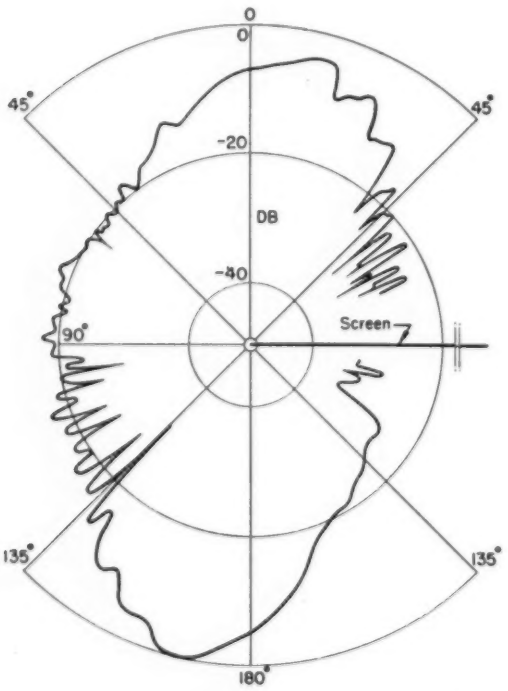

FIG. 6. Experimental diffraction pattern for semi-infinite screen for normal incidence, with incident wave from 0° direction. Receiving horn rotated in 15″ circle about center of diffracting edge. Electric vector parallel to diffracting edge.

Figures 6 and 7 show the patterns for the case of the electric vector parallel and perpendicular respectively to the diffracting edge when the radius of the circle is 15 inches. The patterns were measured at the midpoint of the edge of the screen. The effective aperture angle of the horn is twice as large as in the case of the 30-inch circle and so the size of the lobes is correspondingly reduced.

Although an inspection of Figs. 2–5 is sufficient to show that there is good agreement between experiment and theory through all the angular range of the measurements it is of interest to compare for the shadow zone only the ratios of the amplitudes for the two cases of the electric vector parallel and perpendicular to the edge of the screen. Figure 8 shows the theoretical values of this ratio, the observed values for a circle of 15″ measured at the midpoint and at 6″ from the midpoint of the diffracting edge, and the values given by Maey[8] and Jentzsch[9] obtained by optical measurements. The

[8] E. Maey, Wied. Ann. **28**, 117–130 (1886).

[9] F. Jentzsch, Ann. d. Phys. **84**, 292–312 (1927). It might be mentioned that when Wolfsohn (reference 1, Fig. 6a, p. 275) cites Jentzsch's data, he titles the figure "intensity ratio" whereas the values plotted are "amplitude ratios."

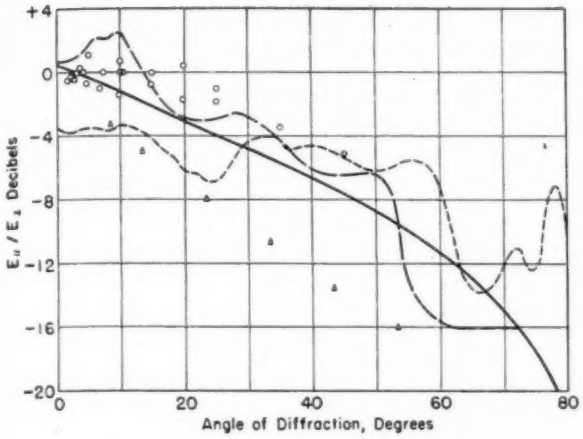

FIG. 8. Ratio of the amplitude of the measured electric vector for electric vector parallel to diffracting edge ($E_{\parallel}$) to that for electric vector perpendicular to diffracting edge ($E_{\perp}$) in the shadow zone behind the screen, *versus* diffraction angle. Normal incidence and semi-infinite screen. ——— Theory. - - - - Receiving horn rotated on 15″ circle, about center of diffracting edge. — — — Receiving horn rotated on 15″ circle, about point 6″ from center of diffracting edge. O, Optical data, Maey. Δ, Optical data, Jentzsch.

experimental data in Fig. 8 show clearly the effect of the interference fringes produced by the diffracted waves that come from the other three edges of the screen. It is difficult to draw a satisfactory average through the experimental curves. The general trend, however, is the same as the theoretical curve. Agreement is found with Maey's data, but Jentzsch's data

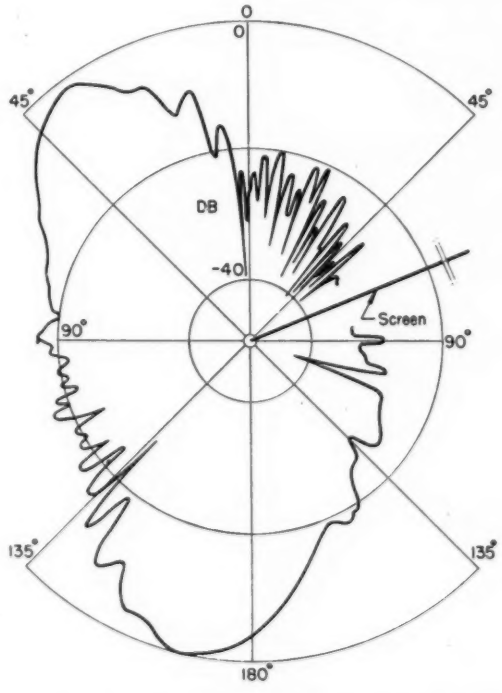

FIG. 9. Experimental diffraction pattern for semi-infinite screen for $-22\frac{1}{2}°$ incidence, with incident wave from 0° direction. Receiving horn rotated in 15″ circle about center of diffracting edge. Electric vector parallel to diffracting edge.

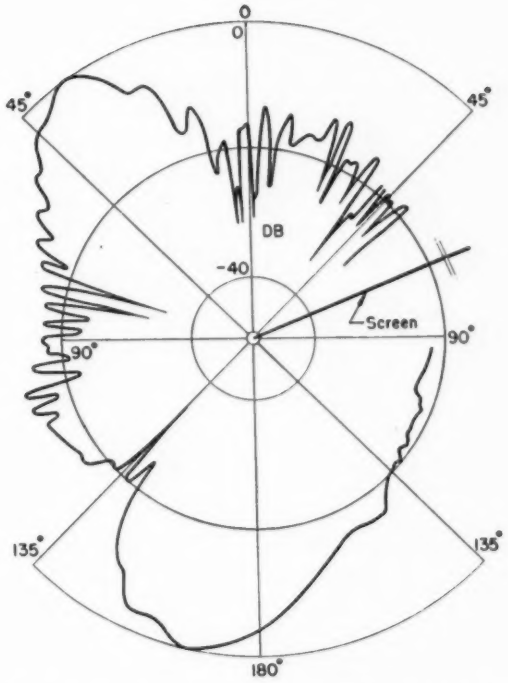

FIG. 10. Experimental diffraction pattern for the conditions of Fig. 9, except electric vector perpendicular to diffracting edge.

lie considerably below both the experimental and theoretical curves. At large angles the experimental data fall in general slightly above the theory. This effect may be in part explained by the smallness of the component values used in calculating the ratios. For such small values, inherent noise in the measuring apparatus plus diffracted contributions from surrounding objects as well as the other three edges of the screen may well increase the smaller component value more than the larger, and thus increase the ratio. Similar curves of $E_{\parallel}/E_{\perp}$ are obtained for the measurements at a radius of 30″ but the errors of measurement are larger because of the increased diffraction about the other three edges.

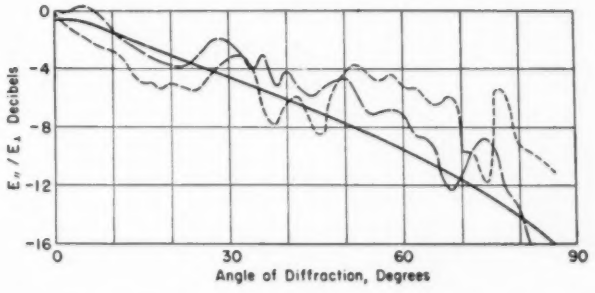

FIG. 11. Ratio of the amplitude of the measured electric vector for electric vector parallel to diffracting edge to that for electric vector perpendicular to diffracting edge in the shadow zone behind the screen, *versus* diffraction angle. Angle of incidence $= -22\frac{1}{2}°$; semi-infinite screen. ——— Theory. - - - - Receiving horn rotated on 15″ circle, about center of diffracting edge. — — — Receiving horn rotated on 15″ circle, about point 6″ from center of diffracting edge.

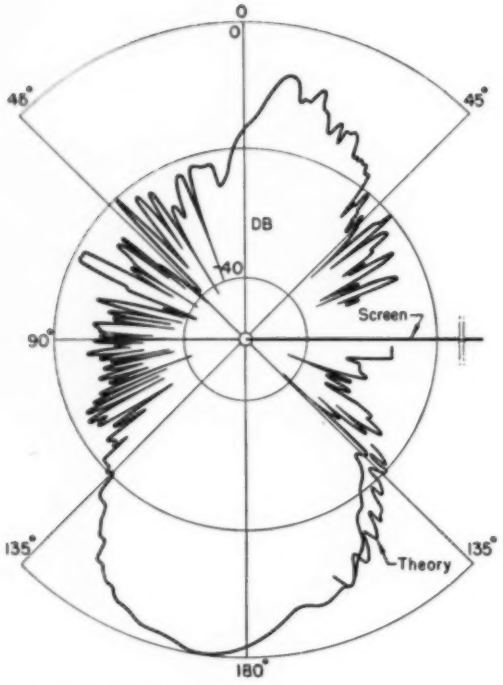

FIG. 12. Experimental and theoretical diffraction patterns for quarter-infinite screen for normal incidence, with incident wave from 0° direction. Receiving horn rotated in 30″ circle about top diffracting edge. Electric vector parallel to vertical diffracting edge.

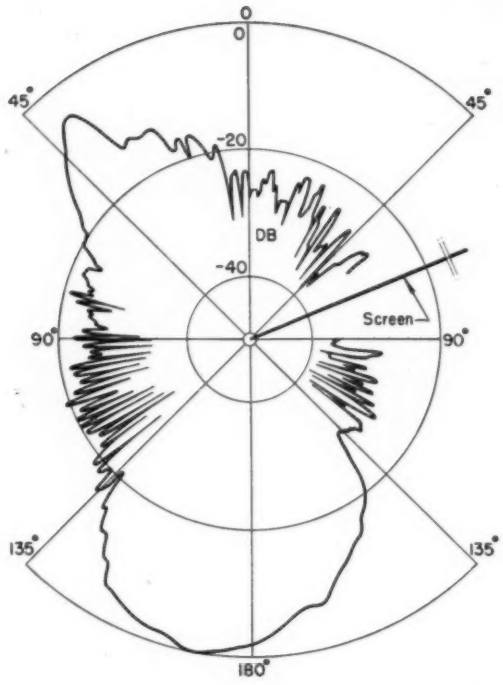

FIG. 14. Experimental diffraction pattern for quarter-infinite screen for $-22\frac{1}{2}°$ incidence, with incident wave from 0° direction. Receiving horn rotated in 30″ circle about top diffracting edge. Electric vector parallel to vertical diffracting edge.

IV. ANGLE OF INCIDENCE −22.5 DEGREES

The measurements described above were repeated for the case that the direction of propagation of the incident wave made an angle of −22.5 degrees with the normal to the screen. Figures 9 and 10 show the two patterns for the cases of the electric vector parallel

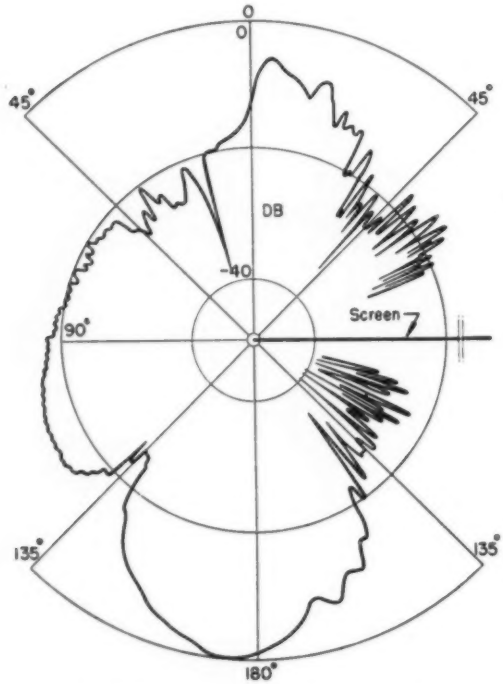

FIG. 13. Experimental diffraction pattern for the conditions of Fig. 12, except electric vector perpendicular to vertical diffracting edge.

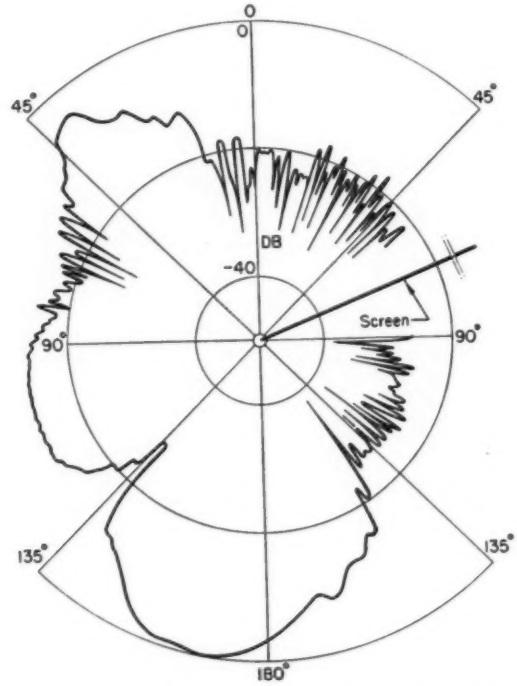

FIG. 15. Experimental diffraction pattern for the conditions of Fig. 14, except electric vector perpendicular to vertical diffracting edge.

and perpendicular to the diffracting edge of the screen respectively. Figure 11 shows a comparison between the theoretical and experimental values of the ratio of the amplitudes for the electric vector parallel and perpendicular to the edge of the screen. The experimental curves in Fig. 11 follow the theory quite well, with some deviations due to effects of extraneous diffraction. The experimental points tend to rise slightly above the theory at large angles, due in part to incidental noise and diffraction effects from the other edges.

V. QUARTER-INFINITE SCREEN

A rigorous theoretical solution of the diffraction pattern of a quarter-infinite screen has not been obtained. A first approximation is obtained by assuming both edges of the quarter screen to be infinite in extent so that the analysis described above may be applied to each edge. The effect of termination of the edges at the point of intersection is recognized by assuming a source of spherical waves at the corner. Contributions from the two diffracting edges, the incident wave, and the point at the corner are then added together to give the solution. Detailed calculations were carried out for the case of the electric vector parallel to the vertical diffracting edge, when the receiving horn is rotated in a circle whose plane contains the upper edge of the screen. These calculations were made for normal incidence only, and were restricted to the region in the shadow zone in which the angle of diffraction with respect to the vertical edge was between 20° and 50°. This restriction was made since it was felt that such an approximate analysis should apply best in the shadow region behind the screen.

Figures 12 and 13 show the experimental measurements, which were carried out for all angles for the case of normal incidence on the quarter-infinite screen. The theoretical data are plotted in the lower right quadrant of Fig. 12. The experimental and theoretical curves are much alike, but the theory shows larger lobes and a somewhat different slope from the experiment. A comparison of Figs. 12 and 13 with Figs. 2 and 4, respectively, shows that the diffraction pattern of a quarter-infinite screen is surprisingly similar to that of a semi-infinite screen.

Figures 14 and 15 show the experimental measurements for a quarter-infinite screen when the normal to the screen makes an angle of $-22.5°$ with the direction of the incident wave. Further similarity to patterns for the semi-infinite screen is observed by comparison with Figs. 9 and 10.

Measurement of the Surface Temperature of Evaporating Water Drops*

JOHN C. JOHNSON
Massachusetts Institute of Technology, Cambridge, Massachusetts
(Received July 14, 1949)

Measurements made of the surface temperature of evaporating water drops are in agreement with the requirements of the theory ennunciated by Fuchs which states that the temperature is determined by the difference between the ambient and saturated vapor density of the drop.

INTRODUCTION AND THEORY

FOR some years, studies, both theoretical and experimental, have been conducted on the rate of evaporation of liquids in the form of spherical drops. Studies using water droplets have been of particular interest to meteorologists, but evaporation processes are of concern in studies of liquid smokes, in atomizing fuel oils, and in studies of other volatile liquids. Both theory and experiment show that the drop diameter varies as a parabolic function of time when evaporation (or condensation) occurs, so that the surface area changes directly with the lapse in time. This leads to an expression of the type (Houghton 1933)

$$a^2=a_0^2-(8k/\bar{\rho})(\rho_0-\rho)t \tag{1}$$

obtained from the differential equation

$$dM/dt=-2\pi ka(\rho_0-\rho), \tag{2}$$

where dM/dt=the rate of change of the mass of the liquid, k=diffusivity of the vapor in the atmosphere surrounding the drop, a=diameter of the drop at time t, a_0=diameter at $t=0$, $\bar{\rho}$=density of the liquid, and $(\rho_0-\rho)$ is the difference in vapor density at the surface of the drop and the surroundings, the latter ambient condition being essentially the concentration of the vapor in the atmosphere in the absence of or at infinite distance from the drop.

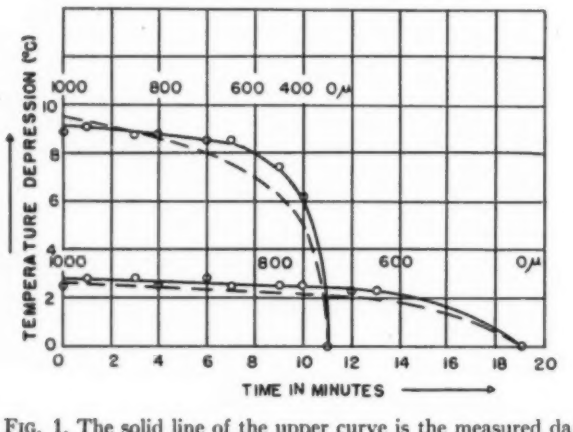

FIG. 1. The solid line of the upper curve is the measured data for a drop evaporating in an atmosphere with temperature and relative humidity of 25.4°C and 37 percent respectively. Number 2 thermocouple was used. The lower solid curve shows the experimental results using thermocouple No. 4, where the ambient temperature and relative humidity were 23.9°C and 68 percent respectively. The dashed curves are a plot of Eq. (6) using the same values of $(\rho-\rho_0)$ that were measured experimentally. $C=2.1\times10^{-3}$ was used.

In practice, the use of Eq. (1) requires a knowledge of the quantity $(\rho_0-\rho)$. Confining the discussion for the moment to water vapor, ρ is the ambient vapor density evaluated from the measurement of the relative humidity of the air, the temperature of the air, and a set of vapor pressure tables for water (neglecting the slight effect on this pressure by the pressure of a neutral gas). The quantity ρ_0, is the saturation vapor density at the temperature of the surface of the evaporating drop. Reason dictates that this latter temperature be colder than the surrounding atmosphere for an evaporating drop. The wet bulb temperature has been suggested for this temperature, but does not give the correct result. Fuchs (1934) [see Houghton (1938)] attacked this problem by considering the energy lost to the drop by diffusion to be balanced in the steady state by the conduction of heat from the air to the surface of the drop. If Eq. (2) be multiplied by the latent heat of vaporization, L, and equated to the expression for the radial conduction of heat by the air to the drop

$$dQ/dt=-2\pi K(T-T_0)a \tag{3}$$

where K is the thermal conductivity of the air, there is obtained a thermal condition

$$T-T_0=(kL/K)(\rho_0-\rho) \tag{4}$$

which must be satisfied as evaporation (or condensation) occurs. T and ρ are the ambient temperature and vapor density, while T_0 and ρ_0 refer to saturation conditions at the drop surface. As $\rho_0=f(T_0)$, Eq. (4) leads to a "cut and trial" solution. It is the purpose of this paper to present an experimental verification of Eq. (4), by direct measurement of the surface temperatures of evaporating water drops.

DISCUSSION OF EXPERIMENTAL PROCEDURE AND CORRECTIONS

The drop under consideration can be suspended from a small thermocouple in a suitable chamber where the humidity and temperature of the chamber's atmosphere can be controlled and measured. If there were no thermal losses due to heat from the air being conducted to the thermocouple junction by the thermocouple wires

* Work done in connection with the partial fulfillment of the degree Sc.D. at Massachusetts Institute of Technology, July 1948.

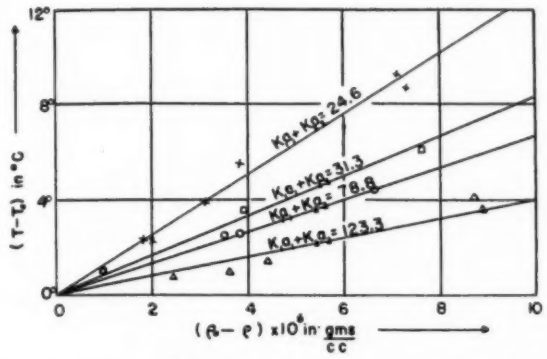

FIG. 2. Data used in determining the best value of A for the four different thermocouples. A is the slope of the curve, $(T-T_0)/(\rho_0-\rho)$.

TABLE I. Thermocouple data.

Thermocouple	No. 1	No. 2	No. 3	No. 4	Units
a_1	127	24	28	79	microns
a_2	127	49	104	117	microns
K_1	0.918	0.918	0.918	0.918	cal./cm°C
K_2	0.054	0.054	0.054	0.054	cal./cm°C
$K_1a_1+K_2a_2$	123.3	24.6	31.3	78.8	cal. microns / cm °C

$$\left(\frac{kL}{K}\right)_{20°C}=2.45\times10^{6}\frac{°C}{g}cc$$

themselves, and thereby helping to compensate the cooling effect of the evaporating drop on the thermocouple junction, the ratio $(T-T_0)/(\rho_0-\rho)$ could be directly measured and compared at once with the constant kL/K predicted by theory. Due to the error introduced by any real thermocouple, it is necessary to use several thermocouples with different heat losses for the measurements, extrapolating the results to one of zero loss for the comparison. If the two lead wires to the thermocouple junction are considered to be cylinders of uniform diameters a_1 and a_2, with conductivities K_1 and K_2 respectively, the heat loss from the wires is to the first approximation (Johnson 1948)

$$(dQ/dt)_{\text{wire}}=-2\pi C(K_1a_1+K_2a_2)(T-T_0), \qquad (5)$$

where C is a dimensionless constant due to the geometry of the system having an empirical value of $2.5\pm0.4\times10^{-3}$. The loss of energy by diffusion (Eq. (2) multiplied by the latent heat of vaporization of the liquid) is just balanced by the conduction of heat to the thermocouple junction both from the surface of the drop and from the wire to give

$$T-T_0=\frac{kL(\rho-\rho_0)}{K\{1+C[(K_1a_1+K_2a_2)/Ka]\}}=A(\rho-\rho_0). \qquad (6)$$

An inspection of Eq. (6) shows that A is a function of the drop diameter for a given thermocouple. For large drops or very fine wires $A\rightarrow kL/K$ and the second term in the denominator is small. At the other limit where the drop is very small in relation to the wires, $A\rightarrow0$ and no difference in temperature is measured. There is an

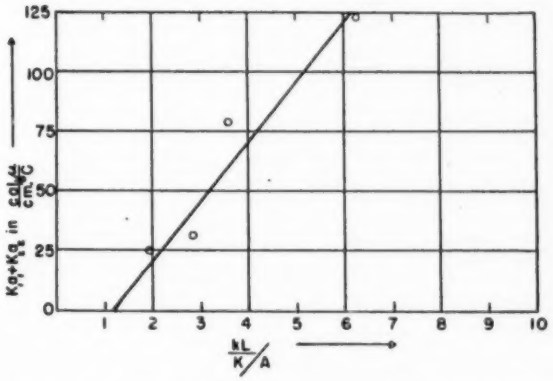

FIG. 3. An extrapolation of the observed data to a thermocouple having no thermal influence on the evaporating drop, to approximate the conditions of a cloud or small rain drop evaporating in the free atmosphere (assuming zero fall velocity).

intermediary region where $a\cong C(K_1a_1+K_2a_2/K)$ causing A to change rapidly. An example of this is given in Fig. 1. The temperature changes for the evaporating drop are shown for two constant vapor density differences.

RESULTS AND CONCLUSIONS

By observing the evaporation of several drops from a given thermocouple, the best value of A can be determined for the thermocouple. This was done for four thermocouples at a drop diameter where the temperature difference was large and nearly independent of drop diameter. The results are given in Fig. 2. Finally the ratio $(kL/K)/A$ is plotted against the wire constant $K_1a_1+K_2a_2$ and extrapolated to zero. Equation (6) on rearranging to

$$(kL/K)/A=(C/Ka)(K_1a_1+K_2a_2)+1 \qquad (7)$$

indicates that the relationship is linear when all measurements are made at one value of the drop diameter. This latter condition has been substantially met in Fig. 3. Least square analysis indicates that

$$(kL/K)/A_0=1.15 \quad A\rightarrow A_0 \text{ as } K_1a_1+K_2a_2\rightarrow0$$

for this series of measurements. From the experimental evidence, it appears that Eq. (4) adequately describes the surface temperature of an evaporation drop of water under steady state conditions where extreme conditions of radiation and convection are lacking. The values of the wire constants are given in Table I.

BIBLIOGRAPHY

(1) N. Fuchs, "Uber die Verdampfungsgeschwindigkeit kleiner Tröpfchen in einer Gasatomsphäre," Physik. Zeits. d. Sowjetunion **6**, 224–243.
(2) H. G. Houghton, Physics **4**, 419 (1933).
(3) H. G. Houghton and W. H. Radford, "On the Local Dissipation of Natural Fog," Papers in Physical Oceanography and Meteorology, Mass. Inst. of Technology and Woods Hole Oceanographic Institute **6**, No. 3, pp. 1–63 (October 1938).
(4) J. C. Johnson, "A Study of the Freezing Temperature of Supercooled Water with Special Reference to Drops Having Diameters from 150 to 1700 Microns," Sc.D. thesis, M.I.T. (July 1948).

X-Ray Measurement of Order in Single Crystals of Cu_3Au*,**

J. M. COWLEY†
Massachusetts Institute of Technology, Cambridge, Massachusetts
(Received August 4, 1949)

X-ray diffraction methods have been used to measure long- and short-range order parameters for single crystals of the alloy Cu_3Au held at elevated temperatures. It is shown that short-range order parameters may be obtained by a three-dimensional Fourier analysis of the "scattering power" for the diffuse background scattering of x-rays, expressed as a function of reciprocal lattice coordinates. Appropriate experimental and computational procedures are outlined. Intensity measurements have been made with a special arrangement of a bent-crystal monochromator and a Geiger-counter spectrometer. Short-range parameters are given for the first ten shells of atoms surrounding a given atom for three temperatures above the critical temperature of Cu_3Au. These results, and those for the long-range order parameter agree well with theoretical predictions.

INTRODUCTION

X-RAY diffraction methods allow quantitative determinations to be made of the amount of order present in an alloy. When long-range order is present, super-lattice reflections appear in the x-ray diffraction pattern with intensity proportional to the square of S, the long-range order parameter defined by Bragg and Williams.[1] Above the critical temperature of ordering of the alloy, the long-range order is zero, but short-range order persists in that there is a tendency for each atom to be surrounded by more than an average number of unlike atoms. In this case, the randomness in the lattice gives rise to a diffuse background scattering of x-rays, and the presence of short-range order gives broad maxima in this diffuse background at the positions of the super-lattice reflections of the ordered lattice. Values of the parameters defining short-range order may be obtained by an analysis of the diffuse scattering.

Measurements of short-range order parameters have been made by Wilchinsky[2] using powder samples of the alloy Cu_3Au. The accuracy of this work was limited by the difficulty of making an accurate separation of the diffuse scattering due to the thermal motion of the atoms from that due to the state of short-range order. This difficulty is largely overcome by the use of a single crystal. In a single-crystal diffraction pattern, the thermal diffuse scattering occurs mostly about the strong "fundamental" reflections, well separated from the maxima of the diffuse scattering due to short-range order. Hence the two effects may be distinguished.

Measurements of long-range order in Cu_3Au have been made by Wilchinsky[2] and by Komar and Buinov,[3] using powder samples. Chipman and Warren[4] have measured the long-range order in a single crystal of the alloy CuZn. The single crystal method has the advantage of giving greater intensity for Geiger-counter measurements, and also permits the detailed study of the time-variation of intensity and shape of super-lattice reflections.

MEASUREMENT OF SHORT-RANGE ORDER IN CU_3AU

Diffraction Theory for Short-Range Order

When an x-ray beam is reflected from a crystal, the intensity reflected in a given direction may be expressed in electron units, in the form

$$I=\sum_m \sum_n f_m f_n \exp\left[\frac{2\pi i}{\lambda}(\bar{S}-\bar{S}_0)\cdot(\bar{r}_m-\bar{r}_n)\right],$$

where f_m and f_n are the atomic scattering factors for the atoms at the end points of the vectors $\bar{r}_m$ and $\bar{r}_n$ drawn from some origin, and $\bar{S}_0$ and $\bar{S}$ are the unit vectors representing the incident and reflected beams. The summations are made over all atoms of the crystal.

We consider a crystal composed of N unit cells of simple structure, such as body-centered or face-centered cubic, with A and B atoms present in the proportions m_A and m_B. If short-range order is present in the crystal, there will be a relationship between the value of f_m and the values of the f_n for atoms close to the atom denoted by m. We say that among the c_i atoms which are i^{th} nearest neighbors of a B atom, on the average n_i are A atoms. If, then, such relationships are incorporated in the expression for the intensity, the scattered intensity is found to consist of sharp "crystalline" reflections plus a diffuse background intensity given by

$$I_D=Nm_Am_B(f_A-f_B)^2 \times\left\{1+\sum_{i=1}^{\infty}\sum_{j=1}^{c_i}\left(1-\frac{n_i}{m_AC_i}\right)\exp\left[\frac{2\pi i}{\lambda}(\bar{S}-\bar{S}_0)\cdot\bar{r}_{ij}\right]\right\},$$

where $\bar{r}_{ij}$ is the vector from the origin to the j^{th} atom

* Extract from a thesis submitted in partial fulfillment of the requirements for the degree of Doctor of Philosophy in Physics at the Massachusetts Institute of Technology.

** Work supported in part by the ONR.

† Now with the Division of Industrial Chemistry, Commonwealth Scientific and Industrial Research Organization, Australia.

[1] Bragg and Williams, Proc. Roy. Soc. **A145**, 699 (1934).
[2] Z. W. Wilchinsky, J. App. Phys. **15**, 806 (1944).
[3] Komar and Buinov, J. Phys. (USSR) **11**, No. 5 (1947).
[4] B. E. Warren and D. Chipman, Phys. Rev. **75**, 1629 (1949).

of the i^{th} shell of atoms surrounding a B atom. The vector $\bar{S}-\bar{S}_0$ may be expressed in terms of the continuous coordinates h_1, h_2, h_3, and the vectors $\bar{b}_1$, $\bar{b}_2$, $\bar{b}_3$, of the reciprocal lattice as

$$\bar{S}-\bar{S}_0=(h_1\bar{b}_1+h_2\bar{b}_2+h_3\bar{b}_3)\lambda.$$

Similarly the vector $\bar{r}_{ij}$ may be expressed in terms of the coordinates l,m,n, of the atoms, and the vectors $\bar{a}_1$, $\bar{a}_2$, $\bar{a}_3$, of the crystal lattice, as $\bar{r}_{ij}=l\bar{a}_1+m\bar{a}_2+n\bar{a}_3$. Putting $\alpha_{lmn}=\alpha_i=l-(n_i/m_AC_i)$, the summation in the intensity expression, abbreviated by I_D', then becomes

$$I_D'=\sum_{l=-\infty}^{+\infty}\sum_{m=-\infty}^{+\infty}\sum_{n=-\infty}^{+\infty}\alpha_{lmn}\exp[-2\pi i(lh_1+mh_2+nh_3)].$$

Thus I_D' is expressed by a three-dimensional Fourier series in terms of the reciprocal lattice coordinates, and is a periodic function with the periodicity of the reciprocal-lattice unit cell.

The coefficients of the Fourier series are given in the usual way as

$$\alpha_{lmn}=\int_0^1\int_0^1\int_0^1 I_D'\exp[2\pi i(lh_1+mh_2+nh_3)]dh_1dh_2dh_3.$$

From the diffraction theory, these Fourier coefficients are given as $\alpha_{lmn}=\alpha_i=l-(n_i/m_AC_i)$; or, in terms of the probability p_{lmn} that the atom with coordinates l,m,n with respect to a B atom should be an A atom, $\alpha_{lmn}=1-p_{lmn}/m_A$.

The probability that an atom is an A atom is given by $P_{lmn}=m_A(1-\alpha_{lmn})$ if a B atom is at the origin, and by $P_{lmn}=m_A+m_B\alpha_{lmn}$ if the origin is an A atom.

The Fourier coefficients have the conventional features of short-range order parameters in that they are zero for the completely random arrangement, and have a maximum (absolute) value for the perfectly ordered state. For even-numbered shells the value for perfect order is unity. For odd-numbered shells the value for perfect order is unity. For odd-numbered shells, the value for perfect order is negative and may be fractional. For example, for Cu_3Au type alloys, α_i°, the value of α_i for perfect order, is equal to $-1/3$, for i odd. It is evident that short-range order parameters defined in this way are the best suited to considerations of the x-ray diffraction effects. It has also been found that they are very convenient for theoretical considerations of order in alloys.[5] Hence the coefficients α_{lmn} or α_i have been used as short-range order parameters in preference to parameters defined in analogy with Bethe's[6] σ. For AB alloys, such as CuZn, the α_{lmn} are equivalent to the r_{hkl} defined by Zernike,[7] and for this case, $\alpha_1=-\sigma$.

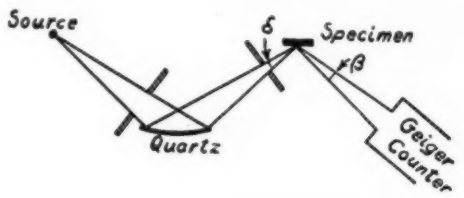

FIG. 1. Arrangement used for measurements of diffuse scattering from single crystals, using a bent-crystal monochromator.

It may be shown readily[6] that the limiting value of α_i for i very large is given by $\alpha_i^\circ\cdot S^2$. Thus the value of α_i falls off to zero with increasing distance from the origin above the critical temperature, but approaches a finite limit when long-range order is present. For the case of finite long-range order, the Fourier series representing the scattering power in reciprocal lattice space may be divided into two series, as MacGillavry and Strijk[8] have suggested: one series with coefficients equal to $\alpha_i^\circ\cdot S^2$, representing the sharp super-lattice reflections with integrated intensity proportional to S^2, and the other with coefficients $\alpha_i-\alpha_i^\circ\cdot S^2$, giving broad maxima in the diffuse background surrounding the sharp super-lattice reflections.

The experimental determination of short-range order parameters involves the measurement of a large number of intensities of the diffuse background scattering of x-rays from a single crystal, the calculation of the quantity I_D' as a function of the reciprocal lattice coordinates, and the three-dimensional Fourier analysis of this function.

Experimental Methods

Measurements were made of the intensity of reflection of copper $K\alpha$ radiation from the face of a single crystal of Cu_3Au cut parallel to the (1,0,0) lattice plane. The crystal was held at a temperature above the critical temperature of Cu_3Au, and intensity measurements were made with a conventional Geiger counter and scaling circuit.

For measurements of diffuse background intensities it is necessary to use monochromatic radiation such as that given by a crystal monochromator. However, it was found that the intensity given by a plane monochromator, such as a well-ground rocksalt cube face,

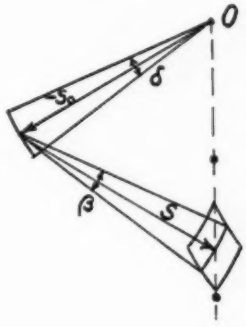

FIG. 2. The volume-element of reciprocal lattice space defined by the divergence of the x-ray beams.

[5] J. M. Cowley, "An approximate theory of order in alloys" (submitted for publication in Phys. Rev.).
[6] H. A. Bethe, Proc. Roy. Soc. **A150**, 552 (1935).
[7] F. Zernike, Physica **7**, 565 (1940).
[8] C. H. MacGillavry and B. Strikj, Physica **11**, 369 (1946).

was insufficient to allow accurate intensity measurements with a Geiger counter. Hence a focusing monochromator, using an elastically bent quartz crystal, was employed in an arrangement sketched in Fig. 1. This arrangement gives sufficient intensity by taking advantage of the fact that a low divergence beam, such as that given by a plane crystal monochromator, is not necessary for the measurement of slowly-varying background intensities, but a relatively large divergence of incident and reflected beams may be used without serious decrease in the accuracy of measurement. In

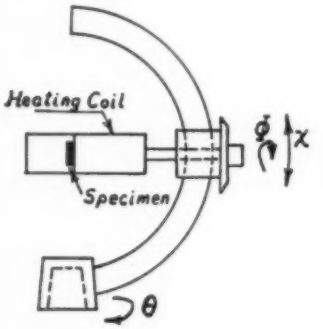

FIG. 3. Specimen mount, for measurement of intensities reflected from single crystal faces at elevated temperatures.

Fig. 1, the incident beam has an effective divergence δ in the horizontal plane. The rectangular aperture at the entrance to the Geiger counter gives the reflected beam a divergence β in the same plane and a divergence γ, not shown, in the perpendicular plane. Figure 2 shows the equivalent of this arrangement in the reciprocal lattice. The vector, S_0, representing the incident beam, varies through an angle δ. The vector S representing the reflected beam varies through an angle β in the same plane and an angle γ in the perpendicular plane. All the "scattering power" contained in the volume element of reciprocal space so defined contributes to the measured intensity. In practice the angles δ, β and γ were made equal to three degrees.

In order to obtain measurements of the intensity for orientations of the single crystal corresponding to various positions of the volume element in reciprocal lattice space, the specimen mount sketched in Fig. 3 was used. The large semicircular arcs stood in a vertical plane on the table of a spectrometer. The specimen was heated by a heating coil and surrounded by a shield having nickel or beryllium windows. An atmosphere of hydrogen was maintained within the shield to prevent oxidation of the surface of the crystal. Three calibrated rotations are provided; rotation through the Bragg angle θ, rotation about the (1,0,0) crystal axis, perpendicular to the crystal face, through the angle Φ, and a tilting of this axis through an angle χ in a vertical plane.

The function I_D' may be found throughout the whole of a unit cell of the reciprocal lattice by applying symmetry operations to values found for a relatively small portion of the unit cell. Thus, for Cu_3Au, intensity measurements were made, and values of I_D' were calculated only for the region contained in the triangular prism $ABCDEF$ shown in Fig. 4. This prism has one thirty-second of the volume of the whole unit cell, which may be built up from the prism by use of the center of symmetry, G, and planes of symmetry.

From the observed intensities, the values of I_D' were calculated using the relation

$$I_D' = K(I_{\text{Obs}} - I_T - I_C)\left[\frac{(\sin 2\theta)}{(1+\cos^2 2\theta)}\right]\frac{1}{(f_{\text{Au}} - f_{\text{Cu}})^2}\frac{1}{A(\theta)},$$

where I_T and I_C represent the "temperature-diffuse" and Compton scattering contributions to the diffuse background intensity, K is a constant, and $A(\theta)$ is a correction for the absorption in the nickel or beryllium foil surrounding the specimen. Since the experimental conditions were such that the angles made by the incident and reflected beams with the crystal face were equal, no correction for absorption in the specimen was necessary.

The contribution of the Compton scattering was calculated to be approximately one-tenth of the average value of I_D'. The temperature diffuse scattering was evaluated by measuring diffuse background intensities at temperatures of 360°C, which is just below the critical temperature of about 385°C, and room temperature. At 360°C, the diffuse scattering consisted of temperature-diffuse scattering, Compton scattering, and a small amount of scattering due to disorder. For a specimen cooled quickly from 360°C to room temperature, the amounts of Compton and disorder scattering were unchanged, but the temperature-diffuse scattering was decreased. Thus the rate of variation of the temperature-diffuse scattering was obtained, and by extrapolation to absolute zero of temperature, the amount of disorder scattering at 360°C was found. The correction term for temperature-diffuse and Compton scattering, to be subtracted from the observed intensity at any elevated temperature, was then defined as the intensity measured at 360°C, minus the contribution of the disorder scattering at 360°C, plus a term proportional to the difference between the temperature of observation and 360°C.

At each of three temperatures greater than the critical temperature, more than 450 intensity measurements were made for settings of the angles θ, Φ, and χ, corresponding to positions of the measuring volume-element spaced regularly throughout the portion of the reciprocal lattice cell shown in Fig. 4. The value of I_D' was calculated for each position. Values of I_D' were then interpolated on to a cubic net of points spaced at intervals of 0.05 in the coordinates h_1, h_2, h_3, which are so defined that the unit of distance is the distance of the (2,0,0) reflection from the origin of the reciprocal lattice. By use of appropriate symmetry operations, the values of I_D' at the 8000 points of this cubic net within the unit cell were obtained.

The values of the Fourier coefficients α_{lmn} are given

by the integration of the product of I_D' and the appropriate exponential function throughout the unit cell of the reciprocal lattice. In practice, the presence of a center of symmetry allows the exponential functions to be replaced by cosines, and the integration is approximated by a summation of the values of the product at regularly spaced points. Thus,

$$\alpha_{lmn}=K\sum_{h_1}\sum_{h_2}\sum_{h_3} I_D' \cos 2\pi(lh_1+mh_2+nh_3).$$

The summation was carried out over the 4000 points of the cubic net contained in half of the unit cell. The normalizing constant, k, was obtained from the relation,

$$\alpha_{000}=K\sum_{h_1}\sum_{h_2}\sum_{h_3} I_D'.$$

The summation was greatly simplified when one or two of the atom coordinates were zero. Thus

$$\alpha_{l00}=K\sum_{h_1}(\sum_{h_2}\sum_{h_3} I_D') \cos 2\pi lh_1$$

and

$$\alpha_{lm0}=K\sum_{h_1}\sum_{h_2}(\sum_{h_3} I_D') \cos 2\pi(lh_1+mh_2).$$

For the general case, in which no such simplification was possible, a "template" method of performing the multiplication and addition was used. The values of I_D' were tabulated at regularly spaced positions for values of h_2 and h_3 from 0 to 1, for each value of h_1. Templates were made by cutting holes in stiff paper so that, when the templates were placed over the tables of values of I_D', only numbers to be multiplied by given values of the cosine functions were visible.

In some cases the values of the α_{lmn} so obtained did not show symmetry with respect to the three reciprocal lattice aces. Thus, for example, the values obtained for α_{200} and α_{020} were different. Such differences arose from imperfect correction for temperature-diffuse scattering, and were small for carefully determined backgrounds. In order to minimize the errors arising from such asymmetry, the values of the α_{lmn} were obtained for various permutations of the indices, and the weighted average was found.

Experimental Results for Short-Range Order

Intensity measurements were made for Cu_3Au at temperatures of 405, 460, and 550°C. The distribution of scattering power in the reciprocal lattice, calculated from these measurements, showed interesting features. Figure 5 is a contour plot of the scattering power due to short-range order, in arbitrary units, in the (1,0,0) plane of the reciprocal lattice of Cu_3Au at 405°C. The corners of the square are sites of the sharp fundamental reflections. The diffuse maxima at the super-lattice reflection positions appear to be flattened into a disk-like shape. At the center of the square, one of these disks is seen in section by the plane of the disk, and on each side of the square is the section of a disk with its plane perpendicular to the plane of the section. It is seen that the flattened sides of the disks face the nearest fundamental reflections, and each fundamental reflection is surrounded by six such flattened sides.

The disk-like shape of the diffuse maxima seems to be a consequence of the structure of the Cu_3Au lattice, rather than any particular values for the short-range order parameters. Qualitatively, the same shape is given by calculation assuming a wide variety of values for the order parameters for the first two shells, ignoring the effects of further parameters.

The same disk-like shape has been found, on a much smaller scale, for the relatively sharp super-lattice reflections from single crystals of Cu_3Au[9,10] for temperatures below the critical temperature. For this case, the shape of the super-lattice reflections was explained by Wilson[11] in terms of the domain-structure of the ordered alloy.

The short-range order parameters calculated by Fourier analysis of such distributions of scattering-power are given in Table I. The third column of the table gives the coordinates of representative points of the successive shells, referred to half of the length of the face-centered cubic unit cell as unit distance. The values of the order parameters for a perfectly ordered lattice are given in the fourth column. The magnitudes of the short-range order parameters decrease, in general, with increasing temperature and with increasing distance from the origin. At 405°C, the magnitude of the nearest-neighbor order parameter is seen to be almost half that for perfect order. The parameters for the fifth and tenth shells indicate that, with a gold atom at the center, there is an excess of one copper atom among the 24 atoms of the fifth shell, and a defect of half a copper atom among the 24 atoms of the tenth shell. Thus the influence of the atom at the origin is appreciable at greater distances than those which have been considered in previous theoretical and experimental work.

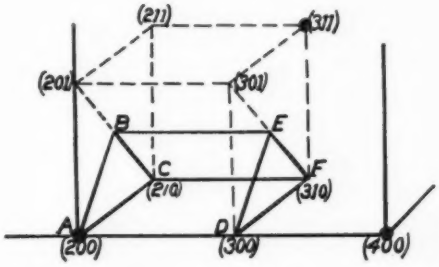

FIG. 4. The prism-shaped portion of reciprocal-lattice space, *ABCDEF*, throughout which the scattering power was determined.

[9] B. Strijk and C. H. MacGillavry, Physica **12**, 129 (1946).
[10] Edmunds, Hinde, and Lipson, Nature **160**, 304 (1947).
[11] A. J. C. Wilson, Proc. Roy. Soc. **A181** (1943), Nature **160**, 305 (1947).

It is difficult to make an accurate estimate of the probable error in the values of the short-range order parameters found. However, it is believed that the error in the parameters for the inner shells does not exceed 0.01. For more distant shells, the absolute error is probably slightly less, and the relative error greater. The principal sources of error are inaccuracies in the correction for temperature-diffuse scattering and in the interpolation of the values of I_D' from a conical-polar to a cubic net of points.

In general, the experimental order parameters given

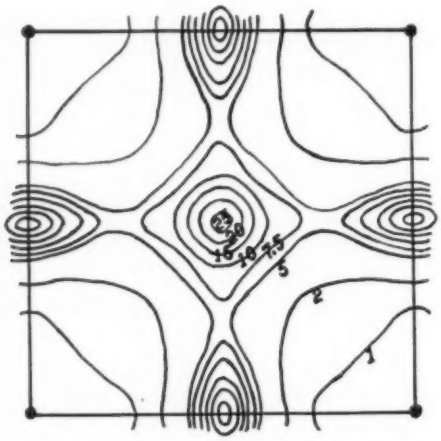

FIG. 5. Contour plot of scattering power due to short-range order in the (1,0,0) plane of the reciprocal lattice of Cu_3Au at 405°C.

in Table I have the same sign as the corresponding parameters for the case of perfect order. However, for some of the parameters for the third, sixth, and ninth shells, the signs are reversed, indicating a defect of copper atoms in a shell surrounding a gold atom instead of an excess, or an excess instead of a defect. The significance of these reversals of sign becomes apparent when the number of copper atoms in excess or defect in each shell is considered as a function of the radius of the shell. In Fig. 6 the number of copper atoms in defect (as compared with the number for a completely random arrangement) for each shell, given by the product $\frac{3}{4}c_i\alpha_i$, is plotted as a vertical line at the abscissa value corresponding to the radius of the shell. This is done for perfect order and for temperatures of 405 and 550°C. For the case of perfect order, alternate shells show an excess and a defect. However, for the elevated temperatures there is a marked tendency for groups of shells to show a common excess or defect, so that the alternation is less rapid. Thus, after the large excess of copper atoms in the first shell about a gold atom, the next three shells have a defect, the next three have a common tendency to show an excess, and so on.

One way of interpreting this behavior is to consider that the predominating force is that tending to surround each atom with unlike neighbors. The first shell surrounding a gold atom is thus copper-rich. All atomic sites which are nearest neighbors to atoms in this first shell will then tend to be gold-rich. The atoms of the second, third, and fourth shells are all nearest neighbors of points in the first shell, and so will show a common defect in copper atoms. Similarly, the atoms of the fifth, sixth, and seventh shells are nearest neighbors of atoms in these three shells, and will tend to be copper-rich, and so on.

Such a variation in density of copper atoms with radial distance from the origin is analagous to the variation in density of the atoms about a given atom in a monatomic liquid. Debye and Menke[12] determined the radial distribution of the density of mercury atoms about a given atom in the liquid by x-ray methods. Their curve has been added in Fig. 6 with the dimensions adjusted so that the first peak coincides with the point representing the excess of copper atoms in the first shell. It is seen that the positive and negative portions of the curve coincide with the regions of copper defect and excess. The curve as drawn would represent the distribution in a liquid of "atoms" consisting of a copper atom plus half of its gold-rich shell of nearest neighbors. The distribution of copper atoms about a gold atom may thus be likened to a "melting" of the ordered structure to give a "liquid-like" arrangement of the atoms on the atomic sites.

This liquid-like dependence of the density of copper atoms on the radial distance is combined with the dependence on the lattice coordinates associated with ordering. The radial dependence becomes more important as the temperature is raised, and seems to predominate at temperatures as high as 550°C.

MEASUREMENT OF LONG-RANGE ORDER IN Cu_3Au

When an x-ray beam is reflected at the face of a single crystal by planes parallel to the face, the integrated intensity of the reflection is given by

$$E=K(N^2F^2/\mu)[(1+\cos^2 2\theta)/(2\sin 2\theta)]\exp(-2M),$$

where N = number of unit cells per unit volume, K = constant for given primary beam conditions, F = structure factor for the given reflection, μ = linear

TABLE I. Experimental values of short-range order parameters for Cu_3Au at temperatures above the critical temperature.

i	c_i	Coords.	Perfect order	405°C	460°C	550°C
1	12	1,1,0	−0.333	−0.152	−0.148	−0.131
2	6	2,0,0	1.00	0.186	0.172	0.105
3	24	2,1,1	−0.333	0.009	0.019	0.026
4	12	2,2,0	1.00	0.095	0.068	0.045
5	24	3,1,0	−0.333	−0.053	−0.049	−0.032
6	8	2,2,2	1.00	0.025	0.007	−0.009
7	48	3,2,1	−0.333	−0.016	−0.008	−0.003
8	6	4,0,0	1.00	0.048	0.042	0.019
9	12	3,3,0	−0.333	−0.026	−0.022	−0.011
	24	4,1,1	−0.333	0.011	0.020	0.007
10	24	4,2,0	1.00	0.026	0.025	0.007

[12] Debye and Menke, Physik. Zeits. **31**, 797 (1930).

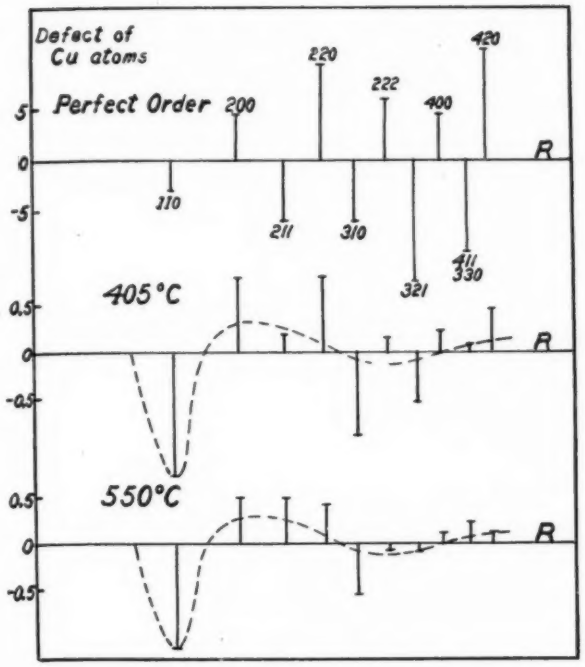

FIG. 6. The number of copper atoms in defect at various radial distances from a gold atom.

absorption coefficient of the crystal, $\exp(-2M)$ = correction factor for thermal vibration of atoms.

For a single crystal of Cu_3Au, with long-range order parameter S, the structure-factor for the super-lattice reflections is given by $F^2=(f_{Au}-f_{Cu})^2\cdot S^2$.

Wilchinsky[2] used the fundamental lines of Cu_3Au as intensity standards in his determination of S from powdered samples. Such a standardization is not possible when a single crystal is used, because the intensities of the strong fundamental reflections are decreased by an unpredictable amount by extinction effects. Hence an intensity standard was used; namely, the (600) reflection from a well-ground rocksalt cube face.

Measurements of the integrated intensities of super-lattice reflections from single crystals of Cu_3Au were made using the same apparatus as for the short-range order measurements outlined above. The entrance slit of the monochromator was narrowed to reduce the divergence of the primary beam to less than half a degree. Thus the volume element of reciprocal-lattice space shown in Fig. 2 was reduced to a thin plate-like element. This plate was swept through the region of a super-lattice reflection by a rotation of the single crystal specimen. The measured intensity was plotted against angle of rotation of the specimen. The area of the resultant peak was then proportional to the integrated intensity of the reflection. Similar measurements on the rocksalt reflection provided the standardization from which the value of S could be calculated. The results of two series of measurements are summarized in Fig. 7 and compared with the predictions of theory.[6]

The experimental results show agreement with the theory in the slow decrease in S and then the sharp fall to zero S at the critical temperature. The drop in S at the critical temperature was observed experimentally to take place within a temperature range of two or three degrees.

For such measurements, the single-crystal specimen was first heated at some temperature below the critical temperature for 70 to 100 hours. It was then found that, on raising or lowering the temperature, the integrated intensity reached a new equilibrium value in one hour or less. When the critical temperature was exceeded, the intensity of the super-lattice reflection became too small to measure within 15 minutes. Once the crystal was disordered, an annealing time of 70 hours or more was required to bring it to an equilibrium ordered state again.

These observations confirm the results and conclusions of Sykes and Evans,[13] who measured the electrical resistance of Cu_3Au as a function of time and temperature. They showed that two processes with very different time-constants could be distinguished; the slow growth of "anti-phase domains," and the much more rapid increase of order within the domains. Starting from a disordered sample, a long annealing time is necessary for the domains to grow large enough so that the presence of the domain boundaries has no appreciable effect on the electrical resistance or the integrated intensity of x-ray reflection. Once this domain size has been attained, an equilibrium state may be obtained rapidly at another temperature by increase or decrease of order within the domains.

A few observations have been made of the changes of integrated intensity, peak intensity, and half-width of super-lattice reflections from an initially disordered specimen heated below the critical temperature. A crystal, previously heated to 410°C to disorder it, was held at 360°C. After 15 minutes the integrated intensity of the reflection was about half of its maximum value, but the width of the reflection was much greater than

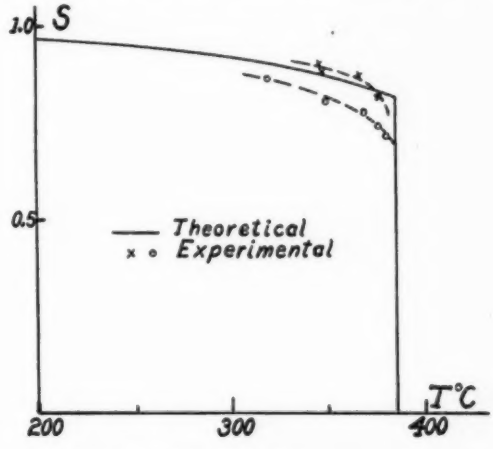

FIG. 7. Experimental values of the long-range order parameter, S, for Cu_3Au, compared with a theoretical curve.

[13] C. Sykes and H. Evans, J. Inst. Metals **58**, 255 (1936).

for long annealing times. With further heating, the integrated intensity of the reflection increased more and more slowly. The rapid initial increase in intensity presumably corresponded to the propagation of order in the lattice outward from a number of nuclei until the domains so formed either coalesced or formed inter-domain boundaries. From a more detailed study of the shape and size of the super-lattice reflections at the end of this initial stage of growth, it should be possible to deduce the shape and size of the initially formed domains, and hence the directions of growth from the nuclei, and the number of nuclei.

The author wishes to express his indebtedness to Professor B. E. Warren, who suggested this research and provided valuable discussion and advice during the course of the work.

Integrating Crystal Detectors for High Energy Photons and Particles*,**

R. S. Alger
Laboratory for Insulation Research, Massachusetts Institute of Technology, Cambridge, Massachusetts
(Received July 18, 1949)

Three of the alkali halides, LiF, KBr, and NaCl were examined as integrating detectors for high energy photons and particles. Dosage measurements were based on the number of color centers formed in single crystals under x- and cathode-ray bombardment. Exposures of 20 to 10^4r (30-kv x-rays) were measured photoelectrically and 10^6 to 10^7r (3 Mev x- and cathode rays) were measured optically. The crystals have advantages in measurements where wide range, high absorption, small size, and simplicity are desirable; however, their use is restricted by the length of the bleaching period required between exposures.

INTRODUCTION

CERTAIN of the effects produced in the alkali halides under high energy particle or photon bombardment, namely, color center formation and photoconductivity, suggest the possibility of a simple type of integrating detector which uses these materials. Quantitative measurements can be made, either of the optical absorption or the photoelectric currents, and the high absorption coefficients of the heavier crystals such as KBr would permit the detection of high energy particles with a relatively small volume of crystal. Consequently, three of the alkali halides, LiF, NaCl, and KBr were examined as to their characteristics as integrating detectors for x- and cathode rays up to energies of 3 Mev. Although, in this study, the emphasis was placed on experiments clarifying the usefulness of the crystals as detectors, data were obtained on the trapping and migration of electrons which, when further expanded, promise to give new information of general interest.

COLOR CENTERS IN THE ALKALI HALIDES

The following known facts concern the problem at hand. When the crystals are exposed to high energy photons or particles, they become colored by the F-absorption bands, which appear in the visible or ultraviolet region of the spectrum.[1] The F-centers responsible for this absorption seem to be electrons trapped at halogen ion vacancies;[2] such vacancies are always present in the alkali halides as Schottky defects.[3]

When x-ray photons transfer energy to the crystal, either by photoelectric absorption, Compton absorption, or pair production, primary electrons of high energy are released which dissipate their energy in secondary ionization processes, thus creating a number of conducting electrons and neutral halogen atoms. The electrons move through the crystal until they recombine with neutral halogen atoms or are trapped by negative ion vacancies to form F-centers. When crystals are bombarded with electrons, the final result is the same as with x-rays. Cathode and beta-rays may be stopped in the crystal and trapped as additional F-centers, but this contribution is negligible because of the space charge formed.

The F-center density can be calculated from the bell-shaped optical absorption band by an expression derived by Smakula.[4] Seitz[5] has simplified Smakula's equation, for the case where the half-band width is small compared to the frequency of the absorption maximum, to the form

$$N_0 f = 1.31\times 10^{17} K W \frac{n_0'}{(n_0'^2+2)^2} \qquad (1)$$

where N_0 = number of F-centers per cc, f = oscillator strength of the absorbing center, K = maximum optical absorption coefficient in cm^{-1}, n_0' = refractive index at K, W = interval from K to $K/2$ in e.v. If an oscillator strength of 0.7 is used for NaCl at room temperature, Eq. (1) reduces to

$$N_0 = CK. \qquad (2)$$

Values of the constant C listed by Hilsch and Pohl[6] for

* Sponsored by the ONR, the Army Signal Corps, and the Air Force under ONR Contract N5ori-07801.
** From a Master's Thesis in Electrical Engineering, M.I.T.
[1] R. W. Pohl, Proc. Phys. Soc. London **49**, E3 (1937).
[2] J. H. DeBoer, Rec. Trav. Chim. Pays-Bas **56**, 301 (1937).
[3] C. Wagner and W. Schottky, Zeits. f. physik. Chemie (B) **11**, 163 (1930).
[4] A. Smakula, Zeits. f. Physik **59**, 603 (1930).
[5] F. Seitz, *The Modern Theory of Solids* (McGraw-Hill Book Company, Inc., New York, 1940) p. 664.
[6] R. Hilsch and R. Pohl, Zeits. f. Physik **64**, 606 (1930).

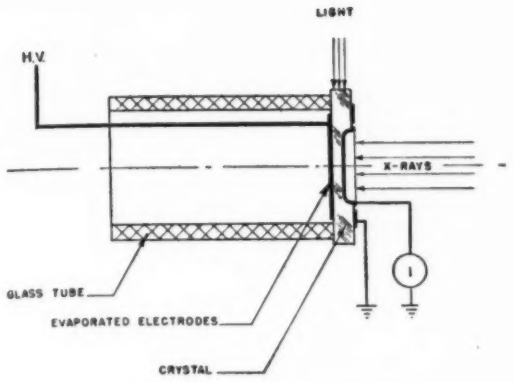

FIG. 1. Photoelectric dosimeter.

NaCl and KBr at room temperature are 3.6×10^{15} and 4.45×10^{15} respectively.

In addition to the principal absorption bands, for which the F-centers are responsible, a number of subsidiary bands have been observed at longer wavelengths, e.g., the F'-, R_1-, R_2-, and M-bands. Molnar[7] has measured the F-bands and the subsidiary bands for the majority of the common alkali halides.

When crystals colored with x-rays are heated or illuminated with light in the F-band, the whole F-band bleaches out uniformly; simultaneously some of the subsidiary bands may appear and a photo-current will be observed in case an external field is applied. Pohl and his co-workers,[1] who investigated the photoelectric processes extensively, found that one F-center was destroyed for every quantum of light absorbed. The conducting electrons move through the crystal until they are trapped by a vacancy or recombine with a halogen atom. The drift distance in the field direction depends on the strength of the electric field and the number of traps present. Pohl and his co-workers[1] designated the current due to photo-electrons as the "primary photoelectric current" whereas other currents resulting from the primary current flow were called "secondary photo-currents." These secondary effects occurred only above room temperature and were not observed in the experiments reported here. Since the electron drift distance is proportional to the field strength, the photo-current can be enhanced by the use of very strong electric fields. With photo-currents of the order of 10^{-10} amp., von Hippel[8] observed a photo-current saturation in thin KCl crystals beginning at a field strength of about 0.6 million volt/cm. Under more intense illumination thicker crystals break down electrically before a saturated photo-current can be obtained. At the saturation point the electron drift distance becomes equal to the thickness of the crystal, and all the electrons released in the crystal are swept to the anode.

When a very weak source of illumination was used for short intervals of time, in which case the charge released was of the order of 10^{-12} coulomb, Pohl[1] found the primary photo-current remained nearly constant with time and had a magnitude proportional to the light intensity. When larger amounts of charge, e.g., 10^{-9} coulomb, are released, a space charge builds up in the crystal, which may nullify the external field, and no further photo-current is obtained. Because the range of the electrons is altered due to the field distortion, not all the photo-electrons contribute equally to the photo-current in this space charge region. Thus it becomes difficult to determine the F-center density from photo-electric measurements at high light intensities.

EXPERIMENTAL PROCEDURE

Crystal Preparation and Crystal Holders

For our photoelectric measurements NaCl and KBr crystals† were split to a size of $\frac{1}{2}\times\frac{1}{2}\times\frac{1}{16}$ in. and hollowed on one side to keep the electric field low at the edge of the electrode. The cavities were produced with an automatic wet cloth lap. Gold electrodes were evaporated onto the polished crystals after they had been heated to 350°C in vacuum to expel surface moisture. Figure 1 gives a schematic view of a finished crystal mounted for photoelectric measurements. The glass tube, cemented to the crystal with polybutyl methacrylate, supports the sample and prevents surface flashover. X-rays are admitted through the concave electrode and the light is focused on the edge of the crystal.

LiF, NaCl, and KBr samples, $1\times1\times0.1$ in. and $1\times1\times0.01$ in., were prepared with optical surfaces for the F-band absorption measurements.

Exposure Methods

Two radiation sources were used; a Machlett x-ray diffraction tube at 30 to 45 kv with a copper target and a 1 mil thick nickel filter, and a 3-million volt source for x- and cathode rays (van de Graaff generator).

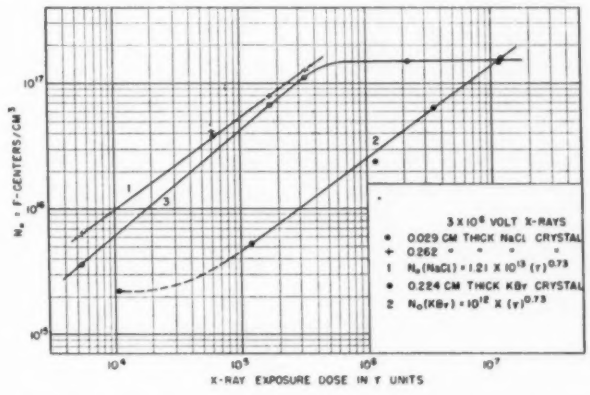
N_a = F-CENTERS/CM^3
X-RAY EXPOSURE DOSE IN r UNITS
3 X 10^6 VOLT X-RAYS
0.029 CM THICK NaCl CRYSTAL
0.262 " " " "
1 N_a(NaCl) = 1.21 X 10^{15} (r)$^{0.73}$
0.224 CM THICK KBr CRYSTAL
2 N_a(KBr) = 10^{12} X (r)$^{0.73}$

FIG. 2. F-center concentration as function of x-ray exposure.

[7] J. P. Molnar, thesis, Physics Department, M.I.T. (October, 1940).

[8] A. von, Hippel Phys. Rev. **54**, 1096 (1938).

† Harshaw Chemical Company, Cleveland, Ohio.

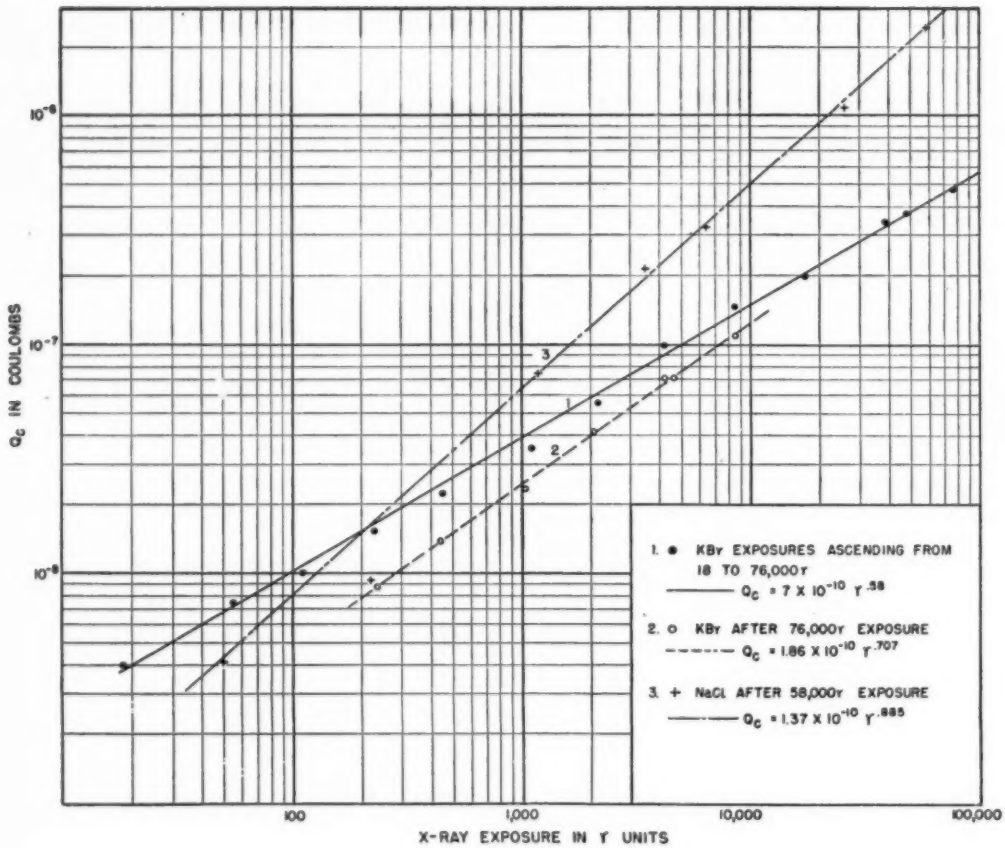

FIG. 3. Charge bleached from crystals as function of x-ray exposure.

All x-ray exposures were measured in roentgens (r units) with air ionization chambers. The chamber used with the diffraction tube was copied, with some change of dimensions, from a design of Taylor and Stoneburner.[9] Exposures to 3-million volt x-rays were measured with a roentgen meter built into the van de Graaff generator. While the relative values measured with this meter are accurate to better than 5 percent, the actual calibration in roentgens may be in error by a factor of 2. Cathode-ray exposures were measured in joules and converted to roentgen-equivalent-physical (rep) units in air for comparison with the x-ray doses. (1r$\simeq$83.8 ergs/g of air at standard conditions and 1 rep=83.0 ergs/g of material.) Due to the simplifying assumption of a uniform ionization intensity and the unknown distribution of cathode rays over the target plate, the accuracy of the rep values is probably less than that of the r.

Since the production of F-centers depends on ionization, the F-center concentration will vary throughout the crystal according to the ionization intensity. For the 30 to 45-kv x-rays the ionization is most intense at the incident surface and decreases rapidly in accordance with the large coefficient of absorption for the crystals. At 30 kv and exposures up to 10^4 r, the visible coloring extended less than 1 mm into the KBr crystals. Photoelectrons resulting from the absorption of 3-Mev photons have an appreciable velocity in the direction of the x-ray beam; therefore, the peak ionization intensity occurs beyond the incident surface and may well be at the exit surface of a thin crystal. Consequently a given x-ray exposure below the saturation value might produce a smaller average F-center concentration in a thin crystal than in a slightly thicker one because the latter contains more of the peak ionization.

Photoelectric and Absorption Measurements

The coloration produced in the crystals by exposure to an x-ray dose of from 20 to 10^4 roentgens was measured photoelectrically by the charge Q_c traversing the crystal under strong illumination. After the crystal had been colored (Fig. 1), an electric field of about 10^5 volts/cm was applied, the crystal illuminated and the photo-current recorded as function of time. The space charge formed during the measurement of Q_c cuts off the photo-current before all of the F-centers are removed; the remaining centers can be bleached by illuminating the crystal until no photo-current is obtained with either polarity of the external field.

The coloration of crystals given larger exposures (10^4 to 10^7 r or rep, of 3-million volt rays) can be measured optically. Values of the maximum absorption co-

[9] L. S. Taylor and C. F. Stoneburner, Bur. Stand. J. Research **9**, 769 (1932).

efficient K, from which N_0 is obtained by Eq. (2), were measured with a Model 12M Cary recording spectrophotometer. The minimum measurable transmission was about 0.03 percent, and no F-center bleaching due to the scanning beam could be detected. Absorption measurements covered the region from 3400 to 7200A in KBr and NaCl, and from 2100 to 3400A in LiF. Desiccated holders protected optical surfaces of the hygroscopic crystals from atmospheric moisture.

The KBr and NaCl crystals were bleached with white light between experiments, while a 4-watt germicidal lamp, which has its major intensity concentrated in the 2537-Hg line, was used to bleach LiF. A residual absorption was bleached out by heat.

Parameters influencing both N_0 and Q_c are: besides the crystal material and prehistory, the energy and intensity of the radiation, the temperature and time of storage, the voltage and crystal thickness used. The effects of each of these variables were examined in turn.

RESULTS

Effect of Exposure

The relation between the F-center concentration N_0 in KBr and NaCl and the x-ray exposure in roentgens over the range from 10^4 to 10^7 r is shown in Fig. 2. N_0 increases with exposure until an equilibrium condition is reached (curve 3), where a saturation value of 1.5×10^{17} F-centers per cc was obtained for NaCl. This saturation can be measured only in thin crystals; in thicker crystals (curves 1 and 2) practically all the light is already absorbed at lower concentrations, and the sensitivity range of the spectrophotometer is exceeded. Over the straight line portion of the log-log curves 2 and 3 the F-center concentration fits the empirical relation

$$N_0 = C_1 r^{0.73}, \tag{3}$$

where $C_1 = 1.0 \times 10^{12}$ for KBr and 1.2×10^{13} for NaCl. Since the F-band was barely detectable in KBr at $r = 10^4$, this point may be considerably in error.

Typical photoelectric measurements of Q_c for 30-kv x-rays and exposures ranging from 20 to 10^4 r are given for KBr and NaCl in Fig. 3. The empirical equations obtained between Q_c and the x-ray exposure in roentgens are similar to Eq. (3).

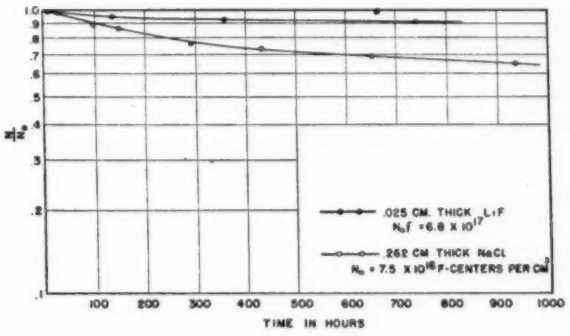

FIG. 5. F-center decay at 21°C due to thermal release.

For KBr (curve 1) $Q_c = 7 \times 10^{-10}\ r^{0.58}$, KBr (curve 2) $Q_c = 1.86 \times 10^{-10}\ r^{0.707}$, NaCl (curve 3) $Q_c = 1.37 \times 10^{-10}\ r^{0.885}$.

It becomes apparent from curves 1 and 2 that a preceding exposure can affect the characteristics obtained in later measurements (see later section on Polarization).

Influence of Crystal Type and Thickness

The crystal material has a pronounced effect on the F-center density N_0 and charge Q_c obtained for a given x-ray exposure (Figs. 2 and 3). When the crystals are exposed to x-rays, the F-center formation rate (i.e., N_0/roentgen) diminishes in the order LiF→NaCl→KBr. Comparing LiF with NaCl for an exposure of 10^7 rep, the ratio $N_0 f_{(\mathrm{LiF})}/N_0 f_{(\mathrm{NaCl})} = 4.6$ was found (see Eq. (1)). A 1 mil thick crystal of LiF became practically opaque under a 3-million volt x-ray bombardment before the F-band of a similarly treated KBr crystal was readily detectable. In Fig. 2 the F-center density $N_{0(\mathrm{NaCl})}$ is seen to be greater than $10 N_{0(\mathrm{KBr})}$ for identical x-ray exposures below the saturation value.

Since the optical measurements show more F-centers formed in NaCl than KBr, it would be expected that for crystals of the same thickness and subjected to the same electric field, a larger charge Q_c would be obtained for NaCl. A comparison of the curves in Fig. 3 shows that this is the case; $Q_{c(\mathrm{NaCl})}/Q_{c(\mathrm{KBr})}$ varied from about 2 to 4. Selection of the proper crystal material provides some control over sensitivity and usable range of these integrating detectors.

N_0 is slightly higher in a thicker crystal for a given exposure of 3-Mev x-rays (Fig. 2), which agrees with

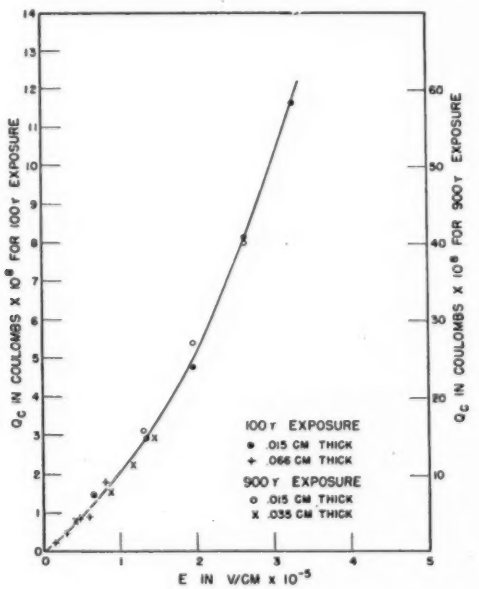

FIG. 4. Effect of applied field on charge bleached from KBr crystals.

the result predicted by the distribution of the ionization intensity. This variation should affect N_0 only before the crystal becomes saturated. Figure 4 shows Q_e as a function of the applied field strength for 3-crystal thicknesses. No definite thickness effect is apparent over the limited region covered.

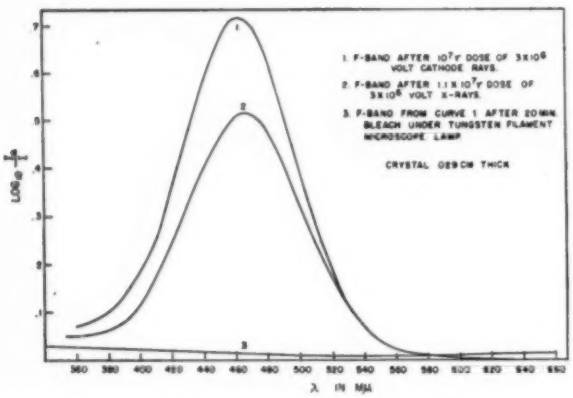
1. F-BAND AFTER 10⁷r DOSE OF 3X10⁶ VOLT CATHODE RAYS.
2. F-BAND AFTER 1.1 X 10⁷r DOSE OF 3X10⁶ VOLT X-RAYS.
3. F-BAND FROM CURVE 1 AFTER 20 MIN. BLEACH UNDER TUNGSTEN FILAMENT MICROSCOPE LAMP
CRYSTAL 0.63CM THICK
λ IN MμA

FIG. 6. Bleaching of F-centers in NaCl.

Thermal Bleaching

In alkali halide crystals colored by x-rays, some thermal bleaching occurs at room temperature. The bleaching rate may be very slow, e.g., Joffé observed some color centers remaining in an x-ray colored NaCl crystal after it had been stored in the dark for about 20 years.[10] The heavier crystals, with their lower activation energy, bleach more rapidly than the crystals composed of the lighter elements. Since the thermal bleaching would produce an error in dosimeter readings, a series of measurements were made on colored NaCl, LiF, and KBr crystals to determine the bleaching rate. The results for NaCl colored by 3-million volt x-rays, and LiF colored by 3-million volt cathode rays are given in Fig. 5 which shows N/N_0 plotted as a function of time. (N = the F-center concentration at any time t and N_0 = the initial concentration.) The decay curves are not simply exponential, but a half-life of about 0.87 year fits the LiF characteristic quite well.

A consideration of the mechanism of decay indicates that a more complicated expression would be required to describe completely the decrease in the F-center density as a function of time. When the electron is thermally released from an F-center, it has the possibility of being captured by a neutral halogen atom or another halogen lattice vacancy. Each time an electron is captured by a neutral halogen atom the number of neutral halogen traps is decreased by one, and at the same time the ionized F-center increases the number of lattice vacancies by one. Consequently, as bleaching continues, the ratio of halogen vacancies to halogen neutral atoms increases, and the probability that the thermally released electron will be captured by a lattice vacancy to reform an F-center also increases. Therefore the F-center density decreases more rapidly the higher the coloration. Thus the thermal bleaching produces a larger error in the optical measurements where high F-center densities are employed than in the photoelectric measurements. In the case of photoelectric measurements with KBr, the time between x-ray exposure and the photoelectric measurement was allowed to vary from a few seconds up to 20 hr. at room temperature, and no decrease in the charge Q_e was observed. However, a slight decrease in the optical density of the F-band in highly colored KBr and NaCl can be detected after several hours.

Optical Bleaching

If the crystals are to be used more than once, the remaining color centers must be removed and the space charge redistributed between measurements. The required bleaching period depends on the F-center density, bleaching light intensity, and the crystal material. For example, 5 minutes of illumination were sufficient to bleach a KBr crystal exposed to a 100-r dose, while an NaCl crystal given the same dose required 30 minutes of illumination.

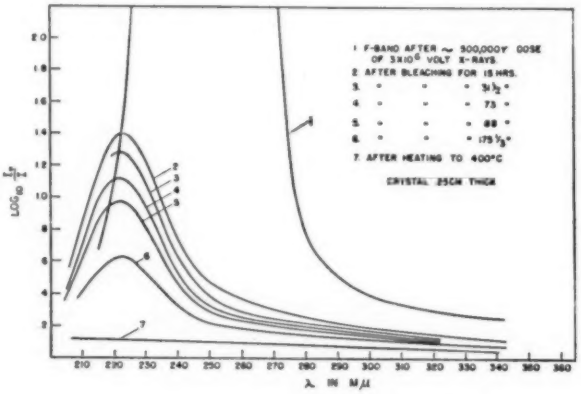
1. F-BAND AFTER ~ 500,000r DOSE OF 3X10⁶ VOLT X-RAYS.
2. AFTER BLEACHING FOR 15 HRS.
3. " " " 31½ "
4. " " " 73 "
5. " " " 88 "
6. " " " 175⅓"
7. AFTER HEATING TO 400°C
CRYSTAL 25CM THICK
λ IN Mμ

FIG. 7. Bleaching of F-band in LiF.

The optical measurements show the results of photo- and thermal bleaching more directly. Curve 3 of Fig. 6 gives the result of 30-minutes' bleaching with white light of the F-band absorption (curve 1) in an NaCl crystal exposed to approximately 10^7 rep. The F-band has been completely bleached, and no R- or M-bands are present; however, the absorption through the entire spectrum has increased from 0.015 to 0.02 density units.

The bleaching of LiF produced an effect not encountered thus far in the other crystals. An LiF crystal with an F-band absorption well above the upper limit of measurement (Fig. 7, curve 1) was exposed to the light from a 4-watt germicidal lamp for 175 hours. After the first 15 hr., the F-band was almost completely bleached except for a small peak centered at 2230A (curve 2). With continued bleaching the subsidiary

[10] A. F. Joffé, *The Physics of Crystals* (McGraw-Hill Book Company, Inc., New York, 1928) p. 128.

peak decayed symmetrically as shown in curves 2 to 6. Normally, illumination with any frequency in the F-band causes the whole band to decay symmetrically with the possibility of the F'-, R-, and M-bands appearing at longer wave-lengths. The auxiliary band at 2230A is singularly different from the usually subsidiary bands since it is on the short wave-length side of the F-band. When the crystal was heated to 400°C and allowed to cool, the F-band and the subsidiary peak were eliminated (curve 7). Once more, the final curve (7) exhibits some neutral absorption over the entire spectrum investigated; it may be due to surface deterioration.

Effect of Vacancies on Performance

Since the number of vacancies is dependent on the crystal temperature, the vacancy concentration can be increased by heating the crystals almost to the melting point and cooling them rapidly to room temperature. The number of vacancies frozen into the crystals quenched in this way will correspond to some intermediate temperature. Many of the vacancies appear to be paired up, i.e., halogen and alkali vacancies are attached to each other. A method for determining the number of paired vacancies from low frequency dispersion measurements has been described by Breckenridge.[11]

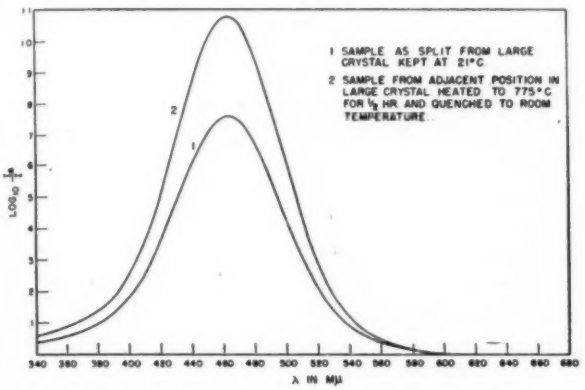
1 SAMPLE AS SPLIT FROM LARGE CRYSTAL KEPT AT 21°C
2 SAMPLE FROM ADJACENT POSITION IN LARGE CRYSTAL HEATED TO 775°C FOR ½ HR. AND QUENCHED TO ROOM TEMPERATURE.
λ IN Mμ

FIG. 8. Effect of vacancies on F-band in NaCl crystals.

If the dielectric loss ($\tan\delta$) is measured at a constant frequency of about 10^4 cycles/sec. over a range of temperatures, the alkali halide crystals containing sufficient vacancies exhibit a peak in the $\tan\delta$-curve at a temperature characteristic of the crystal. The number of paired vacancies can be determined from the height of the $\tan\delta$-peak by the following equation:[11]

$$n=\tan\delta_{\max}\frac{(18\epsilon_0 k)T\kappa_\infty'}{(Zea)^2(\kappa_\infty'+2)^2}, \qquad (4)$$

where $\epsilon_0=8.856\times10^{-12}$ farad/meter, $e=1.59\times10^{-19}$ coulomb, $k=1.38\times10^{-23}$ joule/degree centigrade, $\kappa_\infty'\simeq\kappa'=5.9$ for NaCl. By measuring $\tan\delta$ as a function of temperature before and after a crystal has been heat-treated, the number of paired vacancies produced by the heat treatment can be determined from the above relation. Crystals of LiF, KBr, and NaCl, which had been heated to increase the number of vacancies present, were compared with unheated crystals by measuring both the number of paired vacancies and F-centers formed in the crystals with a given dose of x-rays. Since electrodes were required for the dispersion measurements, two sets of crystals were used, one for the electrical and one for the optical measurements. The crystals to be compared were split from adjacent positions in the original crystal. NaCl was kept at 775°C for 30 minutes, KBr at 710°C for 30 minutes, and LiF at 825°C for 60 minutes and all were quenched to room temperature. This heat treatment produced only a slight hump in the $\tan\delta$-curves for KBr and LiF, and a more pronounced jump in NaCl, which, according to Eq. (4) corresponded to $n=1.5\times10^{15}$ vacancy pairs/cm.[3]

A 250,000-r dose of 3-million volt x-rays produced a stronger coloration in the heated samples; the effect was larger in NaCl than in either LiF or KBr as was to be expected from the $\tan\delta$-characteristics. Figure 8 shows the result for NaCl. The values found for the F-center densities per cc were:

$$\left.\begin{aligned} N_{0_1}&=5.8\times10^{16}\text{ for the heated samples}\\ N_{0_2}&=4.1\times10^{16}\\ \Delta N_0&=1.7\times10^{16}\end{aligned}\right\}\text{ for the unheated samples.}$$

The value of N_{0_1} is a factor of 40 higher than the number n of paired holes obtained from the dispersion measurements (see Eq. (4)), although the F-center concentration is less than half the saturation concentration shown in Fig. 5. If, as Seitz suggests,[12] the vacancies are completely paired after the crystal stands for a few days at room temperature, the maximum number of F-centers should not exceed the number of

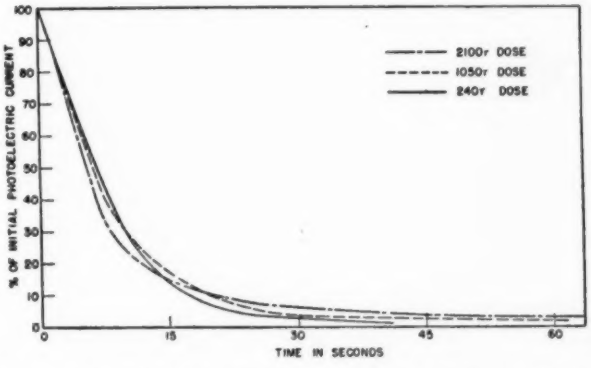

FIG. 9. Reduction in photo-current in KBr due to polarization.

[11] R. G. Breckenridge, Technical Report XI, Lab. Ins. Res., M.I.T. (April, 1948).

[12] F. Seitz, Rev. Mod. Phys. 18, 384 (1946).

paired vacancies if no new vacancies are created by the x-ray bombardment. The ratio of $n/N_0=0.025$ obtained in this experiment would indicate that only a small percent of the vacancies were paired.

The rate of F-center formation was increased in the crystals containing the larger concentration of vacancies. Consequently, crystals containing the largest possible number of vacancies might make the most sensitive detectors, but the effect is not very large.

Polarization

In photoelectric measurements, the space charge formed has a pronounced effect on the value of Q_e observed. When the crystal is illuminated in a strong electric field the electrons released from the F-centers will move toward the anode. Some electrons will be removed from the crystal while others are retrapped to form new F-centers or trapped by neutral halogen atoms to form ions. A positive space charge, presumably of neutral halogen atoms, develops in the vicinity of the cathode, and reduces the primary photo-current essentially to zero as the applied field is nullified. This behavior is illustrated by the curves of photo-current *vs.* illumination time in Fig. 9. Some of the reduction in primary photo-current is due to the loss of charge carriers to halogen neutral traps; however, the reduction in current shown in Fig. 9 is primarily related to space charge.

Increasing the F-center concentration results in a greater space charge density and consequently a steeper potential gradient at the cathode. When the gradient becomes sufficiently steep, electrons can enter the crystal and a semicontinuous photo-current is observed. After the electrons have entered the crystal they are indistinguishable from the electrons released from F-centers. Gradually the competing neutral halogen traps reduce the F-center concentration thereby preventing continuous photo-conductivity. In KBr crystals exposed to 10^7 rep of 3 million-volt cathode rays the total photo-current may drop by a factor of 3 during half an hour with the rate diminishing with time as the ratio of halogen vacancies to halogen neutral atoms increases. At high F-center concentrations Q_e is dominated by the rate of trapping by halogen neutral atoms, while at low F-center concentrations, the polarization predominates. With the equipment used in these experiments a practical upper limit of about 50,000 r for KBr was dictated by the bleaching time required to reduce the total current to zero. Bleaching the crystal with light does not restore the crystal completely to the initial condition of electrical neutrality. After the initial exposure r_1, with subsequent bleach and polarization, a series of reproducible values of Q_e can be obtained for exposures less than r_1. However, with $r_n > r_1$, a change occurs in the charge distribution when Q_{e_n} is measured and a pronounced decrease in Q_e is observed for all future exposures less than r_1. This effect is illustrated in Fig. 3. Curve 1 was obtained for exposures progressing from 18 to 78,000 r. After the 78,000-r exposure, smaller exposures fall along curve 2. The same effect was observed with NaCl before curve 3 was obtained. The polarization effects are being studied in more detail.

CONCLUSIONS

The results obtained demonstrate that the color centers in the alkali halides can be used to measure radiation or particle exposures. However, there are a number of restrictions which limit the usefulness of crystal dosimeters.

The main advantages of the crystal dosimeters are: small size, high absorption, wide range, and simplicity of the detecting element. Although the smallest crystals used in the experiments were $\frac{1}{2}\times\frac{1}{2}\times\frac{1}{16}$ in. in size, smaller crystals could be used if desired. When compared to gas-filled detectors such as ionization chambers, the higher absorption coefficient of the crystals is an advantage, especially when high energy radiations are being detected. Exposures of 20 to 10^7 r measured with KBr crystals illustrate the wide range possible. The crystal material offers some choice in the range and sensitivity that can be obtained. Based on the optical measurements, the crystals listed in descending order of sensitivity are: LiF, NaCl, and KBr.

The bleaching period required to eliminate the F-centers between successive measurements is a major limitation of the speed with which measurements can be repeated.

The polarization effects complicate the photoelectric measurements and make frequent calibrations necessary; consequently the optical method is more attractive for exposures above 10^5 r.

The vacancy concentration has only a slight effect on the F-center formation rate, and thermal bleaching at room temperature can be neglected except in the case of large F-center concentrations or long storage periods.

The author is indebted to Professor A. von Hippel under whose supervision this work was carried out, to Professor G. J. Trump for the use of the 3-million volt generator, to K. A. Wright who operated the generator and to M. A. Gilleo for assistance with the optical measurements.

Thermionic Emission from Oxide Cathodes: Retarding and Accelerating Fields*,†

C. S. HUNG‡
Massachusetts Institute of Technology, Cambridge, Massachusetts
(Received August 3, 1949)

An experimental investigation of the thermionic emission from oxide-coated cathodes is presented in which the applied voltage range extends from the retarding potential region through zero field and up to an average accelerating field of 50,000 volts per cm. The retarding potential range yields information concerning the energy distribution of the electrons emitted, and indicates an excellent agreement between theory and experiment for high retarding fields. Near zero field, cathode inhomogeneity or patch effect may be responsible for the deviations found. Consideration is given to the influence of a possible reflection effect, but theoretical calculation indicates that with the large area cathode used, the simultaneous reflection at the emitter and the collector surfaces so alter the observed current voltage relationship, that the existence or non-existence of a reflection effect cannot be determined by the experiment. Results shown in the accelerating field region up to 50,000 volts per cm are accounted for on the bases of two assumptions which are (1) patch effect for small accelerating fields and (2), the intensification of the field at sharp points expected in view of the inherent roughness of the cathodes studied. The deviation of the experimental results from those predicted by the Schottky mirror image theory is explained over the whole range of observation by these two assumptions.

INTRODUCTION

THE object of this work is to study two of the properties of the surface potential barrier of an oxide cathode. The first is the reflection effect on electrons crossing this barrier, and the second is the lowering of this barrier height in the presence of an external electric field. The surface potential barrier of a uniform thermionic emitter is usually assumed, for distances large compared to the lattice constant, to be due to the mirror image force alone. The quantum-mechanical reflection coefficient for an image force barrier, according to Frank and Young,[1] is only six percent for the low energy electrons and is a slowly varying function of the electron energy in the direction normal to the cathode surface. One way of determining the reflection coefficient experimentally is to measure the electron current to the anode as a function of the retarding potential of the anode relative to the cathode. The thermal equilibrium energy distribution of electrons in the emitter, with energies above the height of this barrier, is known to be Maxwellian since the height of the barrier from the μ-level is always large compared to kT at all operating temperatures of the cathode. This retarding field current, for cylindrical electrodes and assuming zero reflection coefficient is, as given by Schottky:[2]

$$J_v = J_0[2/(\pi)^{\frac{1}{2}}]\left\{e^{-n}\int_0^{(\lambda n)^{\frac{1}{2}}} \exp(-\theta^2 x^2)dx + \int_{(\lambda n)^{\frac{1}{2}}}^{\infty} \exp(-x^2)dx\right\}, \quad (1)$$

where J_v, and J_0 denote the currents per unit length of the cathode when the retarding potentials are V and zero respectively. And $n=eV/kT$, $\theta=r/R$, $\lambda=R^2/(R^2-r^2)$, where r, R denote the radii of the cathode and the anode respectively. The J_v/J_0 *vs.* V/T curves are independent of T under the conditions of this equation. Using this retarding potential method, Nottingham[3] found that for pure tungsten and thoriated tungsten of all degrees of coverage at the same temperature, the plots of $\log(i_v/i_0)$ against V/T all coincide, but the plots for different temperatures differ from each other and from the theoretical curve assuming no reflection

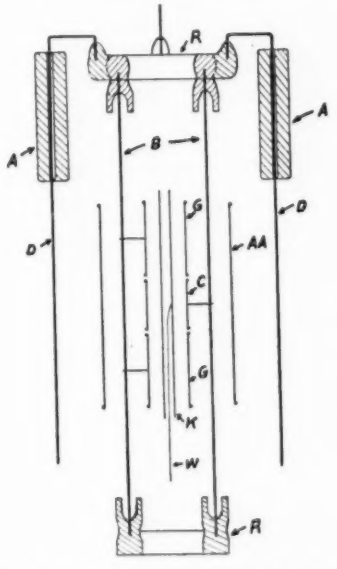

FIG. 1. The sliding anode structure. Fixed elements: K—cathode, 0.2 cm in diameter and 4.5 cm long; AA—auxiliary anode, 2.5 cm in diameter; W—0.002-in. tungsten wire as one element of the thermocouple; A—glass sleeves for guiding the motion of the sliding structure. Sliding structure includes: G—guard rings, 0.8 cm in diameter; C—collector, 0.8 cm in diameter; R—glass rings as insulation and support; B—6 tungsten rods sealed in R for supporting the guard rings and the collector; D—tungsten rods sealed in R, sliding in A. The sliding structure is in the normal position for emission measurements.

* From a thesis paper submitted to the Department of Physics, M.I.T., in partial fulfillment of the requirements for the degree of Doctor of Science.

† This work was done with the support extended to the M.I.T., Research Laboratory of Electronics, jointly by the Army Signal Corps, the Navy Department (ONR), and the Air Force (Air Material Command).

‡ Now at the Department of Physics, Purdue University.

[1] N. H. Frank and L. A. Young, Phys. Rev. **38**, 80 (1931).

[2] W. Schottky, Ann. d. Physik **44**, 1011 (1914).

[3] W. B. Nottingham, Phys. Rev. **49**, 78 (1936).

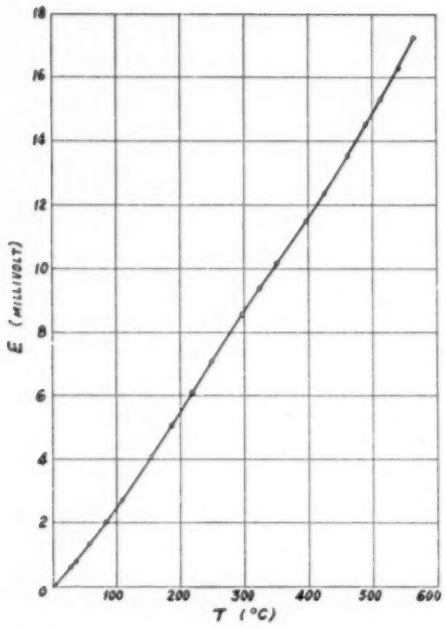

FIG. 2. Calibration curve of tungsten-nickel thermocouple. T is temperature of hot junction above that of cold junction (at 25°C).

as given by Eq. (1). A reflection coefficient of the form

$$R(p_z)=\exp(-p_z^2/2m\omega) \tag{2}$$

was proposed, where p_z denotes the momentum normal to the cathode surface that the electrons would have with zero applied field at distances beyond the range of mirror image forces. With the constant $k/\omega=4.5\times10^{-4}$ (deg.)$^{-1}$, all his data could be explained. This result was interpreted to mean that this reflection coefficient is probably related to the image field and not the surface patches, and therefore a reflection effect of at least this amount should exist at the surfaces of all electrodes including the anodes and the oxide cathode. Experiments on oxide cathodes by Heinze and Hass,[4] Fan,[5] and Brown,[6] have shown agreement with Eq. (1) for high retarding potentials. Deviations at low retarding potentials were reported and demand further study.

The lowering of the image force barrier in an external field is, according to Schottky,[2]

$$\Delta\phi=(eE)^{\frac{1}{2}} \tag{3}$$

and the anode current in an accelerating field is

$$J_v=J_0\exp[(eE)^{\frac{1}{2}}\cdot e/kT] \tag{4}$$

where E is the accelerating field at the cathode surface. Equation (4) is exact in the case of parallel plane electrodes and is also valid in the case of cylindrical electrodes except at very low anode voltages. Investigations on tungsten and thoriated tungsten cathodes by Nottingham[3] have shown agreement with Eq. (4) except for deviations at low accelerating potentials which have been explained satisfactorily by the patch theory. Measurements on oxide cathodes by Fan,[5] Mahlman,[7] Sproull,[8] and others have shown that the slopes of the Schottky plots, $\log(J_v/J_0)$ *vs.* $(E)^{\frac{1}{2}}/T$, in accelerating fields up to 10,000 volt/cm are 2 to 6 times higher than

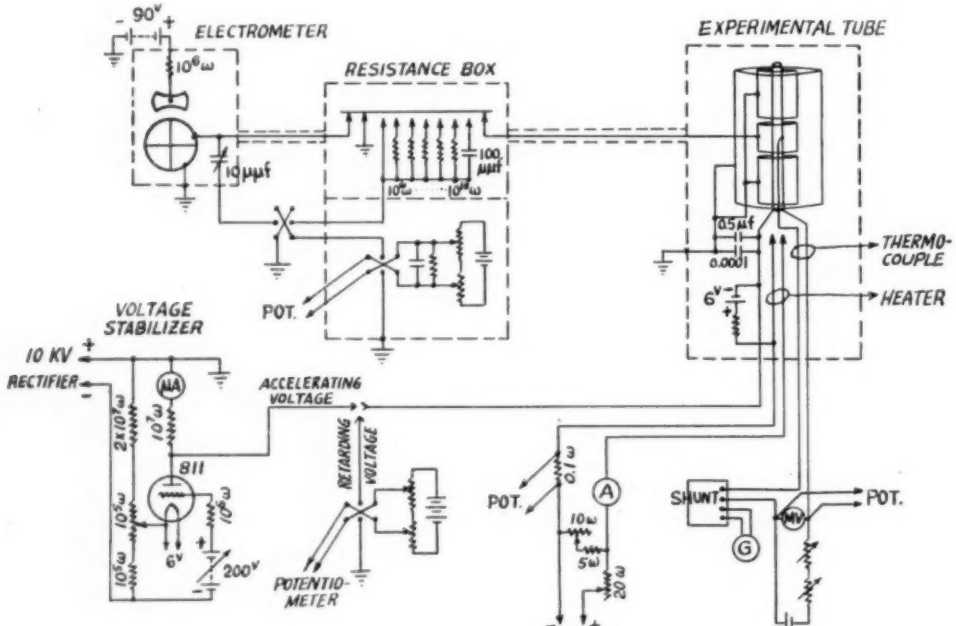

FIG. 3. The measuring circuit.

[4] W. Heinze and W. Hass, Zeits. f. tech. Physik **19**, 166 (1938).
[5] H. Y. Fan, J. App. Phys. **14**, 552 (1943).
[6] B. B. Brown, M. I. T. thesis, (1942).
[7] G. W. Mahlman, M. I. T. thesis (1948).
[8] R. L. Sproull, Phys. Rev. **67**, 166 (1945).

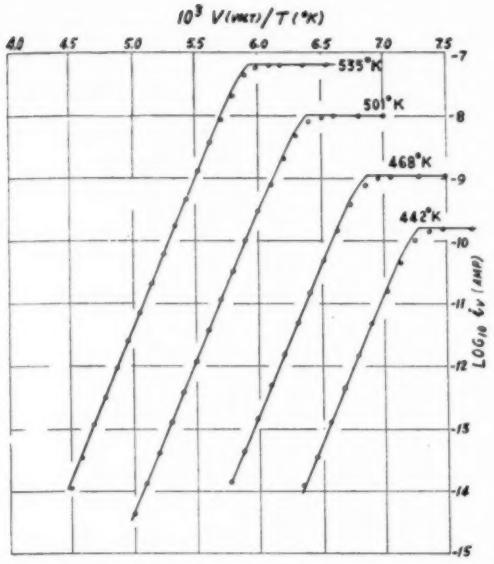

FIG. 4. Retarding field plots. Circles indicate the experimental points, and solid line the theoretical Schottky curves.

the theoretical image theory line. This effect was usually attributed to the patches, and it was suggested that the theoretical line might be approached at high enough accelerating fields.

In making further studies of these properties of the surface potential barrier, we notice that there are two more defects of the oxide cathode which should be considered: namely, the non-uniformity of the work function of the anode due to contamination, and the roughness of the oxide cathode surface. In this work we have managed to keep the anode free from the materials evaporated from the cathode so that the anode work function was uniform and did not change with the anode current. The roughness of the oxide cathode surface has been taken account of in analyzing our results.

EXPERIMENTAL SET-UP

The Experimental Tube

The main feature in the design of the experimental tube involved the use of a sliding anode structure in order to keep the anodes clean. A drawing of the sliding structure is shown in Fig. 1. The cathode (K) and the auxiliarly anode (AA) are fixed in position while the main anodes, the collector (C) and the guard rings (G), are removable. During the processing of the tube, the main anodes (GCG) were drawn up and were kept hot during the breakdown and the activation of the cathode so that materials evaporated from the cathode did not contaminate them. The auxiliary anode served as anode for drawing emission during activation. After the tube was sealed off, when the main anodes were suspected of being dirty, they were drawn up and heated to high temperatures to drive off the deposits. The collector and the guard rings were supported by a "bird-cage-like" structure, which is restricted to up and down motion through the use of the glass sleeves (A). The main anodes and the auxiliary anode were made of tantalum which does not show "anode effect"[3] after it has been properly cleaned.

The cathode sleeve was made of 2-mm diameter grade A nickel tubing. The cathode temperature was determined by the thermocouple method as used by Fan[5] and others. A 2-mil tungsten wire was welded to the center of the inside of the cathode sleeve. The point of welding served as the hot junction. The tungsten wire and a 5-mil nickel wire welded to the end of the cathode sleeve were brought out through a separate press. This press was immersed in an oil bath to keep the cold junction temperature constant. The disturbance of the cathode sleeve temperature[5] by this tungsten wire may be neglected. The temperature of the coating surface is believed to be within a few degrees of the sleeve temperature at all operating temperatures.[9] The tungsten-nickel thermocouple was calibrated against Chromel-P-Alumel thermocouple and checked against the readings of a glass thermometer for every hundred degrees. The calibration curve is shown in Fig. 2.

The main anodes and the auxiliary anode were chemically cleaned and induction heated to 1600°C for a prolonged period.

The cathode coating consisted of $(BaSr)CO_3$ sprayed onto the sleeve to an amount of 5 mg/cm^2. The tube was baked out thoroughly at 500°C, and after this the cathode was broken down and activated. The pressure of the tube after seal-off was around 10^{-8} mm Hg with the use of getter.

The Measuring Circuit

The measuring circuit is as shown in Fig. 3. The experimental tube was shielded in a copper box against disturbances. All leads coming out of the box were shielded. The heater current was measured by the

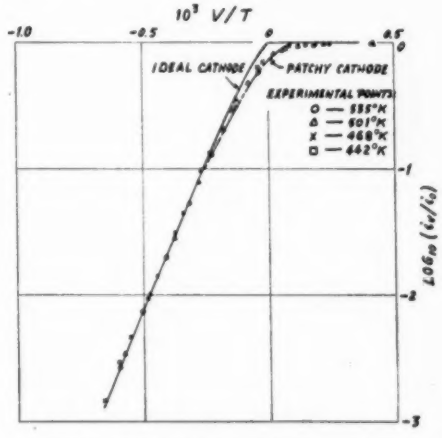

FIG. 5. Retarding field plots matched together. Solid line—theoretical Schottky curve; dot-dash line—calculated curve for a patch model at 500°K assuming no reflection.

[9] G. E. Moore and H. W. Allison, J. App. Phys. 12, 431 (1941).

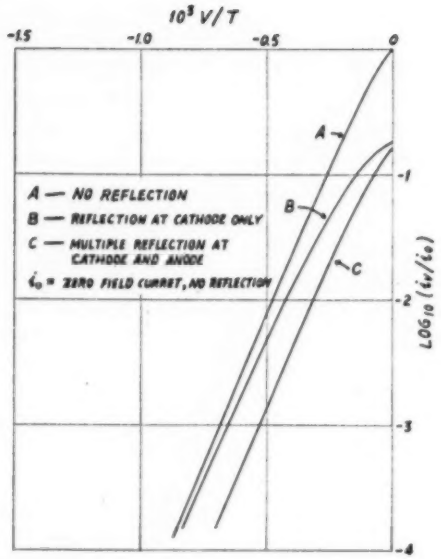

FIG. 6. Calculated retarding field plots for a uniform cathode with different assumptions of reflection effect.

voltage drop across a 0.1 ohm resistance with a Leeds and Northrup K-2 potentiometer. The negative lead of the heater was made 6 volts positive with respect to the cathode to suppress electron emission from the heater. The connections for thermocouple e.m.f. measurement were all copper wires from the cold junction to the meter. A change of cathode temperature by 0.2°C, resulting in a change of thermocouple e.m.f. of 0.007 mv, was indicated by a deflection of 0.2 mm on the galvanometer scale. The cathode was grounded through a 0.5 μf condenser in parallel with a 100 $\mu\mu$f mica condenser to shunt off electrical disturbances. The anodes were grounded and the cathode voltage was variable. Retarding voltages were obtained from dry cells and measured with the K-2 potentiometer. Accelerating voltages below 200 volts were obtained from dry cells, while those from 200 up to 8000 volts were obtained from a high voltage rectifier and controlled by a voltage stabilizer. The voltage stabilizer employed an amplification factor bridge circuit with an 811 tube. When properly adjusted, the variation in output voltage of the stabilizer was below 1 percent of the input variation for all load currents up to 1 μamp. The guard rings and the auxiliary anode were connected directly to ground, while the collector lead was led to the current measuring equipment through a coaxial copper tubing which was grounded. The wire was insulated from the tubing using polystyrene disks. The current measuring equipment consisted of a resistance and balancing e.m.f. circuit and a Compton quadrant electrometer. The voltage drop across a high resistance or a condenser due to the collector current was balanced out, as indicated by the zero deflection of the electrometer, and measured with the potentiometer. Vacuum tube platinum resistors up to 10^{10} ohms were used for current measurement down to 10^{-12} amp. and the charge accumulation method employing a 100 $\mu\mu$f air condenser, and a 10 $\mu\mu$f air condenser (built in the electrometer) were used for current measurement down to 10^{-14} amp.

RETARDING FIELD STUDIES

Retarding Field Current from a Non-Uniform Cathode

It is known that because of the different crystal faces, the crystal defects, and the various amounts of foreign matter adsorbed on the crystal faces, the work function of an oxide cathode is not uniform but varies over short distances along its surface. This non-uniformity of the cathode work function, the patches, causes the retarding field current to be different from

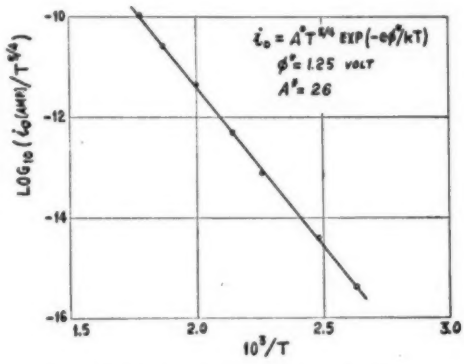

FIG. 7. Observed saturation current against temperature.

that predicted by Eq. (1) which is derived for an ideal uniform cathode. In the actual case, electrons emitted from the various parts of the cathode experience different retarding fields. The retarding potential which an electron experiences in going from the cathode to the anode is the difference between the height of the potential barrier at the anode surface and that near the patch from which the electron is emitted. The total retarding field current is the sum of the component currents from the various patches, each of which varies according to Eq. (1) when the proper value of retarding potential is used, and each saturates at a different anode potential. A plot of this total current against the applied retarding potential would show a slower approach to the saturation current than in the ideal case of a uniform cathode, and consequently an apparent shortage of slow electrons in the energy distribution of the emitted electrons. The effective work function of the non-uniform cathode can be defined as ϕ^* in the following equation:

$$J_0 = A^* T^{5/4} \exp(-e\phi^*/kT), \qquad (5)$$

where J_0 is the observed saturation current, and A^* is the effective A constant. Since in general the plot of $\log(J_0/T^{5/4})$ *vs.* $1/T$ for oxide cathodes can be represented by a straight line, this effective work function is equivalent to the work function for an ideal uniform

cathode which has the same thermionic emission as the actual cathode over the temperature range studied. The effective zero field V_0^* can be defined from the following equation:

$$V_0^* = \phi_{\text{anode}} - \phi^*. \tag{6}$$

It is determined from experiment by matching the experimental retarding field plot to the theoretical Schottky plot at both high retarding fields and at saturation. The zero field point on the theoretical curve marks the effective zero field, because when thus matched the theoretical curve represents the retarding field plot of an ideal cathode which has its work function equal to ϕ^*. The effective work function and effective zero field defined in Eqs. (5) and (6) are necessarily temperature dependent even if the work functions of the patches are independent of temperature, however the temperature dependences are only slight.

Experimental Result and Interpretation

The experimental study was made at temperatures between 442°K and 535°K. The maximum current density reached in these runs was below 0.1 μamp./cm^2. Experiment shows that at such low temperatures and low current densities no measurable change of the cathode state took place. The curves for increasing and for decreasing retarding potentials coincided very well. The changes in temperature during each run at one particular temperature were always within 0.2°C. Anode effect was found to be not present.

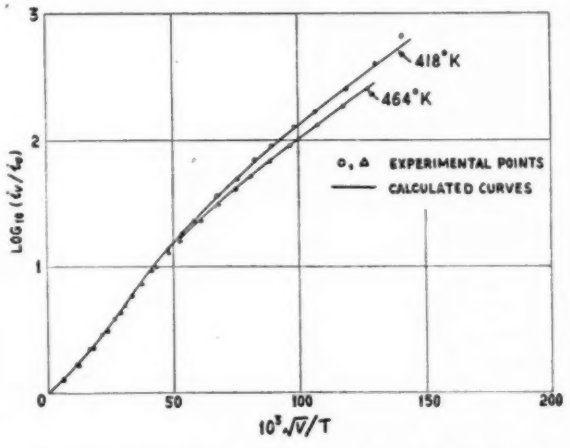

FIG. 8. Accelerating field plots for the same cathode as used for Figs. 4, 5, and 7.

The experimental curves were shown in Fig. 4. An enlarged drawing with all the curves matched together is shown in Fig. 5. It is seen that at retarding potentials above 0.2 volt, all the experimental curves coincide with the theoretical curve assuming no reflection. Therefore, at least for the high energy electrons, the energy distribution obeys Maxwell's law, and the electron temperature agrees with the cathode temperature. The departure of the experimental curves from the theoretical is seen to occur in a range of 0.3 volt. Even at the maximum current density of 0.1 μamp./cm, space charge distortion of the curves should not be detectable. The anode was found to be free from contaminations, so that the condition of uniform anode surface potential is approximately satisfied. Although the temperature of the cathode was not uniform along its whole length, it is believed that the temperature variation over the cathode under the collector was not more than 2 or 3°C, and the temperature variation over the entire cathode was within 30 or 40°C at the measuring temperatures we used. This temperature distribution along the cathode does not make the experimental curve deviate noticeably from the theoretical curve for a cathode with uniform temperature.

It remains now for us to examine the effects of first the non-uniformity of the cathode work function and second the reflection at the surfaces of the electrodes. The distribution of work function along the cathode being unknown, we use a crude model for discussion. We take our cathode as made up of patches that can be grouped into seven equal areas with work functions ranging in equal steps from ϕ to $\phi+0.15$ volt. As a first approximation, we neglect the distortion of the electron trajectories by the patch field, and sum up the component currents from the separate patches directly, using Eq. (1) with different retarding potentials for the different groups of patches. The calculated retarding field curve is shown in dot-dash line in Fig. 5 for the temperature of 500°K. Similarly calculated curves for temperatures from 450°K to 550°K show only slight deviation from each other. The experimental curves for the temperature range of 442°K to 535°K are also seen to be very close. The calculated curve fits the experimental curves quite well, and the use of a more elaborate model with a slightly larger range of work function variation would enable us to make a perfect match. It will be seen in the analysis of our accelerating field measurements that this value of work

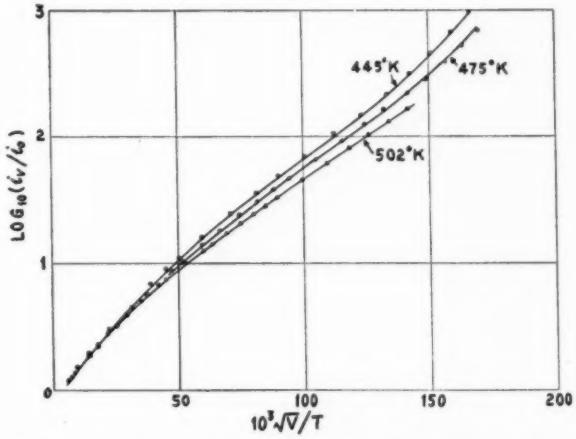

FIG. 9. Accelerating field plots for another oxide cathode; note similarity to plots in Fig. 8.

function variation agrees with the value we found there.¶

The Reflection Effect

As mentioned in the introduction, according to Nottingham's measurements on tungsten and thoriated tungsten filaments, a reflection coefficient as given by Eq. (2) with $k/\omega=4.5\times10^{-4}$ deg.$^{-1}$, should occur at both the cathode and the anode. Electrons that are reflected from the anode should go back to the cathode if the field is strictly radial. Since Nottingham used a filament wire of about 0.08 mm in diameter, a slight departure of the electrodes from being strictly coaxial would cause the electrons that are reflected from the anode to miss the cathode and go back to the anode again. Thus the anode current would not be affected appreciably by the reflection effect at the anode. However, with our tube, the cathode was 2 mm in diameter so that the electrons that are reflected from the anode had very good chance of landing on the cathode as they should in the ideal case. This reflection effect at the anode would reduce the anode current more at high retarding fields than at near zero field. Measurements yield information on the reflection effect only as the reflection near zero field differs relative to that at high retarding fields. Therefore the apparent reflection effect is greatly reduced when the reflection at the anode is included. The current expression for a uniform cathode when reflection effect is present is

$$J_v=(2e/h^3)(2\pi mkT)^{\frac{1}{2}}\exp(-e\phi/kT)\times\int_{-\infty}^{\infty}dp_y\int_{0;\ (2\text{ Mev}-(1-\theta^2)p_y^2)^{\frac{1}{2}}}^{\infty}\times(1-R)\exp\left(-\frac{p_x^2+p_y^2}{2mkT}\right)\frac{p_x}{m}dp_x, \quad (7)$$

where p_x and p_y are the normal and tangential components of the momentum of the electron at the cathode surface (the length of the cathode is along the z axis), and θ is as defined in Eq. (1). R is the reflection coefficient, and is given by Eq. (2) when reflection at the cathode alone is considered. When multiple reflections at both electrodes are considered, it is as follows:

$$1-R=\frac{(1-R_c)(1-R_a)}{1-R_cR_a}, \quad (8)$$

where $R_c=\exp(-p_x^2/2m\omega)$, $R_a=\exp(-P_x^2/2m\omega)$ and $P_x^2=p_x^2+p_y^2(1-\theta^2)-2$ Mev, P_x being the normal component of electron momentum at the anode surface. In Fig. 6 are shown the retarding field currents for different assumptions of reflection effects. It is seen there that while Curve B, where reflection effect at the cathode alone is considered, is markedly different from Curve A for zero reflection; Curve C, for which the multiple reflection effect is considered, has a form very nearly the same as Curve A. Therefore we see that the reflection effect, if it does exist, is not observable in our case. The possibility of the existence of an appreciable reflection effect at the electrode surfaces should not be excluded although we have found a satisfactory explanation of our retarding field measurements with the patch theory. A decisive check on this reflection effect would be to use a fine filament wire, in which case the reflection effect, if it does exist, would show up strongly.

Work Function and Zero Field

The thermionic emission against temperature curve is shown in Fig. 7. The currents used in the plot are the observed saturation currents so that the slope of the plot gives the effective work function. The points lie approximately on a straight line. The effective work function is found to be 1.25 volts and the A value around 26. The effective zero fields obtained from the matching of the experimental retarding field plots to the Schottky plot are shown below:

Temperature in °K	V_0^* in volts
535	3.17
501	3.19
468	3.21
442	3.22

This variation of the effective zero field is quite large and could be due to the changes in work functions of the patches and to the effect of the patch field distortion on the electron trajectories which we have neglected in our previous analysis. The anode work function obtained from the values of ϕ^* and V_0^* given above is around 4.4 volts. This is higher than the thermionic value of 4.07 volts obtained for tantalum by Dushman, Rowe, Ewald, and Kidner;[10] and the photoelectric value of 3.92 to 4.05 volts obtained by Cardwell.[11]

ACCELERATING FIELD STUDIES

Measurements

Emission currents were measured with accelerating potentials up to 7 kv and at temperatures below 500°K. The maximum electric field, calculated from the geometry of the electrodes, was 50,000 volt/cm at the cathode surface. The drop in potential across the coating was negligible according to Mahlman's measurements on the conductivity of oxide coating prepared in the same way as in this experiment. The emission

¶ It should be emphasized that what we mean here by the work function of the patches are the potential barriers, in the presence of the field due to the neighboring patches, which an electron climbs over in traveling along the normal to the patch area. In our later use of Becker's hill and valley checkerboard approximation for accelerating field studies, the work functions of the patches are as defined by Becker, i.e., they are the values when each patch is considered as an infinite plane with no neighboring patches.

[10] Dushman, Rowe, Ewald, and Kidner, Phys. Rev. **25**, 338 (1925).

[11] A. L. Hughes and L. A. Dubridge, *Photoelectric Phenomena* (McGraw-Hill Book Company, Inc., New York, 1932).

current was always below 1 μamp. and therefore there was no heating up of the cathode when high voltage was applied between the electrodes. The current was steady on the application of high accelerating potentials, and the current at low field did not change before and after a run was made. The results for the same cathode as we used in the retarding field studies are shown in Fig. 8. Measurements on two more cathodes show similar current voltage characteristics. Results on one of them are shown in Fig. 9. The curves are seen to decrease in slope as the voltage is increased and remain almost linear for a range of moderate voltages and increase rather fast in slope as 3 kv is exceeded. The minimum slopes near the linear part of the curves in Fig. 8 are about 2.6 times the theoretical Schottky line if one takes the field at the cathode surface to be that calculated according to the dimension of the electrodes. The slopes for the curves at the two temperatures are about the same. According to patch theory, we would expect a deviation of the experimental curve from the Schottky line at low voltages and that deviation should go to zero at high voltages. There are two difficulties if we were to rely on the patch theory alone to explain our results: first the rapidly rising parts of the curves at high voltages cannot be explained; and second, since the curves did not approach the theoretical Schottky line even at 5 kv, the average linear dimensions of the patches would have to be smaller than 10^{-6} cm. It is conceivable that there be patches of that size or smaller, but their contribution to the emission current would not be important owing to their small areas, unless their work functions are greatly reduced by a very strong accelerating field, a point which we will take up immediately.

The Effect of the Roughness of the Cathode Surface

Owing to the difficulties with patch theory alone, it is desirable to look into the other possible reasons for this deviation. It is easy to see that the roughness of the cathode surface has an important effect on the actual fields at the different parts of the cathode. With the oxide cathode built up of crystals of sizes of from one micron to a few tens of microns, piled up on one another, the field variation along the cathode would be very large. And it is likely to have a considerable fraction of the cathode surface with fields ten times or more higher than the average field. At low voltages, this effect will not be important. The lowering of the potential barriers at low accelerating potentials will be small even for the sharp points where the fields are many times higher than the average field. The change in the logarithm of the emission from a small area of the cathode is proportional to the lowering of the potential barrier there. When the latter is small, the change in the emission current itself is also nearly proportional to it, and therefore to the square root of the field. Thus the net field effective in increasing the emission for the entire cathode is close to the average field. (The effective field would be equal to the average field at low accelerating potentials if the lowering of the potential barrier were proportional to the field itself and not to its square root.) At high accelerating potentials, the lowerings of the potential barriers are large, and the change in the emission current at any spot is then no longer proportional to the lowering of the barrier. Emission currents from places where the fields are strong are far more important than those from places where the fields are relatively weak, and the effective field for the entire cathode is then very different from the average field, and is close to the field at the strong field places. It is thus seen that the ratio of the effective field to the average field increases from unity at low accelerating potentials to higher and higher values as the accelerating potential is increased. It is not surprising thus to find that the experimental curves did not approach the theoretical curve even at the highest average field of 50,000 volt/cm as we have used. The explanation of the entire curve is as follows: At low applied accelerating potentials the effective field is approximately the average field and the initial large slope of the curve and the subsequent decrease in slope is mainly due to the patch effect. At higher accelerating potentials, the patch effect becomes smaller but the effective field to average field ratio becomes greater so that the slope of the curve no longer decreases. For voltages above 1 kv, the patch effect becomes almost negligible and the curve has an almost constant slope over a considerable range of voltage. This slope is 2.6

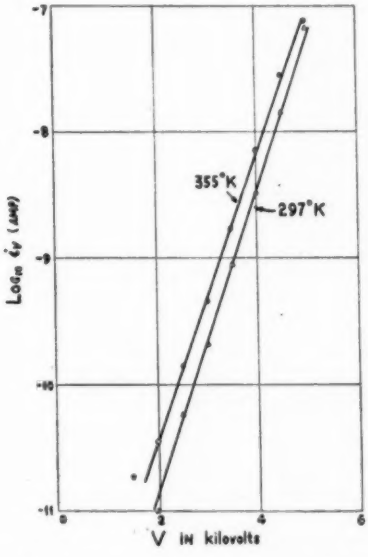

FIG. 10. Electron emission at near room temperatures under high accelerating voltages.

times higher than the slope calculated from the average field because the field effective in increasing the emission current is 2.6^2 times higher than the average field. For accelerating potentials above 5 kv, the slope of the curve increases rather fast because of the further in-

crease of effective field to average field ratio; and probably at some extremely sharp points, field emission was taking place. Based on this explanation, we can estimate the average linear dimension of the patches and the variation in work function of the patches using Becker's hill and valley checkerboard approximation.[12] Estimates have been made for two extreme cases: first, that the effective field to average field ratio is 2.6[2] throughout the whole range of accelerating potential up to 5 kv; and second, this ratio is unity for accelerating potentials below 1 kv and is 2.6[2] for potentials above that. The actual case should lie between these two extremes. The results of estimation are: the maximum work function variation (assuming sinusoidal variations from patch to patch) is 0.16 volt from average for both cases; and the average linear dimension of the patches are 2×10^{-5} cm and 2×10^{-4} cm for the first and the second cases respectively. The calculated curves for the first extreme case are shown in Fig. 8. This value of work function variation agrees with the value of 0.15 volt we have obtained in our analysis of the retarding field measurements. The linear dimensions of the patches of 2×10^{-5} to 2×10^{-4} cm are rather small compared to the sizes of the oxide crystals which run from 10^{-4} to 10^{-2} cm. It should be noted that in our analysis, perhaps it is around the smaller crystals that we have higher fields and therefore more important contributions to the observed current; and it is also likely that the patches correspond to crystal defects and not to the entire crystal faces.

[12] J. A. Becker, Rev. Mod. Phys. **7**, 95 (1935).

Measurements at near room temperatures lend support to this view of the important effect of the roughness of the cathode surface. At high accelerating potentials, fluorescent spots appeared on the glass wall of the experimental tube indicating that the emission came from local spots of the cathode where the fields are very high. Curves in Fig. 10 show that the current is temperature sensitive suggesting that at least part of it is thermionic emission from local sharp points where the potential barriers are lowered to perhaps two- or three-tenths of an electron volt by the extremely high fields there.

It is suggested that further accelerating field measurements be done with single crystals or with cataphoretically deposited cathodes whose surfaces are far more smooth than the ordinary cathodes with sprayed-on coatings.

The author wishes to express his gratitude to Professor W. B. Nottingham for the suggestion of this work, his constant interest in it and his many helpful suggestions.

Augmented Flames in Half-Open Tubes[1,2]

MARJORIE W. EVANS, MILTON D. SCHEER, LOUIS J. SCHOEN, AND EMMY L. MILLER
Research Division, New York University, University Heights, New York City
(Received July 18, 1949)

High velocity flames in half-open tubes produced by placing a grid augmenter in the path of an advancing flame are described. High speed schlieren motion pictures and instantaneous pressure measurements are used to study flame structure and accompanying flow in the tube. It is found that the grid augmenter causes a mixing of burning and unburned gases, resulting in an increase in reaction surface. As a result the total amount of reaction per unit time per unit volume is increased, thus leading to the observed high velocities.

INTRODUCTION

THE velocity of propagation of flames burning in gas is determined by the normal combustion velocity (which is dependent upon thermal conductivity, diffusion, and the detailed reaction kinetics), and by the flow processes in the system. A hydrocarbon-air mixture ignited by a spark at the closed end of a half-open tube (i.e., a tube closed at one end and open at the other), generally has a maximum flame front velocity of about 100 feet per second.[2] Certain flames such as those in pulse jet engines have been observed to move with a considerably greater velocity. Flames of high velocity, in some cases approaching 1000 feet per second, have been produced in this laboratory by placing in the path of the advancing flame a grid augmenter consisting of a sheet of metal containing holes with trailing edges. Such a sharp increase in velocity after the flame front has passed through a twenty-hole grid may be seen in Fig. 1, which shows the flame velocity recorded in an experiment in which the grid was placed two feet from the closed end.

This paper reports investigations into the nature of the high velocity or augmented flame produced by the grid augmenter, utilizing schlieren techniques in conjunction with a high speed motion picture camera, and pressure measurements.

[1] This research was conducted under the auspices of Project Squid, sponsored by the ONR under Contract N6ori-11, Task Order II.

[2] This material is a further development of work first reported at the Third Symposium on Combustion, Flame, and Explosion Phenomena, University of Wisconsin, Madison, Wisconsin, September, 1948, in a paper entitled, "A study of high velocity flames developed by grids in tubes," Evans, Scheer, Schoen, and Miller.

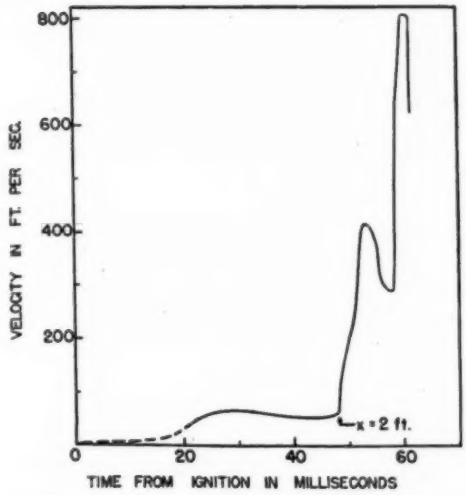

FIG. 1. Velocity-time curve for a flame front in a tube in which a twenty-hole grid augmenter was placed two feet from the closed end.

SCHLIEREN AND PRESSURE MEASUREMENTS

The flame tube was six feet in length with an inner square cross section approximately 3.5 inches on a side. The grid augmenter in these experiments had three rectangular nozzles 0.3 square inch in area with trailing edges 0.3 inch long. The grid was placed 3.1 inches from the spark igniter, which was supplied by a high frequency induction coil. The tube was filled with a 6.6 percent by volume propane-air mixture.

The optical arrangement consisted of a double-mirror knife-edge schlieren system with parabolic mirrors sixteen inches in diameter, having sixty-inch focal lengths. The parallel beam of light between the two mirrors passed through the plate glass side-walls of the flame tube. The light source was a Western Union 100-watt zirconium arc lamp, and a 16 mm Fastax camera, with a speed booster, was used at a speed of 4000–9000 frames per second to record the gas motions in the tube. In order to follow the motion of a particular layer of gas during the flow which accompanies combustion, observations were made of the positions of local thermal gradients produced by stretching across the tube a nichrome wire heated electrically to a temperature well below the ignition point.

Pressure measurements were made with the frequency modulated condenser type pressure gauge developed in this laboratory by J. H. Hett and R. W. King, Jr.[3] The time of ignition, t_{ig}, was correlated with the occurrence of the pressure pulse and with events as recorded in the schlieren motion pictures by means of the circuit shown in Fig. 2. This circuit utilized the light emitted by the igniting spark, as picked up by a photo-cell, to trigger indicating lights which registered on the motion picture film and on the film recording the pressure trace.

Figure 3 is a reproduction of nine selected frames from a schlieren motion picture of the flame as it passes through the grid augmenter. Apparently, in this case only two holes were effective. The flame before reaching the grid shows several large cells and has a relatively smooth surface. These cells strongly resemble those recently observed by Markstein in flames held stationary in tubes by adjustment of the flow velocity.[4] The augmented flame, on the other hand, shows a much more complex structure with fine-grained eddy motion. As it progresses down the tube it assumes a more homogeneous structure. The faint patterns showing gas flow through the grid nozzles in pictures *B*, *C*, and *D*, of Fig. 3 are caused by gas which has been heated by the flame.

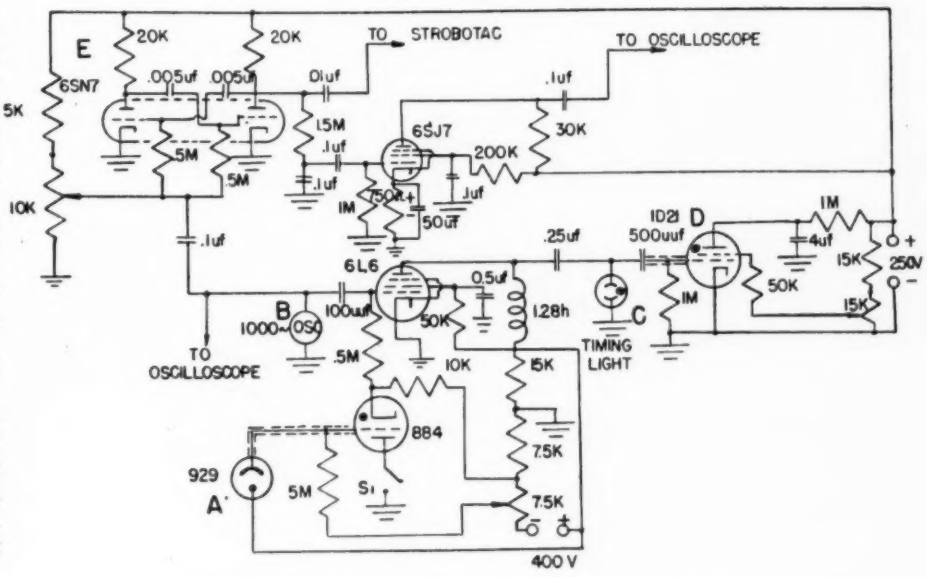

FIG. 2. A circuit for the simultaneous indication of zero time on the schlieren motion picture and pressure recording film. The photocell *A*, picking up light from the igniting spark, triggers a thyratron tube which allows the oscillator *B* to energize the timing light *C* in the Fastax camera, thereby providing a zero time mark t_{ig}, as well as timing marks at 1000 cycles per second for the schlieren motion pictures. *D* is a gas tube which flashes when the photo-cell begins to conduct, thus providing a zero time mark on the pressure recording film. *E* is a frequency divider which divides the 1000-cycle output by 4, thereby furnishing 250 cycles per second to a strobotac which provides timing marks for the pressure recording film. The oscilloscopes were used for the calibration of the oscillator and the frequency divider in conjunction with a 1000 cycle tuning fork oscillator as a standard.

[3] J. H. Hett and R. W. King, Jr., "A frequency modulation pressure recording system," Rev. Sci. Inst. (to be published).
[4] G. Markstein, J. Chem. Phys. **17**, 428 (1949).

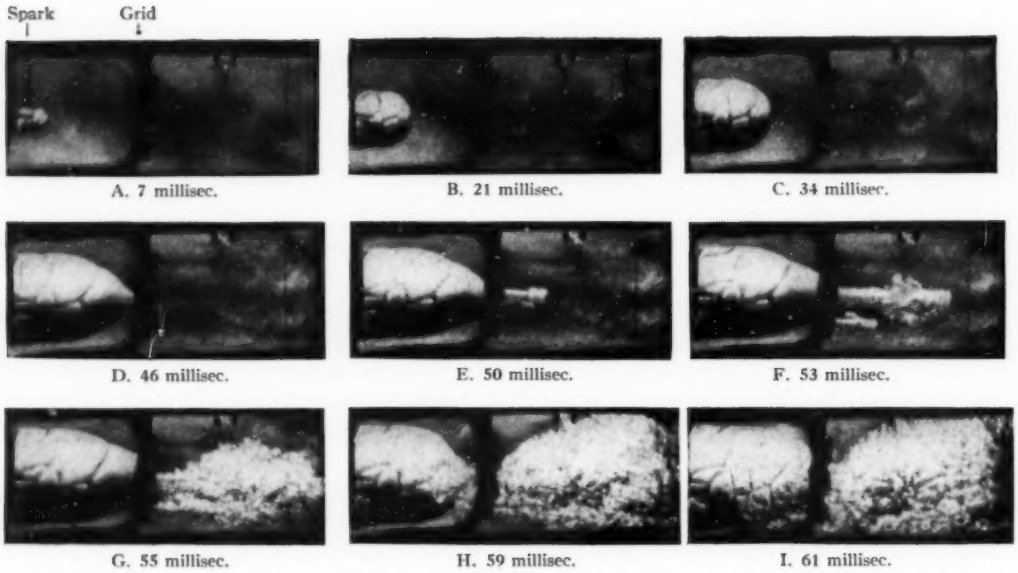

FIG. 3. Schlieren motion pictures taken at 4400 frames per second of flame moving through a three-hole grid augmenter.

Figure 4 shows schlieren pictures of the progress down the tube of a layer of gas in front of the flame. In these early pictures is seen a spark indicator, in series with the igniting spark, placed in the field of view to indicate the time of ignition. This method was later replaced with the timer circuit mentioned above. The position of the heated wire used to produce the thermal gradient is shown in *A*. In subsequent pictures the gradient is observed moving toward the open end. The flame comes into the field of view in *C*, and overtakes the gradient in *E*. The data plotted in Fig. 5 were obtained from measurements made from pictures such as these.

Figure 5 is a plot of position *versus* time for layers of gas as the augmented flame expands and moves down the tube. The solid line represents the motion of the flame front, the dashed lines that of layers of gas which were labeled with thermal gradients. The plot shows that all gas between the grid and a point ten inches from the grid at zero time is enclosed by and becomes part of the augmented flame. This volume is termed the augmentation region. The gas which is initially beyond this ten-inch region is pushed ahead of the flame during the expansion which occurs as a result of the combustion reaction, and is not burned.

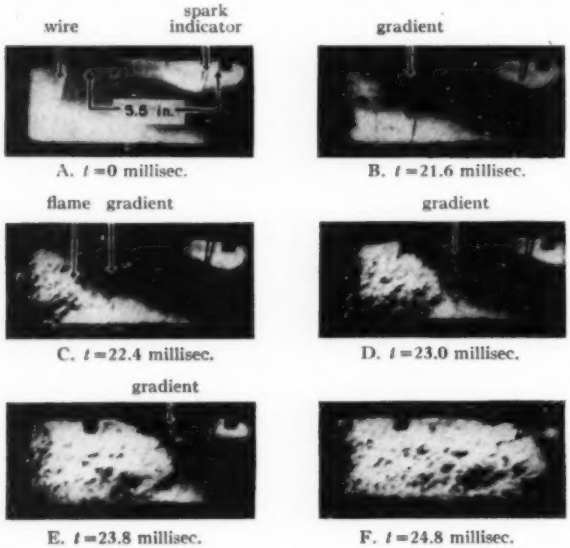

FIG. 4. Schlieren motion pictures taken at 4300 frames per second showing a thermal gradient moving down the tube ahead of an augmented flame.

While the position-time curves for unaugmented flame fronts vary radically from experiment to experiment, the characteristics of the augmented flames are quite reproducible.[2] Under identical experimental conditions the position-time points for several flame fronts fall on the same curve. The lateral growth of the flame in the augmented region is likewise reproducible. A plot of the growth of the augmented flame in the y direction (perpendicular to the axis of the tube) at a point 2.5 inches from the grid augmenter is shown in Fig. 6. It is at this point that the developing augmented flame first reaches the sides of the tube.

Pressure measurements shown in Fig. 7 were made with the gauge placed at points *B*, *C*, and *D*, in the tube as indicated in the figure. The time t_p in Fig. 6, when the flame reaches the sides coincides with the beginning of the first pressure pulse at position *B*. This suggests that the origin of the pressure pulse is in the region near *B*. Pressure measurements in a tube without grid showed only a small rise over atmospheric pressure, the peak pressures being approximately a factor of ten smaller than those shown in Fig. 7. When the tube with grid was filled with propane-air mixture, simultaneous pressure measurements at *B* and in the initiating chamber (i.e., between spark and grid) gave two essentially

identical curves, the method of timing not being accurate enough to indicate the difference in the time of occurrence of the pulse at the two points. When only the initiating chamber was filled with gas, the reaction produced only a small pressure rise. This confirms the conclusion that the pressure pulse is generated near position B, in the augmentation region.

Observation of the schlieren motion pictures shows that at time t_p when the flame reaches the sides of the tube the region 2 to 2.5 inches downstream from the grid augmenter is the center of an expansion of the burning gases. The observation together with the facts cited above indicates that the augmented flame is produced in the augmentation region by a mixing process between t_g (when the flame emerges from the grid augmenter) and t_p. After time t_p the dominant phenomenon is rapid burning and expansion of burning gases with the consequent rapid motion of the flame toward the open end of the tube. It has been previously noted[2] that streak photographs of the augmented flame show that the flame apparently first appeared several inches below the grid, and proceeded to burn simultaneously toward the open end and back toward the grid. This can now be explained, in view of the above observations, by assuming that burning vigorous enough to produce sufficient illumination to record a trace does not occur until time t_p, with the vigorous burning beginning at the center of expansion, 2 to 2.5 inches downstream from the grid.

DISCUSSION

It is clear that the high flame front velocity of the augmented flame is to be attributed to a rapid expansion during the burning of the gas in the augmentation region. In the normal unaugmented flame in the same tube somewhat less gas is burned, but over a longer period of time. This greater rate of burning of the augmented flame is due to an increased burning area or reaction surface. When the burning or burned gas from the initiating chamber flows through the nozzles into the stationary gas a mixing process occurs so that burning surfaces are interspersed with unburned gas. As a result there is more burning area per unit volume than in the normal flame, which presents a relatively smooth surface with a few large cells.

The details of the mixing are not clear. The two-dimensional problem considering the spread of a mixing region in the case of the turbulent mixing of a stream of fluid (of uniform velocity at the mouth of the nozzle) with a fluid at rest has been analyzed by others.[5] The

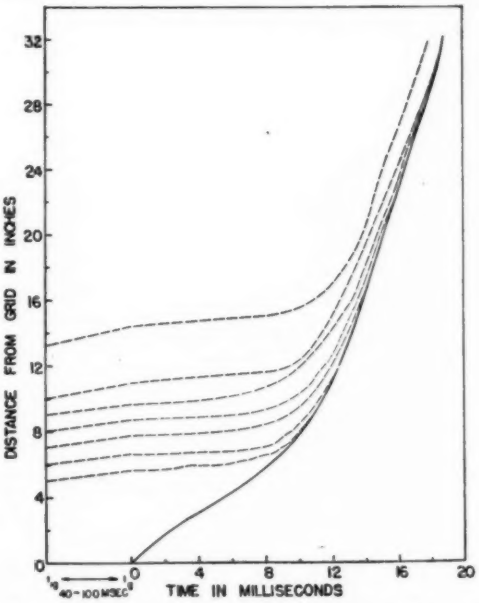

FIG. 5. A plot of the motion of layers of gas as the augmented flame grows and moves down the tube. The solid line represents the flame front, the dashed lines layers of unburned gas ahead of the flame. t_{ig} is the time of ignition, t_g the time of appearance of the flame at the grid. Measurements were made from motion pictures taken at 5000–7500 frames per second.

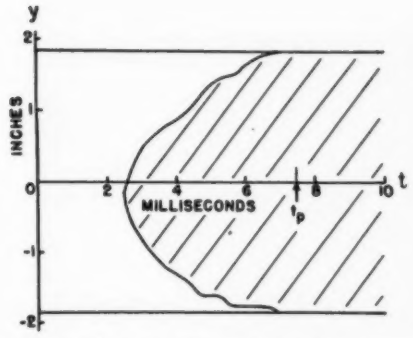

FIG. 6. A plot of the rate of growth, in the y direction, of the mixing region, at a point 2.5 inches below the grid. $y=0$ is the axial line of the tube. Time is measured from the appearance of the flame at the grid. t_p is the time of the beginning of the first pressure pulse shown in B of Fig. 7.

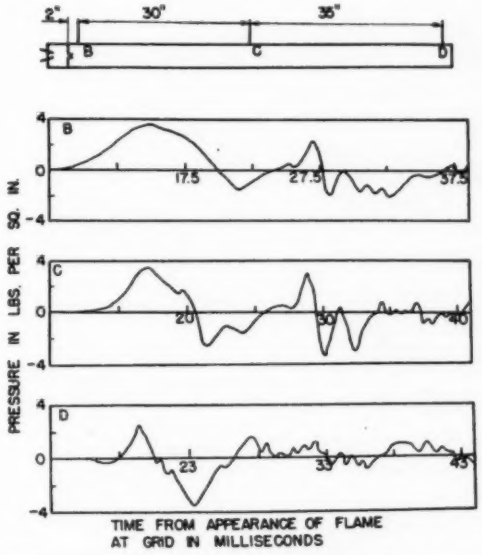

FIG. 7. Pressure-time curves taken with the frequency modulated condenser type pressure gauge at the points B, C, and D, in the augmented flame tube. The flame tube, with spark and grid augmenter, is shown diagrammatically.

[5] *Modern Developments in Fluid Dynamics*, edited by S. Goldstein (Oxford University Press, New York, 1943), Vol. II, p. 597.

TABLE I. Comparison of average pressure and specific impulse of a small pulse jet engine using gasoline as fuel, and the augmented flame tube using a propane-air mixture (6.6 percent by volume) as fuel.

	Small pulse jet	Augmented flame tube
Average pressure (lb./sq.in.)	3.3	1.1
Specific impulse (lb. thrust/lb.fuel/sec.)	760	410

present situation is more complicated in at least four respects, *viz.*, 1) the flow field is not two-dimensional, 2) the velocity of the discharging jet at the mouth of the nozzle is not constant, 3) three or more nozzles are in juxtaposition, and 4) a combustion reaction at an elevated temperature is occurring in the jet and at the boundaries. The qualitative observation may be made from Fig. 3 that the core of fluid in which laminar flow occurs disappears within two or three nozzle diameters downstream, after which the mixing region occupies the whole jet. One can speculate that regions of vorticity and turbulence spread from each jet and ultimately interfere with one another creating additional unstable swirling type flow of an even more complex nature. In this process large vortices may perhaps break up into smaller ones during the lateral growth of the mixing region.

It is of interest to inquire as to whether the augmented burning described here resembles the burning observed in jet engines, particularly with respect to the rate of burning. This is conveniently done by comparing the average pressure in a typical small-scale pulse jet, which uses gasoline as fuel, with the average pressure in the flame tube. In order to carry out this comparison it is assumed that the flame tube could be fired at a frequency which would correspond to a period comprised of the time for the pressure to rise from atmospheric to a peak, back through a minimum, and then to atmospheric again, and that such repetitive firing would not materially alter the pressure record, shown in Fig. 7. Such an assumption is suggested in part by the fact that a similar sequence of pressure changes occurs in a combustion chamber of a pulse jet during a cycle of operation. At any rate, following this hypothesis, if the curve B of Fig. 7 is integrated from 7.5 to 23.9 milliseconds and the result divided by the elapsed time the average pressure in the flame tube is obtained, i.e.,

$$P_{Av}=\left(\int_{7.5}^{23.9} P(t)dt\right)\Big/16.4.$$

The specific impulse is calculated on the assumption that the augmentation region is filled with propane-air mixture at 16.4 millisecond intervals. Inasmuch as the heats released per unit mass for gasoline and propane differ by only 5 percent and the calculations are only approximate, no correction was made for the difference. Table I lists the results in terms of average pressure and specific impulse, and the quantities are found to be of the same order of magnitude for the small pulse jet and the augmented flame tube.

CONCLUSION

Despite an incomplete understanding of the mixing process in the flame tube, it is possible to draw some conclusions with regard to the effect of swirling or eddy motion on combustion processes. Such motion is an important factor in determining the rate at which a given fuel-air mixture can be burned, its function being, at least under the conditions of these experiments, to increase the total reaction surface, thus increasing the amount of mixture reacting per unit time per unit volume.

In situations where sufficient fuel and air are available an increase in the intensity of the swirling and mixing may make possible a greater rate of energy release in the same reaction chamber volume. Conversely, under these conditions for a given desired rate of energy release a smaller volume of combustion chamber may be used. These possibilities could conceivably be of interest in the design and operation of industrial furnaces and internal combustion engines as well as jet engines.

The authors take pleasure in acknowledging their indebtedness to the late Professor J. K. L. MacDonald and to Dr. J. H. Hett, Professor G. E. Hudson, and Messrs. R. W. King, Jr., and Simeon Braunstein for help received during these studies.

Static Magnetic Storage and Delay Line*,**

AN WANG AND WAY DONG WOO
Computation Laboratory, Harvard University, Cambridge, Massachusetts
(Received July 27, 1949)

Magnetic cores with a rectangular hysteresis loop are used in a storage system which requires no mechanical motion and is permanent. The binary digit "1" is stored as a positive residual flux, and the binary digit "0" as a residual flux in the opposite direction. When a negative probing field is applied to the core, a large voltage is induced in another winding if the digit stored has been a "1," and very small voltage if it has been a "0." The induced voltage in the former case is large enough to magnetize another core of identical construction. Binary digits can thus be transferred from one core into another. Many cores are arranged in tandem to form an information delay line. Binary digits can be advanced along the line step by step. The present upper limit of the speed of propagation is about 35,000 digits per second, and there is no lower limit.

I. INTRODUCTION

ONE of the most important research problems in the field of large-scale digital calculating machines is that of information storage. Electronic trigger pair tubes, cathode-ray tubes, acoustic delay lines, rotating drums, or tapes are used in present machines. Electronic trigger pair storage is, of course, the most versatile, but it is extremely expensive and its reliability poor. Cathode-ray tube and acoustic delay line storage systems need constant regeneration to preserve the information stored. All three systems lose the information if there is interruption of power. Magnetic drum or tape storage preserves information indefinitely, but it involves a mechanical system, and the operating speed is limited by mechanical considerations. Both in acoustic delay lines and rotating magnetic drums, the operation is necessarily synchronous. The speed depends upon the physical nature of the system and cannot be changed at will during operation.

This paper describes a storage system which operates like electronic trigger pairs but does not use vacuum tubes other than a relatively small number for control purposes.

A binary digit which takes the value of "0" or "1" is stored in a ferromagnetic core in the form of positive or negative residual magnetism, depending on the direction of the last magnetizing force. As shown in Fig. 1, a binary digit is represented by the point "0" or "1" on the hysteresis curve of the core. To store a binary digit, only the application of a magnetizing pulse of proper polarity is necessary.

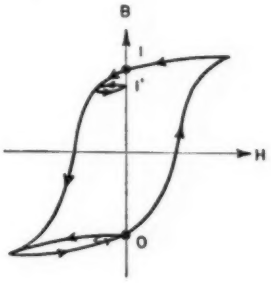

FIG. 1. Hysteresis loop.

The reading out of the stored information presents a more difficult problem. For a small negative pulse of magnetizing force H, applied at point "0," there results less change in the flux density B than for a similar negative pulse applied at point "1." Thus the relative amplitude of the induced voltage indicates what information has been stored in the material. However, this is true only for the first-read-out pulse, since after "0" information has been read out, the material returns to the point "0," whereas after "1" information has been read out, the material goes to a new point "1'" instead of returning to "1." Further negative pulses of H produce very nearly equal changes of B for starting positions "0" and "1'." Thus, whereas small read-out pulses do not actually destroy the positive or negative residual magnetism representing the stored information, they make reading out by like pulses impossible after the first.

When a large negative read-out pulse of H is impressed, the information is destroyed. The state of the material returns to position "0" in the B–H curve, no matter what information was previously stored. However, the secondary induced voltage is much larger when B changes from "1" to "0" than when B changes from "0" to "0." The ratio of these voltages was found to be as high as 30:1 for suitable magnetic materials. The large induced voltage can be made to drive another core from state "0" to "1." Thus one can construct (1) a storage unit in which digits can be stored and read-out continuously, and (2) an information delay line in which a series of binary digits can be propagated at

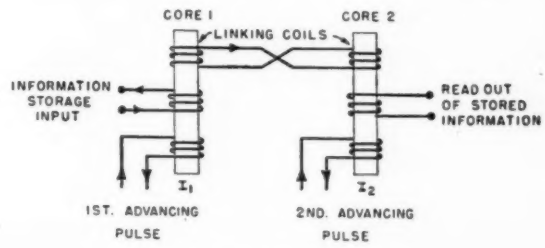

FIG. 2. Two-core storage unit.

* Work done under Contract W19-122-ac-24 between Harvard University and the United States Air Force.
** Presented at the Cambridge Meeting of the American Physical Society (June, 1949).

any desirable speed up to about thirty thousand information pulses per second.

II. A SINGLE-INFORMATION STORAGE UNIT

Since the large secondary induced voltage is sufficient to drive another core of similar size to its saturation, a means is available to transfer the information.[1] Such a storage unit is shown in Fig. 2. Core 1 and Core 2 are wound of strips of material with a nearly rectangular hysteresis loop to insure that the states of residual magnetism, 1 and 0, are well defined and stable. Assume

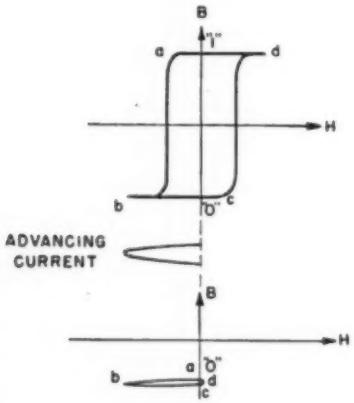

FIG. 3. Flux changing path.

that the 1 state of residual magnetism corresponds to flux in the cores in the upward direction, and the 0 state to flux in the downward direction. Then, whenever a 1 is stored in Core 1 through the information input coil, the first current pulse I_1 will change its state from 1 to 0. This generates a large induced voltage in the linking coil and drives Core 2 to state "1." After that the second current pulse I_2 shifts this state "1" back to Core 1 again. Thus the state "1" is transferred between Core 1 and Core 2 when the current pulses I_1 and I_2 are applied alternately. However, if both cores are originally in the "0" state, the I_1 pulse cannot change much of the flux of Core 1. The linking current is very small, and Core 2 remains in the "0" state. The alternate application of I_1 and I_2, which will be called advancing pulses from now on, therefore will not produce any change of the states of the cores. This constitutes a single-information storage, in which a binary digit can be stored indefinitely and read out at any given time by the application of a pair of advancing pulses.

Physically this is possible due to the existence of two limit cycles of the hysteresis loop when the two alternate advancing pulses are applied. As shown in Fig. 3, the upper loop represents the cyclic change of magnetization of cores when digit "1" is stored. The lower small loop represents the cyclic change of magnetization of cores when digit "0" is stored. In either case an advancing pulse changes the magnetization of one core along the curve a to b to c while that of the other core, through the linking coils, changes from c to d to a. Depending on the initial state of magnetization of the first core, the hysteresis loop follows either the upper or the lower curve.

[1] Chapter IV, Progress Report No. 2, November 10, 1948; the Computation Laboratory, Harvard University, under Contract W19-122-ac-24 with the U. S. Air Force.

III. PROPAGATION OF INFORMATION ALONG A DELAY LINE

The requirement for a magnetic delay line is that it should be able to store a series of information pulses and deliver them back at a later time. A number of magnetic cores are needed. These should be so constructed as to work in the following manner: When the first information pulse has been stored in the first magnetic core, an advancing pulse is applied to this core to transfer the information to the next core. This is necessary in order to make the first core ready to receive and store the second-information pulse. Next, these two signals are advanced further to make room for the storage of the third. This process of advancing and storing continues to the end of the line, where the information signal is sent out. If, after the line is loaded with information, no further advancing pulses are applied, the information will stay in the cores indefinitely. When advancing pulses are once again applied, the stored information is discharged. If the output of the delay line is connected to its input, a closed ring results. Information can be kept circulating around the ring continuously by the advancing pulses, and can be reproduced at any time. The same is true for magnetic recordings on a rotating storage drum, except that in the latter case the mechanical rotation of the drum is used to carry the information along, whereas in the present scheme advancing pulses are used to propagate the information.

Since all the magnetic cores in such a delay line are connected in tandem through the linking coils, two possible effects must be prevented before the desired information transfer can be made. First, an advancing pulse should advance a digit only in the forward direction; any backward flow of information is to be avoided. Second, an advancing pulse should advance a digit to the next core only; any effect of the digit on cores beyond this would interfere with previous digits. Of course it is imperative for successful operation that the signal should not fade along the line.

IV. A DELAY LINE OF THREE CORES PER BINARY DIGIT

A circuit has been developed which is based on the fundamental requirements of a delay line, discussed in Section III. The connections are shown in Fig. 4. Three cores are necessary for the storage of each binary digit. Three such cores together will therefore be referred to as one storage unit. Three successive pulses are required to advance the information from one storage unit to the next. These pulses, respectively, advance the signal from the first core to the second core,

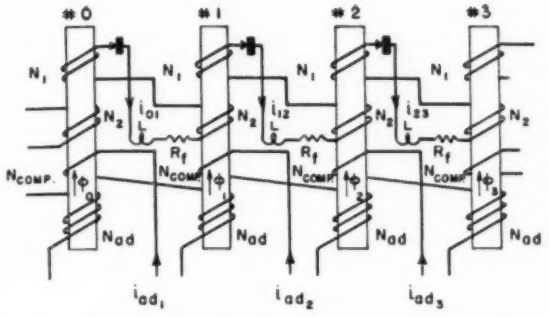

FIG. 4. Delay line structure of three cores per digit.

from the second core to the third core, and then from the third core to the first core of the next storage unit.

The operation can briefly be summarized as follows: All advancing pulses are connected so as to drive all the cores to negative saturation. When there is no information in the line, all the cores have negative residual magnetism and are thus in the "0" state. When information is stored, every third core may be positively or negatively magnetized and thus be in either state "1" or "0." Consider the case of a "0" being stored in Core 1. All advancing pulses are so connected so as to drive the cores to negative saturation. Since the residual magnetism on Core 1 is already negative and the core has essentially a square hysteresis loop, only a very small change of flux results when Advancing Pulse #1 is applied. There is no effect on other cores. The next core remains negatively magnetized. One can consider that the digit "0" information has been transferred to Core 2. On the other hand, if a "1" is stored in Core 1, it is positively magnetized. The application of i_{ad1} drives it to negative saturation. This large change of flux in Core 1 induces a large electromotive force in coils N_1 and N_2 of that core, causing i_{01} and i_{12} to flow. The current i_{12} drives Core 2 from negative magnetization to positive saturation.

The current i_{12} satisfies the following equation

$$N_1(d\phi_1/dt)+N_2(d\phi_2/dt)=[R_f+L(d/dt)]i_{12}, \quad (1)$$

where R_f represents the total resistance of the link circuit in the forward direction of i_{12} and L the leakage inductance of the linking coil. Integrating Eq. (1),

$$N_1\Delta\phi_1+N_2\Delta\phi_2=R_f\int i_{12}dt+L\Delta i_{12}.$$

Note that i_{12} is always a positive quantity due to the presence of the rectifier. Δi_{12} vanishes as the fluxes of Cores 1 and 2 reach a constant value. We get

$$\Delta\phi_2=-(N_1/N_2)\Delta\phi_1+R_f\int i_{12}dt. \quad (2)$$

The last term in Eq. 2 is always a positive quantity. If Cores 1 and 2 have the same dimensions, the flux change of ϕ_2 is not complete unless N_1 is greater than N_2. The optimum ratio of N_1 to N_2 is found to be close to 2:1.[2] The resultant change of flux of Core 2 has no effect on Core 3 because the linking current i_{23} is blocked by the rectifier in the circuit. This satisfies the requirement that information may not advance to cores beyond the next one. The current i_{01} is not desirable because it has the tendency to transfer information backward from Core 1 to Core 0. This current must be balanced by the use of a compensating winding, so that the net magnetizing force is always negative in Core 0 to maintain its negative saturation when information is being transferred from Core 1 to Core 2. Since this process of transfer affects only the three cores 0, 1, and 2, another digit in Core 4 can be transferred at the same time without interference in any other cores except 3, 4, and 5.

A static magnetic storage system is then obtained in which three cores are needed to store each binary digit. Information can be stored in the cores indefinitely and can be stepped along the line in the forward direction by the application of advancing pulses. Three advancing pulses are necessary to advance the information by a single storage unit.

Figure 5 shows a breadboard connection of such a delay line for the storage of four binary digits. The information can be advanced through each storage

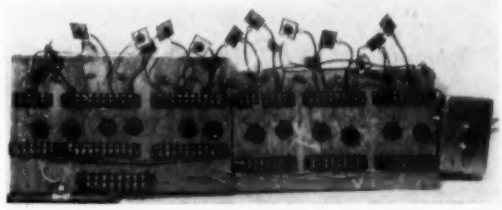

FIG. 5. Four binary digits delay line—three cores per digit.

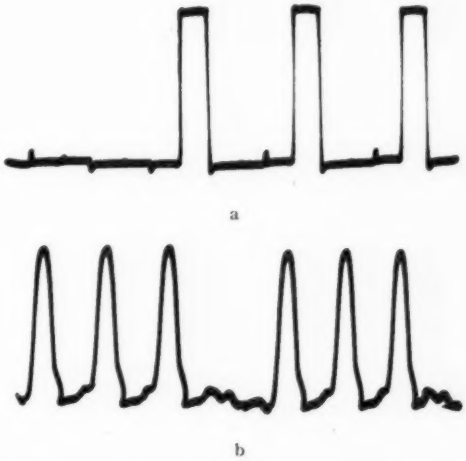

FIG. 6. Flux *vs.* time curve—three cores per digit. a. Information rate=3 kc. Information 0111. b. Information rate=30 kc. Information 1110.

[2] Chapter V, Progress Report No. 3, February 10, 1949; the Computation Laboratory, Harvard University, under Contract W19-122-ac-24 with the U. S. Air Force.

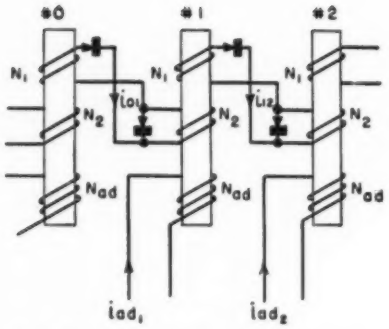

FIG. 7. Delay line structure of two cores per digit.

unit of three cores as fast as thirty thousand digits per second. Oscillographs showing flux variation of a core rate of 3000 and 30,000 digits per second are given in Fig. 6.

Small selenium rectifiers are used in the linking circuit. The rectifiers can be replaced by saturable reactors which offer a high reactance for current in one direction and a low reactance for current in the other direction. But since a reactor is not a highly dissipative element, its use prevents the linking current from dying down fast. This greatly reduces the maximum possible rate of advancing.

An analytical investigation of the sotrage unit in which rectifiers are used in the link circuits is given in reference 2.

V. A DELAY LINE OF TWO CORES PER BINARY DIGIT

As shown in the last section (Fig. 4), the compensating winding is necessary to counteract the effect of the current i_{01} flowing in the coil N_1 of Core 0. If this current can be eliminated, clearly no compensating winding is necessary. It can be done by the introduction of another rectifier,[3] as shown in Fig. 7. In the drawing the leakage inductance and circuit resistance have been omitted in the linking circuit for simplicity. The shunting of a rectifier across the coils N_2 is in such a direction that the current i_{12} is unaffected and produces the useful effect of transferring information from Core 1 to Core 2. But the current i_{01} is greatly reduced by the rectifier which short-circuits the electromotive force generated across N_2 of Core 1. The information then does not flow backward. Since only two cores are now involved in transferring the information, the next two cores can be used for another digit. It is then possible to use only two cores per binary digit.

Figure 8 shows an assembly of a delay line of this design to hold ten digits. Only two advancing pulses are needed to advance the information along the line. A few patterns of the flux variation in cores of this type of delay line are shown in Fig. 9, the repetition rate being 2.5 kc and 25 kc.

The only disadvantage of this connection is that the current flowing in coil N_2 of Core 1 is larger than before. This necessitates a more powerful advancing pulse to change the flux of Core 1.

Another possible arrangement is to apply a series voltage in the link 0–1 when i_{adv} is applied to Core 1 (Fig. 10). This series voltage is opposite to, and slightly greater than, the voltage generated in coil N_2 of Core 1. The transfer of information from Core 1 to Core 2 is made still easier. This scheme has also proved to be successful.

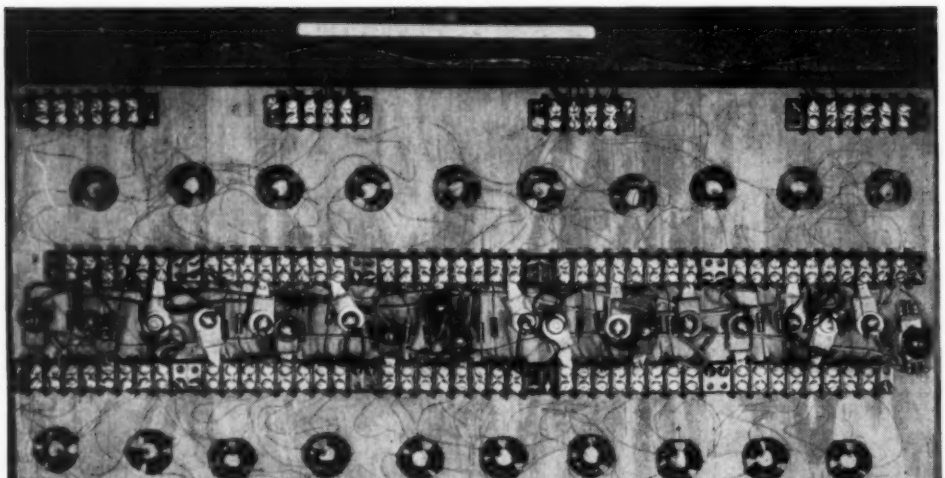

FIG. 8. Ten binary digits delay line—two cores per digit.

[3] Chapter V, Progress Report No. 4, May 10, 1949; the Computation Laboratory, Harvard University, under Contract W19-122-ac-24 with the U. S. Air Force.

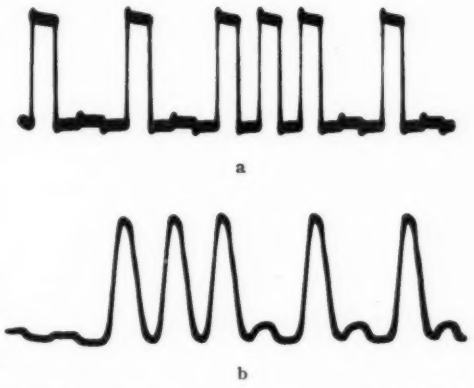

FIG. 9. Flux *vs.* time curve—two cores per digit. a. Information rate=2.5 kc. Information 1010111010. b. Information rate=25 kc. Information 0011101010.

VI. PROPERTIES OF MAGNETIC CORE MATERIAL

As shown in Fig. 11, the ideal hysteresis characteristics of the magnetic storage and delay line are a perfectly rectangular hysteresis loop and a very low coercive force.

In actual practice, unfortunately, such characteristics cannot be realized. Figure 12 shows a typical hysteresis curve for one of the cores manufactured by the Allegheny-Ludlum Steel Corporation of wound strips of Deltamax. The hysteresis loop is close to the ideal; nevertheless, the saturated region is not absolutely of zero slope, and the sharply rising portion is not quite vertical. In addition, the corners are somewhat rounded. But delay lines using such cores have been constructed and operate reliably. The criteria of how good the hysteresis loop is must have been discussed in reference 2.

As the frequency of operation becomes higher, the hysteresis and eddy current losses become appreciable. The heat generated is considerable at the highest frequency of operation. Moreover, the eddy current acts like a short-circuited secondary around the core. The presence of the eddy current requires a larger advancing current to drive the core from one polarity to the other.

At an operating frequency of 50 kc, every core alternates its flux between two saturation values in 10 microseconds. Assume that the flux changes linearly. This is a fairly accurate assumption, as seen from an oscillograph of flux variation. The cores used are made of a strip of one-mil thickness, $\frac{1}{8}$ inch wide, wound into a single-turn core of $\frac{1}{2}$-inch diameter. The hysteresis loss is estimated to be of the order of 7 milliwatt/core, the eddy current loss 25 milliwatt/core, the electrical resistivity of the core being taken as 50 microhm centimeters. For such a core the equivalent demagnetizing ampereturns can be calculated to be about 1.2. It is also equivalent to an increase of coercive force of 0.37 oersted. Apart from the upper frequency limits imposed by these losses, the fundamental operation of the storage and delay line is independent of the frequency.

VII. APPLICATIONS

It may be helpful to point out the unique features of this form of storage. No power is needed to maintain the storage of information. No mechanical movement is needed in recording and pick-up. The speed of recording, transfer, and read out has no lower limit and can be varied to an upper limit which is sufficiently high to be very useful. At the present stage, this maximum rate is of the order of 50 kc. These features represent improvements over the characteristics of the storage devices mentioned in the introduction.

Possible applications include the following:

1. *Information storage.* Individual binary digits can be stored in pairs of cores, as discussed in Section II. If a series of digits is to be stored, the information can be sent into a delay line. After the whole series of digits is in the line, stopping the flow of advancing pulses suffices to store the information indefinitely in the line. It can be read out at any time at the end of the line by applying the advancing pulses again. Development work is being done at the Computation Laboratory of Harvard University to construct a line holding 40 binary digits in a plug-in component container unit which will be no more than two inches in diameter and six inches in length.

2. *Input and output link for high speed computers.* This form of delay line provides an excellent medium for transfer of information between systems of different digital rate. Data and commands can be put into the line manually and then read out to the machine at its operating speed. Again, results from the machine can be fed at high speed into the delay line, from which later a set of slow advancing pulses can step the results out at a speed suitable, say, to operate a typewriter directly.

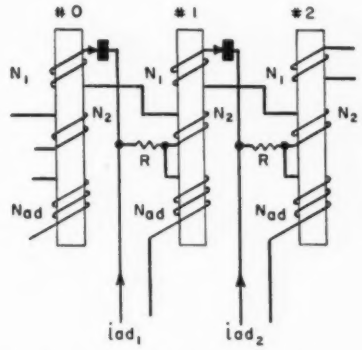

FIG. 10. Another form of delay line of two cores per digit.

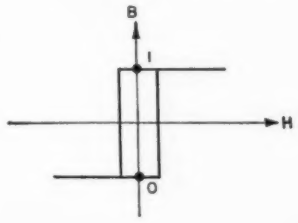

FIG. 11. Ideal hysteresis loop.

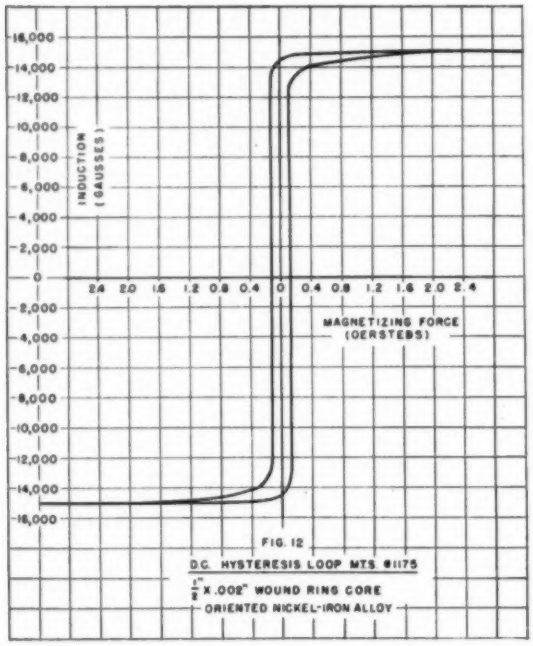

FIG. 12. Typical hysteresis loop of materials used.

3. *Counter.* Since the information stored in the delay line must be stepped along by advancing pulses, it is possible to register a single digit at the beginning of the line, and by the location of this digit along the line at a later instant to determine the number of advancing pulses that have been applied. So far the speed of counting is limited to about 50 kc. This, however, is sufficiently rapid to find wide applications.

4. *Telegraphy.* Because the speed of propagation is variable, a magnetic delay line may serve as the terminal storage for a high speed telegraphy system. The information on a high speed telegraphic line can be distributed to several delay lines. While some lines are being filled, any one of them can be discharged much more slowly to a separate line or directly to a typewriter. Similarly, several slow speed information sources can be read into the magnetic delay lines and then be fed into a high speed telegraphic line by electronic switching control of the advancing pulses.

VIII. ACKNOWLEDGMENTS

The magnetic core materials employed in this research were supplied by the Allegheny Ludlum Steel Corporation, whose cooperation and assistance the authors wish to acknowledge. The use of magnetic cores as a means of obtaining static magnetic storage was originally proposed by Howard H. Aiken, director of the Computation Laboratory, who has worked closely with the authors.

A General Solution for the Bending of Beams on an Elastic Foundation of Arbitrary Continuity*

M. HETÉNYI
Northwestern Technological Institute, Evanston, Illinois
(Received July 29, 1949)

In the analysis of beams which are supported elastically along their entire length, it is usually assumed that the elastic support is provided either by a series of independent springs, or by a completely continuous elastic medium.

The present paper proposes a method of solution for the intermediate cases, that is, for foundations of partial continuity, by assuming that such foundations may be represented by beams imbedded into an otherwise discontinuous supporting material. In a foundation of this type, there are three independent elastic constants, the resilience of the discontinuous spring layers above and below the beam that is within the foundation, and the flexural rigidity of the foundation beam itself. By changing the values of these three constants, elastic foundations of a wide variety may be produced or, conversely, the constants may be adjusted in such a manner as to represent approximately the characteristics of any given elastic supporting medium.

In the paper a general procedure is presented from which solutions can be derived for the bending of beams on such foundations under any loading or end conditions. The method is illustrated by examples showing the range of pressure distributions that may occur under beams supported on foundations of this type.

IN dealing with problems of bending of beams which are supported elastically along their entire length, it is usually assumed that the supporting medium is provided either by a series of independent springs, or by a completely continuous elastic body. Solutions for a large variety of problems were developed in the past on the basis of either of these two assumptions.† There remains an obvious need, however, for a method of analyzing the intermediate cases, where the foundation material may exhibit an arbitrary and partial degree of continuity. The aim of the present paper is to propose a method of solution for problems of this kind.

A partially continuous foundation will be assumed in this analysis as composed of a bending resistant beam, imbedded between two layers of otherwise independent elastic springs. A foundation of this type can be characterized by three elastic constants, the k_1 and k_2 spring constants (lb./in. per inch) of the two layers, and the flexural rigidity EI_2 of the beam within the foundation. If a trial load q lb./in. is placed along a length b on the surface of such a composite foundation, the resulting deflection line may also be defined by three data, namely, by the amount of local deflection δ_1 within the loaded region, by the maximum deflection ordinate δ_2 of the continuous part of the displacement curve, and by the distance d at which displacements vanish [Fig. 1(a)]. The three characteristic constants of the foundation, k_1, k_2, and EI_2, can be calculated from the observation data, δ_1, δ_2, and d, on the basis of the following relationships in the known solution of a single beam on an elastic foundation without continuity: $\delta_1=q/k_1$, $\delta_2=qb(\lambda_2/2k_2)$, and $d=3\pi/4\lambda_2$, where $\lambda_2=(k_2/4EI_2)^{\frac{1}{4}}$.

If a load carrying beam of flexural rigidity EI_1 is placed on a foundation defined by these three constants, k_1, k_2, and EI_2, as shown in Fig. 1(b), the differential equations of bending may be derived as follows: denoting the deflection ordinates of the upper and the lower beam by y_1 and y_2, respectively, we find that the pressure in the foundation under the upper beam is $p_1=k_1(y_1-y_2)$, and under the lower beam $p_2=k_2y_2$, while the resultant pressure acting on the lower beam is $p_2-p_1=(k_1+k_2)y_2-k_1y_1$. Since these pressures are continuously distributed along the two beams, we have from the flexural theory:

$$EI_1(d^4y_1/dx^4)=-p_1=-k_1(y_1-y_2) \tag{a}$$

and

$$EI_2(d^4y_2/dx^4)=-(p_2-p_1)=-(k_1+k_2)y_2+k_1y_1. \tag{b}$$

The pressures in these cases are considered positive when accompanied by positive (downward) deflections. From (a) we have

$$y_2=\frac{EI_1}{k_1}\frac{d^4y_1}{dx^4}+y_1 \tag{c}$$

or

$$\frac{d^4y_2}{dx^4}=\frac{EI_1}{k_1}\frac{d^8y_1}{dx^8}+\frac{d^4y_1}{dx^4}. \tag{d}$$

On substituting these expressions into (b), y_2 will cancel out, and we have the differential equation of the elastic line of the upper beam

$$(d^8y_1/dx^8)+2\alpha(d^4y_1/dx^4)+(\alpha_2-\beta_2)y_1=0,$$

where

$$\alpha=[k_1(I_1+I_2)+k_2I_1]/2EI_1I_2$$

and

$$\beta=[\alpha^2-(k_1/EI_1)(k_2/EI_2)]^{\frac{1}{4}}.$$

* Paper presented at the VII International Congress of Applied Mechanics, London, England, September 5–11, 1948.

† See section on references at the end of this paper.

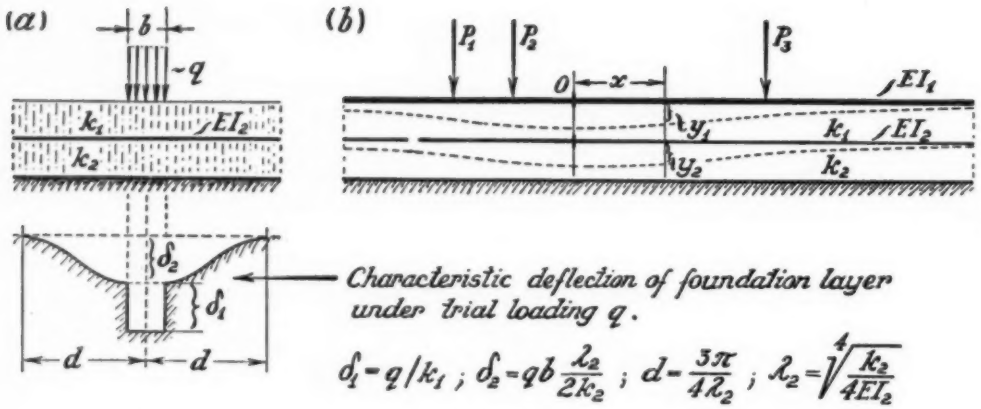

FIG. 1. Foundation layer with an arbitrary degree of continuity.

The general solution of (e) can be written in the form:

$$y_1 = e^{\lambda_1 x}(C_1\cos\lambda_1 x + C_2\sin\lambda_1 x) + e^{-\lambda_1 x}(C_3\cos\lambda_1 x + C_4\sin\lambda_1 x) + e^{\lambda_2 x}(C_5\cos\lambda_2 x + C_6\sin\lambda_2 x) + e^{-\lambda_2 x}(C_7\cos\lambda_2 x + C_8\sin\lambda_2 x), \quad (1)$$

where

$$\lambda_1 = [(\alpha+\beta)/4]^{\frac{1}{4}} \quad \text{and} \quad \lambda_2 = [(\alpha-\beta)/4]^{\frac{1}{4}}.$$

Substituting the solution from (1) into (c), we have the expression for the elastic line of the beam within the foundation:

$$y_2 = [1-(\alpha+\beta)(EI_1/k_1)][e^{\lambda_1 x}(C_1\cos\lambda_1 x + C_2\sin\lambda_1 x) + e^{-\lambda_1 x}(C_3\cos\lambda_1 + C_4\sin\lambda_1 x)] + [1-(\alpha-\beta)(EI_1/k_1)] \times [e^{\lambda_2 x}(C_5\cos\lambda_2 x + C_6\sin\lambda_2 x) + e^{-\lambda_2 x}(C_7\cos\lambda_2 x + C_8\sin\lambda_2 x)]. \quad (2)$$

Expressions for the slope $\theta = dy/dx$, bending moment $M = -EI(d^2y/dx^2)$, and shearing force $Q = -EI(d^3y/dx^3)$ may be obtained for each of the above beams by differentiating the corresponding equation of the elastic line, (1) or (2), respectively.

In applying the above general solutions to the analysis of beams of finite length, the scheme illustrated in Fig. 2 may be the most conveniently used. Here it is first assumed that the beam within the foundation is severed at A and B, resulting in relative displacements and rotations between the severed ends, as the upper beam is loaded. The continuity of slope and deflection in the lower beam is then re-established by the application of end forces P_0 and moments M_0 in the manner shown in the figure.

In using this method of calculation, one needs to know the particular solutions of the elastic lines corresponding to each of the loading cases shown in Fig. 2. The integration constants, C_1 to C_8, in the general solutions (1) and (2) were determined from the prevailing end conditions in each of these particular cases of loading, giving the following results.

Concentrated load P, centrally applied at the upper beam (Fig. 3).

$$C_1 = A\left[\frac{\cosh^2\lambda_1 c + \cos^2\lambda_1 c}{\sinh 2\lambda_1 c + \sin 2\lambda_1 c} - \frac{1}{2}\right]$$

$$C_2 = A\left[\frac{1}{2} - \frac{\sinh^2\lambda_1 c + \sin^2\lambda_1 c}{\sinh 2\lambda_1 c + \sin 2\lambda_1 c}\right]$$

$$C_3 = A\left[\frac{\cosh^2\lambda_1 c + \cos^2\lambda_1 c}{\sinh 2\lambda_1 c + \sin 2\lambda_1 c} + \frac{1}{2}\right]$$

$$C_4 = A\left[\frac{1}{2} + \frac{\sinh^2\lambda_1 c + \sin^2\lambda_1 c}{\sinh 2\lambda_1 c + \sin 2\lambda_1 c}\right]$$

$$C_5 = -B\left[\frac{\cosh^2\lambda_2 c + \cos^2\lambda_2 c}{\sinh 2\lambda_2 c + \sin 2\lambda_2 c} - \frac{1}{2}\right]$$

$$C_6 = -B\left[\frac{1}{2} - \frac{\sinh^2\lambda_2 c + \sin^2\lambda_2 c}{\sinh 2\lambda_2 c + \sin 2\lambda_2 c}\right]$$

$$C_7 = -B\left[\frac{\cosh^2\lambda_2 c + \cos^2\lambda_2 c}{\sinh 2\lambda_2 c + \sin 2\lambda_2 c} + \frac{1}{2}\right]$$

$$C_8 = -B\left[\frac{1}{2} + \frac{\sinh^2\lambda_2 c + \sin^2\lambda_2 c}{\sinh 2\lambda_2 c + \sin 2\lambda_2 c}\right]$$

where:

$$A = \left[\frac{k_1}{EI_1} - \alpha + \beta\right]\frac{P}{EI_1}\frac{1}{16\beta}\frac{1}{\lambda_1^3}$$

and

$$B = \left[\frac{k_1}{EI_1} - \alpha - \beta\right]\frac{P}{EI_1}\frac{1}{16\beta}\frac{1}{\lambda_2^3}.$$

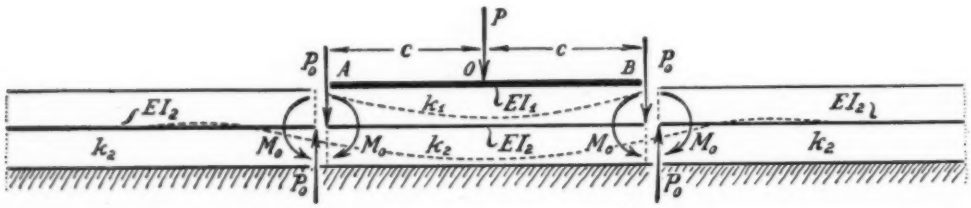

FIG. 2. Method of analyzing a beam of finite length A–B, supported on a foundation layer.

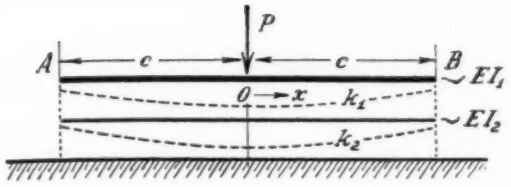

FIG. 3. Particular solution to problem shown in Fig. 2.

Lower beam subjected to equal concentrated end forces P_0 (Fig. 4).

$$C_1=C_3=-\frac{P_0}{EI_2}\frac{k_1}{EI_1}\frac{1}{4\beta\lambda_1^3}\frac{1}{\sinh 2\lambda_1 c+\sin 2\lambda_1 c}\cosh\lambda_1 c\cos\lambda_1 c$$

$$C_2=-C_4=-\frac{P_0}{EI_1}\frac{k_1}{EI_1}\frac{1}{4\beta\lambda_1^3}\frac{1}{\sinh 2\lambda_1 c+\sin 2\lambda_1 c}\sinh\lambda_1 c\sin\lambda_1 c$$

$$C_5=C_7=\frac{P_0}{EI_2}\frac{k_1}{EI_1}\frac{1}{4\beta\lambda_2^3}\frac{1}{\sinh 2\lambda_2 c+\sin 2\lambda_2 c}\cosh\lambda_2 c\cos\lambda_2 c$$

$$C_6=-C_8=\frac{P_0}{EI_2}\frac{k_1}{EI_1}\frac{1}{4\beta\lambda_2^3}\frac{1}{\sinh 2\lambda_2 c+\sin 2\lambda_2 c}\sinh\lambda_2 c\sin\lambda_2 c.$$

Lower beam subjected to equal concentrated end moments M_0 (Fig. 5).

$$C_1=C_3=\frac{M_0}{EI_2}\frac{k_1}{EI_1}\frac{1}{4\beta\lambda_1^2}\frac{1}{\sinh 2\lambda_1 c+\sin 2\lambda_1 c}\sinh\lambda_1 c\cos\lambda_1 c-\cosh\lambda_1 c\sin\lambda_1 c$$

$$C_2=-C_4=\frac{M_0}{EI_2}\frac{k_1}{EI_1}\frac{1}{4\beta\lambda_1^2}\frac{1}{\sinh 2\lambda_1 c+\sin 2\lambda_1 c}\sinh\lambda_1 c\cos\lambda_1 c+\cosh\lambda_1 c\sin\lambda_1 c$$

$$C_5=C_7=-\frac{M_0}{EI_2}\frac{k_1}{EI_1}\frac{1}{4\beta\lambda_2^2}\frac{1}{\sinh 2\lambda_2 c+\sin 2\lambda_2 c}\sinh\lambda_2 c\cos\lambda_2 c-\cosh\lambda_2 c\sin\lambda_2 c$$

$$C_6=-C_8=-\frac{M_0}{EI_2}\frac{k_1}{EI_1}\frac{1}{4\beta\lambda_2^2}\frac{1}{\sinh 2\lambda_2 c+\sin 2\lambda_2 c}\sinh\lambda_2 c\cos\lambda_2 c+\cosh\lambda_2 c\sin\lambda_2 c.$$

Semi-infinite beam on a simple elastic foundation loaded by concentrated end force P_0 and moment M_0 (Fig. 6). Equation of elastic line:

$$y=\frac{2P_0\lambda}{k_2}e^{-\lambda x}\cos\lambda x-\frac{2M_0\lambda^2}{k_2}e^{-\lambda x}(\cos\lambda x-\sin\lambda x),$$

where $\lambda=[(k_2/4EI_2)]^{\frac{1}{4}}$.

The wide range in the pressure distribution types which may be covered by this theory is illustrated in Fig. 7, where a centrally loaded beam of length $2c=280$ in. and flexural rigidity $EI=250\times10^6$ lb. in.^{2} is placed on foundations with increasing degree of continuity. On the left side of the figure the characteristic deflection curves are shown for each of the three types of foundation, as they are subjected to a trial load of $q=10$ lb./in. distributed along a length of 10 in.

The first type of foundation lacks continuity entirely, and its spring constant can be calculated through dividing the applied trial load q by the observed local deflection ordinate $k=10/0.75=13.33$ lb./in.^{2}. The second type of foundation is characterized by a local deflection of $\delta=0.25$ in. and a continuous deflection curve of maximum ordinate of $\delta=0.50$ in. and wave-length $d=50$ in., which define the following elastic constants for the foundation layer: $k_1=20$ lb./in.^{2}, $k_2=8.44$ lb./in.^{2}, and $EI_2=0.476\times10^8$ lb. in.^{2}. The third type of foundation is assumed to have the greatest degree of continuity, with two-thirds of the maximum deflection being of the continuous type, $\delta_1=0.25$ in. and $\delta_2=0.50$ in., and the effect of continuity being observable up to a distance of $d=100$ in. from the center of application of the trial load, which define the following elastic constants for the foundation layer: $k_1=40$ lb./in.^{2}, $k_2=2.36$ lb./in.^{2}, and $EI_2=1.90\times10^6$ lb. in.^{2}.

The pressure distribution under the loaded beam for each of the average pressure $p_0=P/2c$. It is to be noted that the flexural values of the loaded beam ($2c=280$ in., $EI_1=250\times10^6$ lb. in.^{2}) and the total compressibility of the foundations ($\delta_1+\delta_2=0.75$ in.) were the same in each case, thus the pronounced difference in the resulting pressure distributions was due solely to the different degrees of continuity in the material of the foundation.

The outlined method of analysis may be applied to any elastic supporting medium (subsoils, elastic layers, packing or gasket materials etc.) which exhibits a partly local and partly continuous deflection curve when tested under localized pressure. Though in the paper

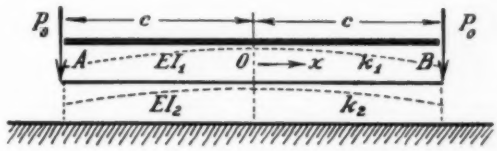

FIG. 4. Particular solution to problem shown in Fig. 2.

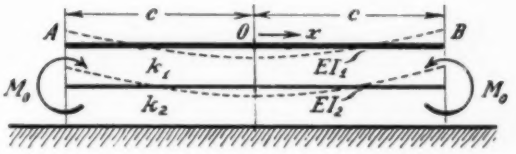

FIG. 5. Particular solution to problem shown in Fig. 2.

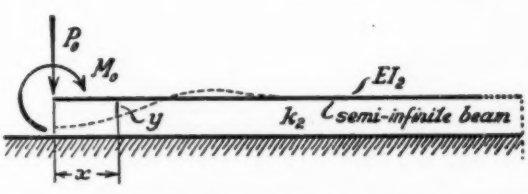

FIG. 6. Particular solution to problem shown in Fig. 2.

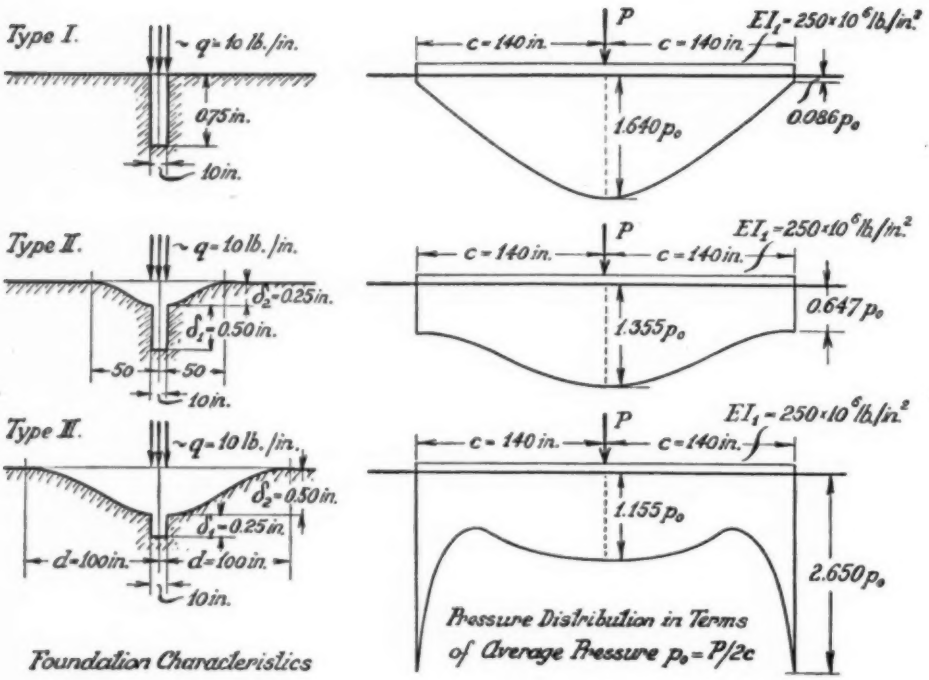

FIG. 7. Pressure distribution under a centrally loaded beam, supported on foundations with various degrees of continuity.

only one-dimensional problems were considered, when beam and foundation are of the same constant width, the same principle may be readily extended to the analysis of corresponding two-dimensional plate problems.

REFERENCES

The discontinuous type of elastic foundation was first introduced by E. Winkler [*Die Lehre von der Elastizität und Festigkeit* (Prague, 1867)]. This type of foundation was assumed in the rail investigations by H. Zimmermann [*Die Berechnung des Eisenbahnoberbaues* (Berlin, 1888)], and a large variety of solutions developed on this basis were discussed by K. Hayashi [*Theorie des Trägers auf elastischer Unterlage* (Berlin, 1921)].

Problems of beams supported on an elastic continuum were investigated, among others, by K. Wieghardt [Zeits. f. angew. Math. Mech. **3**, 165–184 (1922)], M. A. Biot [J. App. Mech. **A**, 1–7 (1937)], and G. Bosson [Phil. Mag. 37–50 (1939)].

A comprehensive study of both types of foundations and the first exposition of the concept of partially continuous foundations may be found in the author's book *Beams on Elastic Foundation* (University of Michigan Press, Ann Arbor, 1946).

Letters to the Editor

Microwave Frequency Dividers

HAROLD LYONS
National Bureau of Standards, Washington, D. C.
August 8, 1949

IN order to extend the range of application of microwave techniques it is becoming more and more important to be able to carry out the operation of frequency division in the microwave region just as at lower frequencies. Such needs are felt, particularly, in connection with spectroscopic or atomic clocks and frequency standards which usually use spectrum lines in the neighborhood of 3000–20,000 Mc or higher.[1] It is therefore necessary to look for a frequency division principle which uses components and techniques that are practicable in the microwave range.[2]

One could inject a signal to be divided into an oscillator operating at a sub-multiple of the injected frequency and lock it in.[3] This well-known principle has obvious disadvantages. If control is lost the lower frequency oscillator will run free. A frequency divider which avoids this difficulty and which is widely used at low frequencies, e.g., in precision quartz-crystal clocks, is the regenerative modulator type.[4] This circuit also works well even in the presence of high noise levels and distorted input signals. It can be designed so that the output will be linearly dependent on the input and maintain a constant phase angle with respect to it. It can generate both sub-multiple and other fractional frequency ratios. Such a circuit to divide down from 9300 Mc to 3100 Mc has been built and tested.[5] A block diagram is shown in Fig. 1. Here it is seen that the 9300 Mc signal is applied to a mixer; to the mixer is also applied a signal at 6200 Mc. This may be a noise component or transient generated by turning the circuit on. The 6200 Mc signal beats with the 9300 Mc input signal to give an output of 3100 Mc. This is amplified by means of the Sperry 2K35 klystron amplifier tubes, and then fed to a Sperry 2K46 klystron multiplier which is tuned to double the input signal to 6200 Mc. After multiplication the signal is amplified at 6200 Mc by means of a Sperry SAC-19 klystron amplifier and fed back to the mixer. If the gain around the feedback loop is great enough, the output signal at 3100 Mc will be maintained independently of the phase shift in the feedback loop. No output will appear unless there is an input signal since the 3100 Mc beat note can only be obtained in this way. If the gain is not high enough in the regenerative circuit it may be necessary to start the operation by injecting some sort of transient. In the circuit shown this was not necessary. Since no attempt was made in this first circuit to design a very efficient mixer, it may not be necessary to use all of the amplification shown in Fig. 1. In principle, the 2K46 frequency multiplier could be replaced by any nonlinear modulator device, such as a crystal rectifier if enough gain were available and the signal level high enough.

Among numerous tests conducted, the input, intermediate, and output frequencies were measured and found to track each other and it was also shown by the insertion of wave-guide filters that no other output signals were present except those in the 3000 Mc range. The output signal was taken from the middle cavity of one of the 2K35 tubes. A definitive test of the accuracy of frequency division was made as follows. The 9300 Mc input signal was fed to a spectrum analyzer where it was viewed on the scope as a pip. The output signal was monitored by means of a frequency meter and second spectrum analyzer. In addition it was fed to a crystal multiplier which multiplied by three and then fed to the same spectrum analyzer as the input frequency. If the output frequency times three is exactly equal to the input frequency, the two pips on the scope should coincide. The two individual pips could be identified by first displaying one and then the other by control of their intensities by means of attenuators. When the two pips were superimposed they blended smoothly into one larger pip; this was done under conditions of highest dispersion in the spectrum analyzer. No beating of the two signals whatsoever could be discerned nor any shift or change in shape of the pulses. If it is assumed rather arbitrarily that a beat note of approximately one cycle per second could be observed, this means that the output frequency times three was equal to the input frequency with an accuracy of at least one part in 10^{10}. In this type of test no difficulty results if the input-oscillator-frequency slowly drifts back and forth since the output frequency drifts with it. It is clear that direct frequency calibrations of extreme accuracy would be necessary to obtain a test with the sensitivity of the one just described.

Since another klystron multiplier tube, the Sperry 2K47, is commercially available and multiplies from approximately 270 Mc up to the 3000 Mc range, frequency dividers could be built to go down to as low a frequency as desired. It is important to note that in this type of circuit it is not necessary to have amplifiers available at the input frequency but only at a lower frequency, essentially a divided frequency. Since klystron multipliers are very efficient and much easier to make than amplifiers, a multiplier tube and frequency divider dividing down from the 24,000 Mc region, rich in spectrum lines, should be possible.

Since amplifiers in this type of circuit are only needed at the divided frequency, some interesting possibilities are opened up by consideration of circuits of the type shown in Fig. 2. In this circuit we make the regenerative-modulator divider provide its own input by providing a second regenerative channel. In this case, if there is enough gain, the circuit should oscillate and divide in frequency at the same time. A more general arrangement allowing more flexibility in the choice of frequencies which can be used with any given set of tubes is shown in Fig. 3. Figures 2 and 3 show a proposed application to an atomic oscillator and atomic clock.[5] Here by atomic oscillator we mean a self-excited or feedback oscillator, the frequency of which is directly controlled by an absorption cell. This is in contra-distinction to the stabilized servo mechanism or frequency discriminator type of spectrum-line controlled oscillators.[1, 6] To make an atomic clock it is then necessary to divide down by means of straight frequency division from the atomic oscillator to a frequency low enough to drive the usual synchronous motor type of clock. Two types of atomic oscillators in which the

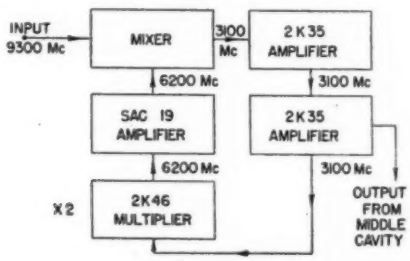

FIG. 1. Microwave regenerative modulator frequency divider, dividing 3 to 1.

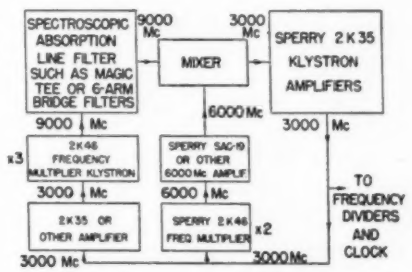

FIG. 2. Proposed combination atomic oscillator and frequency divider, using amplifiers at divided frequencies, applied to an atomic clock.

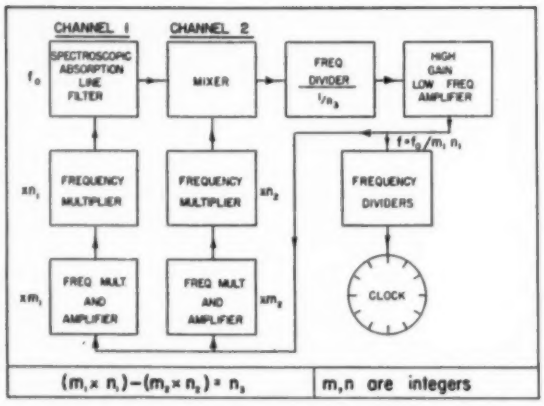

FIG. 3. General and more flexible block diagram of atomic clock using combination oscillator and divider.

feedback frequency is controlled by means of spectroscopic circuits have been described.[1,2,5] Here the spectroscopic filter is based on the use of a magic-tee or a six-arm, wave-guide Wheatstone bridge in which an absorption cell containing ammonia or other absorbing gas at low pressure determines the frequency which will be transmitted by the filter. As shown in Fig. 3, this spectroscopic filter transmits an input frequency to the regenerative modulator only at the frequency of the spectrum line used in the filter. This, therefore, controls the frequency of the oscillator and similarly that of the divided frequency. However, as compared to the atomic oscillators previously described, in this method not only is frequency division carried on simultaneously with controlled oscillation, but an amplifier at the spectrum line frequency is no longer needed.

Although it is very desirable to go back up to the 3,3 line of ammonia at approximately 24,000 Mc, and we are attempting development and procurement of suitable multiplier and amplifier tubes for this purpose, an atomic clock could be developed using a spectrum line in the 9000 Mc range using available amplifier and multiplier tubes and the circuit shown in Fig. 2. For this purpose the various deuterated species of ammonia were prepared and spectrum lines searched for in order to provide a strong absorption line at a lower frequency. Although this work is still incomplete, about 30 lines have been found in the range between 3000 and 10,000 Mc.[5] Such spectrum lines can be used to make a clock following the circuit shown in Fig. 2 or simply used in a separate atomic oscillator driving a frequency divider.

[1] "The Atomic Clock, an Atomic Standard of Frequency and Time," NBS Technical News Bulletin **33**, (February, 1949). Also, Harold Lyons, Phys. Rev. **74**, 1203 (1948).
[2] "Microwave spectroscopic frequency and time standards," Harold Lyons, presented at the AIEE-IRE-NBS Conference on High Frequency Measurements, Washington, D. C., January, 1949. Also, Electrical Engineering **68**, 251 (1949).
[3] E. Norrman, Proc. I.R.E. **34**, 799 (1946).
[4] R. L. Miller, Proc. I.R.E. **27**, 446 (1939). Also, W. A. Morrison, Bur. Stand. Tech. J. **27**, 510 (1948).
[5] Harold Lyons, Phys. Rev. **76**, 161 (1949).
[6] a. Chaffee, Fletcher and Cooke, Harvard University Progress Reports on Contract N5-ORI-76, 1947–1949. b. R. V. Pound, Rev. Sci. Inst. **17**, 490 (1946); Smith, DeQuevedo, Carter, and Bennett, J. App. Phys. **18**, 1112 (1947); DeQuevedo and Smith, J. App. Phys. **19**, 831 (1948); c. W. D. Hershberger and L. E. Norton, RCA Rev. **9**, 38 (1948). d. C. H. Townes, A. N. Holden, and F. R. Merritt, Phys. Rev. **74**, 1113 (1948).

Particle Size of Evaporated Gold

P. G. WILKINSON AND L. S. BIRKS
U. S. Naval Research Laboratory, Washington, D. C.
October 5, 1949

MANY observers have noted that the gold on shadowed electron micrographs granulates when exposed to an intense beam of electrons. It has been generally assumed that before electron bombardment, the gold was a smooth continuous film. Picard and Duffendack[1] published micrographs of gold evaporated at 10^{-6} mm pressure in which the gold appeared as discreet particles. From work[2] we have done on correlating electrical resistance properties of gold with microstructure, we believe that such is generally the condition of evaporated gold except when contaminated by the presence of tungstic oxide. In the usual bell jar conditions for gold shadowing electron micrographs at about 10^{-3} mm pressure, the deposit contained about five percent tungsten by analysis. This gave a characteristic matte background which was observed no matter how careful the operator was to use low beam intensity and fast exposure. When the percentage of tungstic oxide was reduced either by pumping to lower pressure or by flushing the system during evaporation with a few microns of purified nitrogen, free of oxygen, the gold appeared as discreet particles, similar to those observed by Picard and Duffendack. Such deposits showed no tungsten by chemical analysis. Figure 1

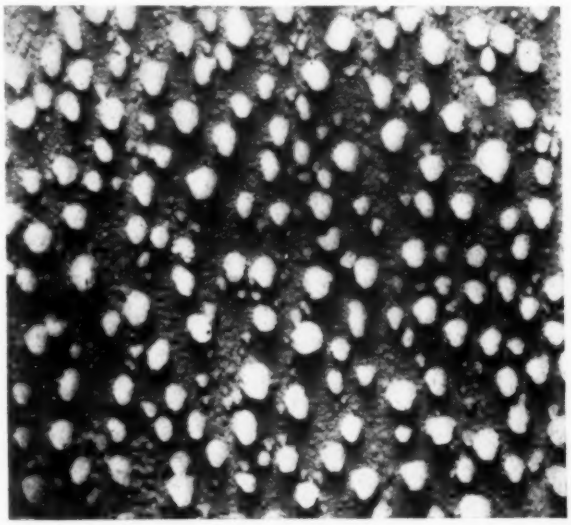

FIG. 1. Gold evaporated at 10^{-6} mm pressure and shadowed with tungstic oxide.

proves the existence of discreet gold particles before electron bombardment. The gold was evaporated at 10^{-6} mm pressure and then shadowed with tungstic oxide before it was placed in the microscope. The shadows could not have appeared if the granulation had taken place in the electron microscope.

Figure 1 is typical of all the tungsten-free gold deposits we have observed.

[1] R. G. Picard and O. S. Duffendack, J. App. Phys. **14**, 291 (1943).
[2] P. G. Wilkinson and L. S. Birks, J. App. Phys. (to be published); P. G. Wilkinson and L. S. Birks, N.R.L. Report No. P-3443.

Energy Partition in Isothermal Fracture*

MARGUERITE M. ROGERS**
The University of North Carolina, Chapel Hill, North Carolina
AND
F. T. ROGERS, JR.†
Oak Ridge National Laboratory, Oak Ridge, Tennessee
October 14, 1949

MEASUREMENTS have been made of the elastic potential energy (e) and absorbed energy (w) associated with the fracture of four-notch specimens ($0.70''\times0.75''\times4.6''$ with 15 percent Izod notches) of a special aluminum-killed mild steel (Bethelehem), by observing for several values of deformation (s),

TABLE I. Relative properties of pre-brittle and ductile specimens, expressed as ratios derivatives for particular pre-brittle specimens to derivatives for the mean of ductile specimens.

x (in.)	Specimen number, B-series	dx_B/dx_D	dw_B/dw_D	G_B/G_D
0.02	208	1.2	0.8	1.1
0.04		1.6	0.3_5	1.0
0.058*		9	0.1_5	0.4
0.04	203	1.10	0.76	1.0_5
0.058		1.13	0.81	1.0_5
0.10		1.16	0.93	1.0_3
0.14		1.19	0.95	0.9_8
0.175		1.54	0.83	0.9_4
0.22		1.90	0.56	0.8_2
0.245		9.5	0.21	0.5
0.04	237	1.10	0.71	1.0_5
0.058		1.13	0.75	1.0_5
0.10		1.16	0.78	0.9_8
0.14		1.54	0.72	0.9_4
0.175*		8.1	0.20	0.7

* Brittle fracture occurred 0.005 in. in excess of these values, for the respective specimens.

the fracture depth (x), and the applied dynamic load. Specimens were held thermostatically at temperatures between 0°F and 50°F so that strain ageing would be small, and deformation was effected very slowly at a constant rate. The essential features of the apparatus have been described elsewhere.[1] At the higher temperatures the specimens fractured in a controlled (ductile) manner, but at the lower ones many ultimately underwent uncontrolled (brittle) fracture during test; however, temperature did not affect the data measureably.

When plotted against s, the data for ductile and pre-brittle specimens were identical. But when plotted against x, the data clearly identified the pre-brittle specimens as different from the ductile ones which were chemically and metallurgically identical with them. As Table I shows (in terms of derivatives), brittle fracture was preceded in the pre-brittle phases by excessive fracture depths and by deficient (in terms of x) energy absorption (see columns 3 and 4, respectively). The three brittle specimens reported in Table I are representative of the many others observed.

Column 5 in Table I refers to the function

$$G=1+de/dw. \tag{1}$$

G. R. Irwin has suggested[2] that a controlled fracture should become uncontrolled when $G\rightarrow 0$, by extending the concepts of A. A. Griffith.[3] Although the present data are not sufficiently precise to provide an ultimate test of Irwin's suggestion, they are in entire accord with it as far as they go, and to that extent serve to emphasize the significance of energy partition in macrofracture phenomena.

* The experimental portions of this work were carried out in the research laboratories of The University of North Carolina under the provisions of Contract No. N6-ori-227 (and Amendment I) of the ONR with the University. Dr. P. E. Shearin and Mr. R. M. Trimble provided material assistance.

** Address at the time of writing: Oak Ridge National Laboratory, Oak Ridge, Tennessee.

† Present address: U. S. Naval Ordnance Test Station, Inyokern, California.

[1] Shearin, Ruark, and Trimble, *Strength of Solids* (Physical Society, London, 1947), p. 158; *Fracturing of Metals* (Am. Soc. Metall., 1948), p. 167.
[2] G. R. Irwin, *Fracturing of Metals* (Am. Soc. Metall., 1948), p. 147.
[3] A. A. Griffith, Phil. Trans. Roy. Soc. (London) **221**, 163 (1920).

A Low Temperature Replica Method for Electron Microscopy

C. E. HALL
Massachusetts Institute of Technology, Cambridge, Massachusetts
September 6, 1949

A REPLICA method has been tested which appears to be of value for the electron microscopy of aqueous substances while they are in the frozen state. The apparatus employed is shown diagrammatically in Fig. 1. The specimen, A, on glass is supported in a vacuum chamber in contact with a copper block, B, which is pre-cooled to liquid air temperature. The block is suspended from a glass rod and can be set at any desired angle by means of a conical vacuum plug. When a vacuum has been obtained, the temperature of the specimen is temporarily raised to about −60° to −90°C with radiant heat from an external microscope lamp in order to sublime ice crystals which may have condensed on the specimen from the atmosphere and also to secure a surface etch. In the absence of an intense source of radiant heat, the conductivity of the supporting glass is sufficient to maintain the specimen at a temperature close to that of the cold sink. After the etching procedure, the specimen is shadowed with Cr and a supporting film of Si evaporated from a BeO crucible[1] is deposited on the surface at normal incidence. (Although Si was used on these experiments, SiO has subsequently proved more convenient for evaporated films since it does not attack tungsten.) Finally, the cold block is removed from the vacuum, the glass plate is detached and the surface film is floated on water after the specimen has warmed to room temperature.

In order to test the feasibility of the method a dilute aqueous suspension of silver halide particles from a photographic plate was used as a test object. Silver halide was removed by floating the replica film on sodium hyposulfite. A micrograph of such a film is shown in Fig. 2. Although the etch was too light to cause the large particles to project far above the surface their outline may be discerned. The surrounding surface of frozen, dilute gelatin displays a crater-like structure, the significance of which is not understood at present. No evidence of gross ice crystals has been observed within quick-frozen specimens.

The micrograph in Fig. 3, for which the etching procedure was omitted, shows ice crystals condensed from air on the surface of frozen distilled water. The micrograph demonstrates the feasibility of obtaining replicas of ice surfaces in this manner and also emphasizes the necessity for either carefully shielding the cold specimen surface or removing the condensed moisture by sublimation before the process is employed.

Since the method depends on the immobilization of a water surface in a vacuum, it is of interest to estimate the rate at which water will sublime from a specimen. The rate of sublimation can be computed[2] for a given temperature from a knowledge of the equilibrium vapor pressure of ice which is tabulated[3] to −98°C and extrapolated values may be obtained with the aid of Clapey-

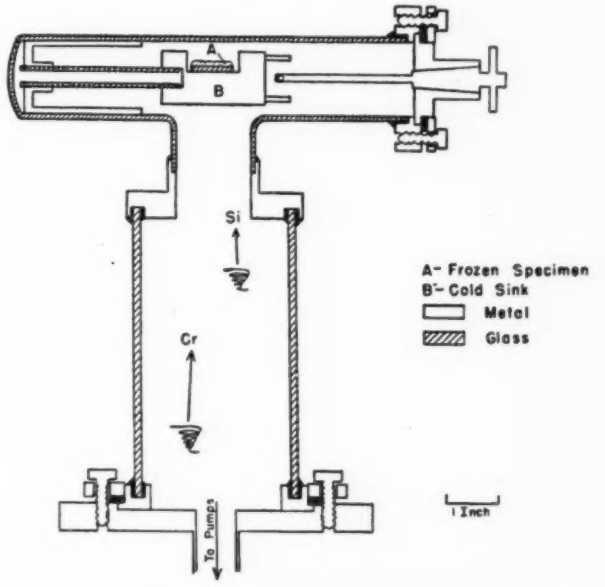

FIG. 1. Apparatus for low temperature replica method.

FIG. 2. Low temperature replica of surface of a frozen dilute suspension of silver halide particles.

FIG. 3. Low temperature replica of ice crystal condensed on frozen distilled water surface, shadow-cast with Cr, but not etched.

ron's equation.[4] The vapor pressures together with the computed rates at which an ice surface would recede in a perfect vacuum at various temperatures of interest are listed in Table I. It is apparent from the table that if the surface is to be maintained over periods of several minutes, the temperature should be in the range −120°C or lower, and that for the etching procedure, the rate of sublimation is reasonably rapid at about −90°C and higher.

TABLE I.* Estimated rate of recession of an ice surface in a vacuum.

Temperature °C	Vapor pressure dynes cm^{-2}	Rate of recession A sec.$^{-1}$
−90	9.3×10^{-3}	140
−100	1.4×10^{-3}	23
−110	1.6×10^{-4}	2.6
−120	1.3×10^{-5}	0.2
−130	7.7×10^{-7}	0.01

* Vapor pressure at −90°C from *Handbook of Chemistry and Physics*; other values calculated from Clapeyron's equation assuming latent heat of sublimation 675 calories per g.

With reasonable assumptions concerning the conductivity between specimen and cold sink, estimates can be made of the rise in specimen temperature due to radiant heat from the hot evaporation filaments and due to heat released through deposition of evaporated shadowing and film materials. Such estimates indicate that under typical conditions the temperature rises about 2°C from radiant heat and is also of negligible magnitude due to condensing Si or shadowing metal. Heat is also absorbed during transfer from liquid air to the vacuum chamber by condensation of moisture from the air and conduction to the atmosphere. When the operation was performed with reasonable speed, the temperature of the block (measured with a platinum resistance thermometer) had usually risen to about −145°C by the time the pressure in the vacuum chamber had reached the point where the oil diffusion pump became effective. The temperature rose at the rate of about 1°C per minute beyond this point. Clearly, in order to complete the process before the specimen warms to a temperature where an ice surface becomes unstable, it is necessary to transfer the cold block rapidly to the vacuum chamber and attain a working vacuum in the shortest possible time. Probably it would be advantageous if thermal contact between specimen and sink could be decreased or broken during the etching procedure to reduce undesirable heating of the cold sink.

[1] Olsen, Smith, and Crittenden, J. App. Phys. **16**, 425 (1945).
[2] L. B. Loeb, *Kinetic Theory of Gases* (McGraw-Hill Book Company, Inc., New York, 1937), p. 96.
[3] *Handbook of Chemistry and Physics* (Chemical Rubber Publishing Company, Cleveland, 1945), 29th edition.
[4] J. C. Slater, *Introduction to Chemical Physics* (McGraw-Hill Book Company, Inc., New York, 1939), p. 176.

Plasma Oscillator

GOTTFRIED WEHNER,
Wright Field, Dayton, Ohio
August 15, 1949

EXPERIMENTS with a stabilized low pressure arc discharge[1] resulted in the discover of a new kind of r-f oscillator. This oscillator is similar to a klystron, whose resonance circuits are formed inside the plasma by thin oscillation layers.[2]

Cathode is either a mercury arc cathode with auxiliary anode or an oxide cathode. The grid completely separates the anode space from the cathode space and has a mesh width (depending on the gas pressure), which makes it possible to stabilize the discharge between fired and unfired operation.[3] The increased voltage drop of such a stabilized discharge is concentrated near the grid.[4] Electrons reaching this region from the cathode side are accelerated into the anode space and form a beam of fast electrons, provided the gas pressure is low (<5 micron) and the mean free path is large compared to the electrode distances.

When another electrode (a plate facing the grid and called repeller) is inserted in the beam and the anode arranged outside the beam, oscillations arise with a well-defined frequency, which are tunable between 1000 and 4000 mc by changing anode voltage and anode current. The grid and repeller (both near cathode potential) are covered with dark sheaths between which the bright anode plasma at high potential is located.

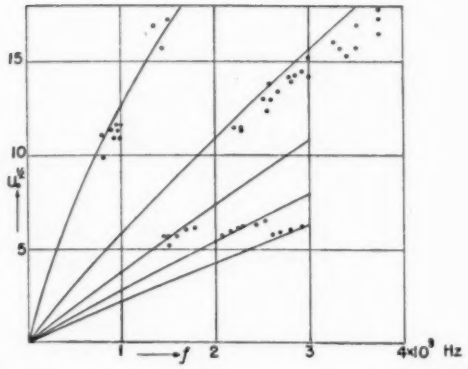

FIG. 1. Velocity *vs.* frequency diagram. Pressure 6 micron.

The investigation of the beam velocity distribution by means of a movable probe resulted in the discovery of a thin r-f velocity modulating layer inside the plasma near the grid ion sheath.[6] Often a second layer is found near the repeller ion sheath. In a suitable arrangement these oscillation layers can be seen as slightly darker zones inside the bright plasma.

Probe measurements showed that the plasma density N is not uniform along the anode space but decreases from the center in direction of the grid as well as of the repeller. Just near the oscillation layer N has a value which is connected with the observed frequency f by Langmuir's equation $f=9000N^{\frac{1}{2}}$. This density distribution provides an infinite number of resonance circuits in line with increasing resonance frequencies to the center. Hence only in one or two layers does the plasma density fit to one frequency. The repeller provides either the second oscillation layer (catcher) or the reversion of the beam when the tube oscillates as a reflex klystron.

Figure 1 shows the beam velocity *vs.* frequency diagram of a sealed-off all metal tube with an electrode arrangement according to Fig. 2. Without changing or matching any resonance circuit,

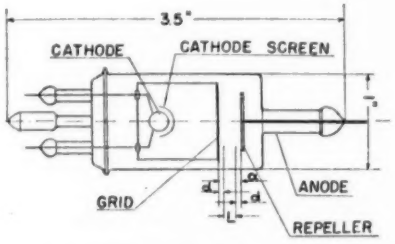

FIG. 2. Sealed-off plasma oscillator tube.

merely by changing anode voltage and anode current the frequency can be changed between 800 to 4000 mc. Oscillations occur along different modes. In case of higher pressures when reflex excitation due to the limited free path of the beam electrons does not exist, these modes are easy to calculate by transit time relations. Identifying the plasma edges near grid and repeller with the oscillation layers and assuming that the two oscillation layers oscillate in opposite phase, excitation should be possible if the transit time t_0 of electrons with the velocity v_0 through the drift space L equals:

$$t_0=\tfrac{1}{4}f\times(4n+1) \quad n=0,1,2,\cdots.$$

Setting

$$f=9000N^{\frac{1}{2}}$$
$$L=a-2d \text{ (Fig. 2)}$$
$$d=550U_0^{\frac{3}{4}}/N^{\frac{1}{2}}{}^{6,7}$$
$$v_0=6\ 10^7U_0^{\frac{1}{2}}$$
$$L=v_0t_0$$

the following relation may be derived:

$$(n+\tfrac{1}{4})\ 6\ 10^7U_0^{\frac{1}{2}}+10^7U_0^{\frac{3}{2}}=af.$$

This is shown with $a=0.6$ cm (Fig. 2) in the curves of Fig. 1. Beside these modes at lower pressures several other modes are detectable. They belong, as can be shown, to an excitation which is similar to the reflex klystron.

[1] W. O. Schumann, Archiv. f. Elektrotechnie **36**, 362 (1942).
[2] H. J. Merril and H. W. Webb, Phys. Rev. **55**, 1191 (1939).
[3] H. Fetz, Ann. d. Physik **37**, 1 (1940).
[4] H. Fetz, Archiv. f. Elektrotechnie **36**, 378 (1942).
[5] G. Wehner, Ann. d. Physik **40**, 501 (1941).
[6] H. Fetz, Ann. d. Physik **40**, 579 (1941).
[7] G. Wehner, Jahrb. d. deutsch. Luftfahrtforschg. III 24.

Wave-Lengths Suitable for X-Ray Microscopy of Biological Specimens

J. L. FARRANT
Division of Industrial Chemistry, Commonwealth Scientific and Industrial Research Organisation, Melbourne, Australia

September 6, 1949

AN x-ray microscope has recently been developed by Kirkpatrick and Baez[1] based on Compton's observation,[2] in 1922, that x-rays incident upon surfaces at glancing angles less than certain small critical angles undergo total specular reflection in accordance with the theory of Drude and Lorentz. The x-ray beam is focused by successive reflections at small glancing angles of incidence from two concave mirrors, having spherical, elliptical or cylindrical cross sections, and set up so that the normals to the two surfaces are mutually perpendicular. In this way one mirror exercises a focusing function for rays in a particular plane, while the other focuses the rays in a plane normal to the first. Kirkpatrick has suggested additional mirrors to reduce the spherical aberration and anamorphotism of the image inherent in the two-mirror system and calculates by means of the theory of Drude and Lorentz that diffraction limits the resolution to about 70A, this limit being independent of the wave-length of the radiation used.[1] In exploratory work with wave-lengths of the order of 1.5A at glancing angles of incidence of less than 30 minutes upon spherical mirrors coated with platinum and gold, Kirkpatrick and his colleagues have already obtained a resolving power of 2 microns.

Radiation of wave-length 1.5A has the advantage of being penetrating enough to allow the specimen to be imaged while in air at normal pressure, provided the absorption of radiation along the path between the mirrors and the image is diminished by the employment of a hydrogen or helium atmosphere.[1] On the other hand only the coarser details of comparatively thick specimens will absorb sufficiently to yield adequate image contrasts, since the "Half-Value Layer (H.V.L.) of organic substances (e.g., cellulose of density 1.3 g/cc) for a wave-length of 1.5A is approximately 0.7 mm, and even for an element of as high an atomic number as copper the H.V.L. is 15 microns. An additional limitation is that such wave-lengths restrict the angle of glancing incidence to a maximum of about 30 minutes, so that images are produced under conditions of extreme obliquity resulting in large aberrations.

In view of these limitations it is suggested by the writer that the realization of a microscope of this type suitable for the examination of bacteria and other organic specimens will entail the use of longer, more absorbable wave-lengths. Besides giving more adequate contrast the use of longer wave-lengths offers the additional advantages that (a) the degree of polish and accuracy of figure of the mirrors would be less critical, (b) the increased critical glancing angle of reflection would allow a greater numerical aperture with consequent increased speed of the optical system and (c) the larger aperture would allow more accurate focusing of the specimen with visible light before making the exposure with x-rays. It is also possible that conditions of less

TABLE I. Limits of resolution set by diffraction.

Mirror material	Wave-length (angstrom units)	$i_c \times 10^3$ (radians)	$d = \lambda/(2i_c)$ (angstrom units)	Observer
Platinum	2.0	14.1	70	E. Dershem[a]
Platinum	7.0	35.5	100	E. Dershem[a]
Gold	8.32	39.0	110	C. B. O. Mohr[b]
Glass	8.32	23.0	180	C. B. O. Mohr[b]
Glass	13.3	37.8	180	C. B. O. Mohr[b]
Glass	44.5	80.0	280	E. Dershem[c]

[a] E. Dershem, Phys. Rev. **33**, 659 (1929).
[b] See reference 4.
[c] E. Dershem, Phys. Rev. **34**, 1015 (1929).

oblique reflection would reduce aberrations, but more work on oblique optics is needed to decide this point.

According to the Drude and Lorentz theory the resolving power of the instrument is independent of the wave-length of the x-rays used.[1] However, the high absorption of long wave-length x-rays results in a less sharply defined critical angle and some of the radiation is specularly reflected at large glancing angles. Hence the Drude and Lorentz theory is inadequate here and even the application of the Fresnel expressions is not completely satisfactory. A closer agreement with experiment is given by the wave-mechanical treatment developed by Hönl,[2] but probably the best estimate of the resolution possible with long wave-lengths is obtained from actual experimental data, even though little information for monochromatic radiation has been published. In Table I is cited the limit d set to the resolution by diffraction, calculated by Kirkpatrick's formula $\lambda/2i_c$ from experimental values of the glancing angle of incidence i_c at which the reflected intensity I is half the intensity I_0 reflected at grazing incidence. The deterioration of resolution at long wave-lengths is not great.

Several investigators[4,5] have found that mirrors composed of light elements are more efficient than heavy metals as reflectors of x-rays of wave-lengths greater than about 8A, and claims have been made for specular reflection of some of the radiation incident at surprisingly large glancing angles. The first observations of this nature were made by Holweck[6] in 1923, but perhaps the most interesting investigations are those of Laby, Bingham and Shearer,[7,8] who examined the reflection of x-rays of wave-length 44.5A ($CK\alpha$) from several substances. At a glancing angle of 6 degrees soda-glass reflected 46 percent of the incident radiation and even at 20 degrees the reflected intensity was 18 percent. The radiation was focused with a concave soda-glass mirror at a glancing angle of incidence of 45 degrees to obtain a diffuse image of the focal spot. The observations made must be accepted with the reservation that part of the effect was due to general long wave-length radiation from the carbon anode employed, but a spectral analysis of the radiation revealed that it consisted largely of the carbon $K\alpha$-line. Although they realized their work established that concave gratings of considerable aperture could be used in this region, these workers unfortunately did not further explore the field of x-ray optics. These and other observations set out in Table II suggest that possibly mirrors of some materials would reflect sufficient of the very long wave-length radiations at close enough to normal incidence to allow the reflecting microscope of Burch[1] with its relatively large aperture to be used in that region.

TABLE II. Observations on the specular reflection of very long wave-length x-rays.

Anode material	Radiation X-ray tube potential (volts)	Mirror material	Glancing angle of incidence	I/I_0 per-cent	Observer
Molybdenum	150	Bronze	11°7′	35	F. Holweck[a]
Molybdenum	200	Bronze	16°2′	10	F. Holweck[a]
Nickel	194	Glass	20°	26	J. E. Henderson and E. R. Laird[b]
Nickel	576	Glass	20°	22	J. E. Henderson and E. R. Laird[b]
Molybdenum	130	Aluminum	15°	22	S. D. Gehman[c]
Molybdenum	150	Aluminum	12°	35	S. D. Gehman[c]
Molybdenum	300	Graphite	14°	22	S. D. Gehman[c]

[a] See reference 6.
[b] J. E. Henderson and E. R. Laird, Proc. Nat. Acad. Sci. **14**, 773 (1928).
[c] S. D. Gehman, Phys. Rev. **33**, 141 (1929).

Work on the specular reflection of x-rays seems to have practically ceased about 1932, but the attractions of x-ray optics are sufficient incentive to reopen investigation of this field. The modern techniques of vacuum evaporation and electron microscopy should greatly facilitate the preparation of mirrors and the examination of the smoothness of their surfaces.

An appreciation of the wave-lengths required to yield adequate image contrast for bacterial and organic specimens is given by the fact that the H.V.L.'s in organic substances for the $K\alpha$-radiations of aluminum (8.3A) and carbon (44.5A) are 5 and 1.4 microns respectively. The corresponding H.V.L.'s for air at N.T.P. are 4.5 and 1.0 mm, so probably the specimen could be imaged while placed in a thin cell filled with air or a lighter gas and sealed off from the x-ray tube and the optical system by thin, small diameter, vacuum-tight windows of collodion or beryllium. Radiation damage to specimens may however restrict the use of the longer wave-lengths.

The low intensity difficulty can be avoided to some extent by using visible light to search and roughly focus the field, while the photography of the image at low magnification with fine-grained plates should reduce exposure time somewhat. Application of the recently-developed x-ray image-intensity multiplier[9] may resolve this difficulty. The obvious advantages of the x-ray microscope are as follows: (i) Thicker specimens may be examined without the use of extremely high potentials. (ii) It may not be necessary to desiccate the specimen by placing it in vacuum. (iii) By choice of appropriate wave-lengths it should be possible to locate specific elements in the specimen. (iv) The x-ray microscope should be capable of use as an x-ray diffraction camera yielding focused diffraction patterns which would be of considerable value, particularly in the investigation of long spacings.

[1] P. Kirkpatrick and A. V. Baez, J. Opt. Soc. Am. **38**, 766 (1948).
[2] A. H. Compton, Phys. Rev. **20**, 84 (1922).
[3] H. Hönl, Ann. d. Physik **18**, 42 and 625 (1933).
[4] C. B. O. Mohr, Proc. Roy. Soc. A**133**, 292 (1931).
[5] T. H. Osgood, Rev. Mod. Phys. **1**, 228 (1929).
[6] F. Holweck, Comptes Rendus **176**, 570 (1923).
[7] Laby, Bingham, and Shearer, Nature **122**, 96 (1928).
[8] T. H. Laby and R. T. W. Bingham, Proc. Roy. Soc. A**133**, 274 (1931).
[9] Westinghouse X-Ray Division, Rev. Sci. Inst. **19**, 477 (1948).

Thin Films Peeled from Teflon

C. K. JONES
Thomson Laboratory, General Electric Company, West Lynn, Massachusetts

July 28, 1949

THERE are many occasions when one has need of thin films of specific materials. These are cometimes difficult to prepare. The method described below was used to prepare films for x-ray absorption measurements.

A thin film of a barium compound was required with a negligible amount of foreign matter of high atomic weight. The specific compounds used were $BaCO_3$, BaF_2 and $BaSO_4$ but the method is equally applicable for a wide variety of such compounds.

The compound in question was mixed with General Electric Sleeving Lacquer #1548 in the ratio of one part compound to two parts lacquer by weight in a ball machine for two hours. A strip of Teflon, a vinyl polymer of the formula

$$\left[\begin{array}{cc} F & F \\ | & | \\ -C- & -C- \\ | & | \\ F & F \end{array}\right]_n,$$

which is attached only by liquid sodium, two inches wide, six inches long, and forty mils thick was mounted on a brass frame. The Teflon was then dipped into the mixture and withdrawn at a slow rate, the optimum being such that the rate of run back is equal to the rate of withdrawal. A Fisher-Payne dip coater is very useful for this purpose. The films were allowed to dry and

then peeled off. In removing the film, lifting at one end was found to be preferable to pulling the film back over itself.

Films prepared in this manner contained sixty percent compound, were as thin as ½-mil thick, and were sufficiently strong to be handled with ease. The thickness of the film could be varied by the dilution of the lacquer. The films were found to vary over a film and between films of roughly one percent.

High Strength Ceramics for High Temperature Use

RESULTS of recent tests at the National Bureau of Standards have shown that several ceramic bodies previously developed by the Bureau have marked superiority, in both strength and creep characteristics at 1800°F and above, over the best available high temperature metal alloys. Laboratory data indicate that these ceramic bodies, especially designed for use in jet engines and gas turbines, possess special properties required at the elevated operating temperatures of these power plants.[1]

The revolutionary developments during the past 30 years, particularly the last 10 years, in both design and efficiency of power plants have emphasized the need for materials of great strength and durability at very high temperatures. This is a natural consequence of the fact that, in any device for the conversion of heat energy into work, the efficiency of that device may be increased by increasing the temperature differential between the beginning and end of the conversion.

Because design engineers projected their plans into regions of temperature and stress far beyond the potentialities of known metallic alloys, a survey of non-metallic compounds, especially the oxides, silicates, carbides, and related combinations peculiar to ceramics became necessary. Little data existed in the literature upon which to base specific designs for the application of ceramics in power plants such as the gas turbine. Some work has been done on feldspathic bodies, which contain a bond of glass and, consequently, have limited use at elevated temperatures. Several reports were also available in the German literature on small specimens of simple oxide bodies with extraordinary resistance to mechanical stress at temperatures above 1800°F. These bodies had been matured, experimentally, at such high temperatures (about 3450° to 3550°F) that their successful production commercially in the United States seemed to be only a remote possibility.

Therefore, when the National Bureau of Standards was requested, by the National Advisory Committee for Aeronautics in 1944, to obtain engineering data on ceramic bodies in tension at elevated temperatures, it was thought advisable to begin the work on bodies which could be produced with available industrial facilities. Leading ceramic concerns were requested to submit specimens for preliminary tests of bending at elevated temperatures and of resistance to thermal shock. Also, six promising bodies were selected from a number developed at the National Bureau of Standards during a previous investigation. These tests, involving bending strength at 1800°F and relative resistance to thermal shock, showed the oxide bodies developed at the Bureau to have superior quality over those then available from commercial concerns. A comprehensive investigation was begun on the high temperature strength and creep in pure tension of six NBS oxide bodies.

For test purposes specimens round in cross section and approximately 0.3 in. in diameter throughout the gauge length were prepared. The adapters for applying the stress were 8½ in. long, $1\frac{3}{16}$ in. in diameter, and were made of one of the bodies under test. Ceramic adapters were used because calculations based on the data available indicated that high temperature alloys would not have sufficient strength at the maximum temperatures and stresses likely to be obtained in some of the tests. Both adapters and test specimens were fabricated under contract by a co-operating industrial concern, using hydrostatic pressure applied by means of rubber molds. The strain gauges, similar in design to those used at the National Bureau of Standards for measuring creep of metals, were fabricated from 90 percent platinum, 10 percent rhodium tubing, and wire.

TABLE I. *Stress-temperature data on four high strength ceramic bodies.*

Temperature (°F)	Maximum stress lb./in.² NBS ceramic bodies No. 358	No. 353	No. 151	No. 4811C
1500	13,000	13,000	12,000	14,000
1700	14,000	13,000	13,000	14,000
1800	17,000	18,000	18,000	18,000
1900	8000	4000	15,000	16,000
2100	...	...	...	6000

Four thermocouples mounted in the vicinity of the specimen provided temperature measurements at the ends and at the center of the gauge length and actuated the temperature controlling and recording instruments. The specimens were heated in conventional wire-wound furnaces equipped with viewing windows to permit the periodic measurement of strain using a Gaertner extensometer-viewing microscope. Loads were applied to the specimen through a lever system.

Four general methods of test were followed, the first two of which may be described as "step testing."

Method 1.—The specimen was heated gradually to the test temperature and a stress considered to be well below the tensile strength of the specimen was applied. After observing length changes for some predetermined time, the stress was increased. Length changes were observed again, whereupon another increment of stress was applied. This was repeated until rupture occurred. It was customary to increase the stress in increments of 1000 lb./in.² at about one-week intervals.

Method 2.—The original temperature and load conditions were essentially as described for Method 1. In this method, however, the load remained constant and the temperature was raised, usually in 100°F steps at about one-week intervals. In some cases, the specimen had not ruptured after prolonged holding at 1800°F. When this occurred in a furnace in which the temperature could not be raised safely above 1800°F, the test was continued by increasing the load in steps while maintaining the 1800°F temperature.

Method 3.—After holding the specimen at 1800°F under a stress of 4000 lb./in.² for 48 hr., stress was increased at the rate of about 1200 lb./in.²/min. to failure. The load was increased by flowing shot into a bucket.

Method 4.—The specimen was held at constant stress and constant temperature to failure, the purpose being to obtain curves of stress against rupture time which could be compared with similar curves for metal alloys.

In general, each combination of stress and temperature was maintained for about 160 hr., or one week. Conditions were then changed by an increment of either stress or temperature, until failure, for a total of 109 tests. Strengths in tension up to 18,000 lb./in.² at 1800°F, and 15,000 lb./in.² at 1900°F were observed. Above 1900°F, however, the strengths drop off rapidly to an average of about 5000 lb./in.² at 2000° to 2200°F.

Resistance to creep also decreases rapidly, for the particular porcelains tested, when temperatures are raised above the range 1800° to 1900°F. Results show that even the comparatively low stress of 6000 lb./in.² has caused more than a tenfold increase in the rate of creep at 2050°F compared to the rate at 1800°F,—and the porcelains on which these tests were made are the most resistant to creep of any investigated. Maximum observed creep rates, for all of the bodies tested, may be summarized as ranging from about 0.0001 to 0.0002 percent per hour at 1700°F for the range of stresses used; from 0.0002 to 0.0008 percent per hour at 1800°F and a stress of 16,000 lb./in.²; and from 0.0030 to 0.0040 percent per hour at 1900°F and 10,000 lb./in.² stress. The maximum stress at rupture for the four NBS ceramic bodies at various temperatures is given in Table I.

Data obtained from the Bureau's tests have revealed that some of the NBS oxide bodies are capable of effectively withstanding high temperature conditions far better than any other material now in use. In fact, an experimental gas turbine, using blades fabricated from the oxide body of the most promising strength and creep characteristics, has been operated successfully in the Cleveland Laboratory of the National Advisory Committee for Aeronautics.

[1] For complete technical details see Burdick, Moreland, and Geller, "Strength and creep characteristics of ceramic bodies at elevated temperatures," NACA Tech. Note No. 1561, available from the National Advisory Committee for Aeronautics, Washington 25, D. C.

PROGRAM

Proceedings of the Electron Microscope Society of America

Chairman: L. MARTON

THE annual meeting of the Electron Microscope Society of America was held at the National Bureau of Standards in Washington, D. C., October 6–8, 1949. Titles and abstracts of the papers presented are given below.

1. The Temperature of Electron Microscope Specimens. G. D. SCOTT AND FRANCES DAWES, *Department of Physics, University of Toronto, Toronto, Ontario.*—It is well known that with the high current densities of the illuminating beam obtainable with a self-biased gun, electron microscope specimens often undergo marked changes. Frequently these changes can be attributed to elevated temperatures. This paper is a discussion of the equilibrium between the energy absorbed by a particle from the electron beam and that which is either radiated to the walls of the surrounding chamber or conducted to the supporting substrate. For the case of an opaque particle on a Formvar film it can be shown that under possible conditions of contact between particle and film, conduction becomes negligible and hence the equilibrium temperature as determined by radiation alone can be 1000°C or more. As there is no mechanism by which the film can absorb any large fraction of the energy either directly from the beam or from the radiation emitted by the adjacent particle, the film itself remains at nearly ambient temperature. The high temperature gradients at the points of contact may, of course, cause instability and ultimately rupture of the film. The temperature conditions of electron microscope specimens are thus seen to be in marked contrast to those which can exist in macroscopic experiments.

2. Vibration Studies: Related to Electron Microscopy. F. A. HAMM AND F. C. SNOWDEN, *General Aniline and Film Corporation, Easton, Pennsylvania.*—This investigation has provided information which is useful as a convenient guide for properly locating the instrument and for high resolution electron microscopy where vibration is a problem. The scheme involves the measurement of an oscillographic trace whose amplitude is proportional to the voltage generated by a piezoelectric crystal pick-up. The essential steps in the calibration and a brief description of the circuit characteristics are given. Electron micrographs relating image shifts with mechanical displacements of the instrument are illustrated. At present these results are only semiquantitative.

3. Performance Tests on the RCA Model EMC Electron Microscope. S. G. ELLIS, *RCA Laboratories, Princeton, New Jersey.*—A standard EMC electron microscope was tested to find the factors which limited its performance. These factors were drifting of the specimen due to thermal motions of the specimen stage and objective lens asymmetry. When these had been reduced, the instrument demonstrated a resolution of approximately 50A. The resolution was now limited by the angular aperture of the illumination. Some of the techniques employed will be described.

4. On the Testing of Electron Microscope Objectives. JAMES HILLIER AND HENRY FROULA,* *RCA Laboratories, Princeton, New Jersey.*—A method of obtaining a quantitative evaluation of electron microscope objectives is described. The axial distance between the line foci produced by an asymmetrical objective is used as a measure of its asymmetries. Using a carefully compensated objective and a carbon black specimen (filmless mount), a photographic chart has been assembled showing the Fresnel fringes in images defocused by known amounts in the range $+100\mu$ to -100μ. These were obtained under standardized conditions of operating of the microscope. To test a lens a single micrograph of a similar specimen is taken near focus and under approximately the same conditions and an enlargement made at the same magnification as the chart. The fringes in the directions of maximum and minimum defocusing are then compared with those of the chart. In this way the amount of defocusing in the two directions can be accurately estimated. The difference between these values is the axial separation of the line foci for the lens tested. It is shown that a separation of $\frac{1}{2}\mu$ can be detected. Preliminary estimates indicate that separations of less than 1μ are necessary for the highest resolution. Lenses with separations greater than $10–15\mu$ are what would be generally considered as unsatisfactory.

* Permanent address: Department of Engineering, University of California, Los Angeles, California.

5. A Technique for the Comparison of Identical Surface Areas in the Light and Electron Microscopes. ERNEST F. FULLAM AND RUTH H. PETCHER, *Knolls Laboratory, General Electric Company, Schenectady, New York.*—To facilitate the interpretation of electron micrographs of surfaces, particularly metals, it is desirable to compare identical areas, at the same magnification, in the light and electron microscopes. The principle difficulty involved is in locating the identical area of the sample in each instrument. This has been done quite successfully by Bryner[1]; however, a simpler and more rapid technique would be more desirable. The proposed simplified technique consists of polishing and etching the metal sample in the usual way. Immediately following the etch an acute angle is scribed lightly on the surface, under the light microscope with a sharpened needle, enclosing or adjacent to the desired area. The needle is placed on the sample by an arm attached to the fine focusing mechanism from another microscope. This insures a very light contact with the metal to minimize the production of a cold-worked structure. The line width is three to ten microns. The angle is reproduced in a nitrocellulose replica cast on and stripped from the surface. This first replica is coated with a thin double film of beryllium and quartz. Quartz films alone do not have sufficient strength. A "Lektromesh" specimen screen with a four-mil hole drilled in its approximate center and polished is cemented to the replica with the apex of the angle visible in the center of the hole. The hole is necessary in order to locate quickly the angle in the electron microscope and to provide sufficient identifiable area adjacent to it for study without the interference of the screen wires. This placing operation is carried out under a dissecting microscope through which the angle in the replica is easily visible. After washing away the nitrocellulose replica by condensation of amyl acetate vapors on it, the remaining thin replica film over the drilled screen is ready for the microscope. Using the apex of the angle as a reference point, many areas adjacent to it may be easily recognized in both the light and electron microscopes even though the surface has no distinctive natural structure that may be readily identified.

[1] J. S. Bryner, "Correlation of optical and electron microscopy," Metals Tech. **15**, No. 4 (June 1948).

6. A Centerable Condenser Aperture for the RCA Model "B" Electron Microscope. F. F. MOREHEAD, *American Viscose Corporation, Marcus Hook, Pennsylvania.*—A modification of the regular condenser aperture that may be centered while the instrument is in operation is described. (5 min.)

7. Permanent Magnet Lenses. JOHN H. REISNER, *RCA Victor Division, Radio Corporation of America, Camden, New Jersey.*—Permanent magnets have been successfully utilized to energize magnetic lens pole pieces for high resolution electron microscopy at direct magnifications of 7000 times with 30-kilovolt electrons, and 5000 times at 50 kilovolts. Stray magnetic fields which have previously limited high magnification and high resolution have been minimized by using two circuit gaps in parallel, and by surrounding the assembly with a magnetic shield connected to the external pole pieces of the two gaps. Magnetomotive forces of 1400 gilberts have been obtained. A single magnet or magnets in bucking arrangement, as well as configurations involving magnets disposed either radially or parallel to the optical axis of the lens, have been successfully utilized. The effects of various magnetic circuit parameters on the design and operation of the lens system have been studied.

8. Beam Deflection Focusing Device. HAROLD T. MERYMAN, *Naval Medical Research Institute, Bethesda, Maryland.*—A beam deflection device operating on an electromagnetic principle has been adapted to the RCA EMU electron microscope. Design and principle of the device will be discussed and its performance demonstrated with micrographs.

9. Motion Pictures of Electron Microscope Images. JOHN H. L. WATSON AND LUTHER E. PREUSS, *Edsel B. Ford Institute for Medical Research, Detroit 2, Michigan.*—The feasibility of taking motion pictures of electron microscope images has been considered on occasion, but the lack of informative, moving subjects has made the project impractical. Lately the technique has been developed as a tool for studying the effects of electron bombardment upon matter[1] and particularly upon tungsten oxide[2] and other tactoid structures. It may be used also to study reticulation of thin metal films under electron bombardment, contamination of microscope specimens due to the electron beam, and for observing the effects of bombardment upon biological and bacteriological specimens. The technique is described and several films are shown illustrating the results. It is found that intensity in the microscope is quite adequate and that contrast is good. Resolution is inferior to stills taken in the normal way, but images are interpreted from "moving micrographs," in conjunction with stills, somewhat more easily by virtue of (1) object movement which often gives a three-dimensional impression, (2) the control of the film which allows the reactions to be observed at a range of speeds and to be studied at close hand repeatedly, and (3) the increased number of single micrographs which are taken in a run and which, because of their number and the speed with which they are taken, are likely to contain more complete information than are a few isolated stills. (20 min.)

[1] John H. L. Watson, J. App. Phys. **19**, 713 (1948).
[2] Heller, Wilfried, Wojtowicz, Wesley, and Watson, J. Chem. Phys. **16**, 998 (1948).

Papers on Sectioning

Chairman: T. F. ANDERSON

10. Improved Sectioning Technique for the Electron Microscope. RICHARD F. BAKER AND DANIEL C. PEASE, *School of Medicine, The University of Southern California, Los Angeles, California.*—Some refinements in a previously described technique[1,2] are described. These include a reliable method of flattening and mounting sections, also a standardized method of knife sharpening. A comparison of fixing agents has been made, using liver and nervous tissue, which indicates the superiority of osmic acid for general use. Perfusion is compared with fluid and vapor immersion as a means of introducing the fixative to the tissue. A discussion of resolving power limitations in thin section microscopy is given. (20 min.)

[1] D. C. Pease and R. F. Baker, Proc. Soc. Exper. Biol. and Med. **67**, 470 (1948).
[2] R. F. Baker and D. C. Pease, J. App. Phys. **20**, 480 (1949).

11. Ultra-Microtomy by a New Method. SANFORD B. NEWMAN, EMIL BORYSKO, AND MAX SWERDLOW, *National Bureau of Standards. Washington, D. C.*—Polymerization of *n*-butyl methacrylate monomer is used as a rapid and simple means for embedding fixed biological material. The solid resin provides an optically clear matrix for cutting very thin sections, one at a time, with a slightly modified conventional rotary microtome. Advance of the embedded specimen toward the knife is obtained from the thermal expansion of a brass specimen holder. These ultra-thin sections have uniform thickness, large area, and integrity of tissue structure. They are suitable for producing transmission images at the higher magnifications of the conventional light, phase-contrast, and electron microscopes. Metallic shadowing of the sections provides greater contrast as well as a three-dimensional aspect to the structural details of the tissue. (20 min.)

12. Electron Microscopy of Renal Morphology. JOHN J. KELSCH AND JOAN BARDET, *Interchemical Corporation, New York, New York.*—The high speed microtome, developed at Interchemical Corporation Research Laboratories, and described by Fullam, Gessler, Grey, Kelsch, and Schuster has been redesigned. The knife is set in a rotatable holder to facilitate the adjustment of the critical clearance angle, which must vary for different materials. The wheel is heavier, and is balanced at three points. The knife edge is at a 45 degree angle to the radius of the wheel to give a slicing action in contrast to the chopping action of the previous model. Cutting speed has been reduced to *ca.* 10,000 r.p.m., and feed speed reduced to 0.5 mm/min. Utilizing the improved high speed microtome, a study of the renal morphology of the mouse was undertaken. The structure of the renal tubules as seen in 0.1μ-sections in the electron microscope is demonstrated, and a series of sections through the cortex and medulla is shown.

13. Some Refinements of the Rotary Microtome Modified for Ultra-Thin Sectioning.* JAMES HILLIER, *RCA Laboratories, Princeton, New Jersey* AND MARK GETTNER, *Sloan-Kettering Institute, New York, New York.*—Using the reservoir described in the accompanying paper accidental distortions of the section by the blade are eliminated with the exception of uniform compression. This appears to be a function of the sharpness of the blade and the thickness of the section cut. Thus with a given blade the compression of each section, which can be easily observed through a low power microscope, provides a reliable indication of the thickness. By this means it has been possible to identify many sources of variations in the thickness of the sections. In the Spencer rotary microtome static friction in the horizontal ways is largely eliminated by the introduction of a 300-micron horizontal excursion of the specimen block during each cutting cycle. This motion must be reproduced to within 0.01 micron if sections of uniform thickness in the 0.05- to 0.1-micron range are to be cut. Static friction in the horizontal ways which has an opportunity to occur during two extremely short intervals in each cutting cycle and is one of the major causes of thickness variation has been reduced by a spring which supports most of the weight of the horizontal member. Variations in the thickness of the

lubricating film in the rear vertical way and on the advance plate constitute a second important source of thickness variations. A definite improvement in performance has been obtained by keeping the thickness of this film to a minimum and by running the mechanism more or less continuously for one-half to one hour before cutting. The third source of variations that has been identified includes vibrations originating in the rachet and other parts of the advance mechanism, from irregularities of hand operation and from accidental table and room vibrations. Laying a finger lightly on any part of the microtome will cause as much as a 0.05-micron variation. The addition of a motor drive has so improved the operation that the variation in 0.02-micron sections cannot be detected visually. It is presumed they are below 40A.

* This work was sponsored in part by the U. S. Navy under Contract N6-ori-99 Task Order I and in part by RCA Laboratories.

14. Serial Sections for Electron Micrography.* MARK GETTNER, *Sloan-Kettering Institute, New York, New York,* AND JAMES HILLIER, *RCA Laboratories, Princeton, New Jersey.*—When a rotary microtome is modified[1] to cut sections of thickness less than 0.2 micron, serial sections cannot be cut in the usual fashion. The extremely low rigidity of such thin sections is not sufficient to overcome the friction between section and the facet of the knife resulting in a rolling and folding of the section. In the present work this has been overcome by the use of a reservoir attached to the blade and filled with a liquid. The height and surface tension of the liquid are adjusted until the meniscus reaches just to the cutting edge. The block and the clearance facet of the blade are kept dry. With this arrangement the sections float as they are being cut, the trailing edge of each section holding to the edge of the blade until the leading edge of the succeeding section attaches itself to it and pushes it on. In this way a chain of sections already flattened, spread and in sequence is obtained floating on the surface of the liquid from which it can be lifted and mounted by any of the usual techniques. The only distortion of the sections observed in this technique is a uniform compression which occurs when sections of less than 0.05 micron are cut or when the blade is dull. The use of different liquids and cutting speeds will be discussed.

* This work was sponsored in part by the U. S. Navy under Contract N6-ori-99, Task Order I and in part by RCA Laboratories.

[1] D. C. Pease and R. F. Baker, Proc. Soc. Exper. Biol. and Med. **67**, 470 (1948).

Chairman: C. M. SCHWARTZ

15. A Technique for the Preparation of Grease or Solid Samples Dispersed in Grease-Like Media for Examination with the Electron Microscope. A. Y. MOTTLAU, *Standard Oil Development Company, Linden, New Jersey.*—The nature of grease as a dispersion of solid particles in oil is briefly discussed, and the value of the electron microscope in studying this solid phase is pointed out. The requirements of a satisfactory grease specimen mounting technique are outlined and a new technique fulfilling these requirements is described. Electron micrographs are presented which demonstrate the usefulness of the technique in disclosing pertinent information on grease structure. The factors involved in the preparation of powder specimens for electron micrography are discussed in relation to the adoption of a modification of the grease mounting technique for this purpose. The modified technique for powders is outlined and illustrated with micrographs.

16. Replication of Frozen Liquids by Vacuum Evaporation. HAROLD T. MERYMAN, *Naval Medical Research Institute, Bethesda, Maryland.*—Silicon monoxide replicas of frozen liquids have been made with particular attention to water. The size and shape of single crystals of ice frozen at various speeds can be demonstrated. The ices have been studied by replication of the surface immediately following freezing, following evaporation from the surface, and of the interior of a fractured crystal. The method has been applied to replication of wet biological specimens and its advantages and limitations will be discussed.

17. Measurement of Cellulose Particle Length by the Electron Microscope. F. F. MOREHEAD, *American Viscose Corporation, Marcus Hook, Pennsylvania.*—The technique for preparing cellulose films from viscose thin enough to examine directly in the electron microscope is described. A difference in particle size on the two sides of cellulose film cast as described on glass is reported and an explanation offered. The average particle length when corrected proportionally to the "skin" and "core" of two types of viscose rayon is compared with the lengths obtained from the measurement of "crystallites" observed after acid hydrolysis plus ultrasonic disintegration. Good agreement is found when the latter are corrected for recrystallization during hydrolysis. The length of the crystalline and amorphous areas of a number of cellulose fibers are calculated from the lengths of the hydrolysis crystallites as measured by the electron microscope. From the calculated results the ratio of the crystalline and amorphous lengths and the number of crystalline plus amorphous lengths per chain is obtained. (15 min.)

18. Reproducibly Representative Specimen Fields in Electron Microscopy. ROBERT C. BACKUS AND ROBLEY C. WILLIAMS, *University of Michigan, Ann Arbor, Michigan.*—Representative specimen fields are highly desirable in electron microscopy whenever one attempts to do precise qualitative or quantitative work. Developments leading toward such fields have been made in the past, but they have not been extensive, nor has there apparently been any adequate appreciation of the unique usefulness of representative fields. The method of producing representative fields by spraying has been extensively developed, and its advantages investigated. The qualitative advantages are the short drying time of spray droplets and the establishment of ideal conditions for both a precise qualitative assay of a single specimen and for a comparison of two or more specimens. The primary quantitative advantage is that counts can be made of the number of specimen particles per unit volume of suspension, by the use of reference particles. The suspending medium should be wholly volatile, in order to realize these advantages, and a volatile, electrolyte-containing buffer has been developed and tested.

19. Determination of the Weight of the Bushy Stunt Virus Particle by Electron Microscopy. ROBLEY C. WILLIAMS AND ROBERT C. BACKUS, *University of Michigan, Ann Arbor, Michigan.*—A method has been developed for determining the weight of macromolecules by counting them directly in electron micrographs. This paper describes the method and the results for the case of the bushy stunt virus particle. The number of virus particles per unit volume of a suspension is determined by counting the virus particles mixed with a known concentration of reference particles, as they appear in representative fields formed by the method described in the preceding abstract. The dry weight of the virus particle in a known volume of the suspension is measured, and hence the weight of a known number of particles is ascertained. Simple division yields the weight of a single particle. In the case of a highly purified suspension of the bushy stunt virus this method has yielded a particle weight of $9.4 \pm 0.7 \times 10^6$.

20. Electron Metallography of Cast Irons. CHARLES H. GEROULD, *The Dow Chemical Company, Midland, Michigan.*—A preliminary report is given on the metallography of cast

irons with emphasis on the formation and distribution of graphite. Electron micrographs are shown comparing typical normal cast iron with malleabilized, magnesium-treated, magnesium-overtreated, and cerium-treated cast irons showing graphite distribution and its relation to properties. Polystyrene-SiO replicas have been used in this work after the etched metal surface has been cleaned by stripping collodion from the surface.

21. Quantitative Metallography with the Electron Microscope. ALFRED L. ELLIS AND F. K. IVERSON, *International Harvester Company, Chicago, Illinois.*—An investigation of the carbide particle size and distribution in five heats of annealed SAE 52100 steel revealed that between 50 and 75 percent of the carbide particles are smaller than 0.5 micron. Since carbide particles smaller than 0.5 micron are difficult to measure at magnifications normally used for lineal analysis (1000×), it was considered desirable to develop an accurate quantitative method using the electron microscope. The accuracy of the replica method was first checked by examining the same carbide particles in the light and electron microscopes. A method was then developed for determining the percentage of carbide from electron micrographs. A statistical analysis of this method revealed that ten plates of five exposures each are required for accuracy within ±0.5 percent of the mean with 95 percent probability. However, only two plates are required for accuracy within approximately ±1 percent of the mean with 65 percent probability. The method of sampling and the statistical data will be presented. The method was applied to determination of the percentage of carbide in heat-treated steels.

22. Electron Metallography of Cemented Carbides. W. L. GRUBE, *General Motors Corporation, Detroit, Michigan.*—In the evaluation of quality and in the correlation of metallurgical properties with the performance of cemented carbide tools various metallographic examinations are utilized. Light-microscopical examinations of this type of material furnish information concerning inherent porosity, bonding, grain size, and grain size distribution. Electron-microscopical examination of cemented carbides has extended the study of the above-listed properties and has also made possible a study of microstructure heretofore unresolved. The metallurgical properties of cemented carbides which have been studied by electron microscopy are: (1) differential etching of binder metal, tungsten carbide, and alloy carbide phases, (2) grain size (below two microns), (3) binder metal distribution, (4) segregation, (5) boundary phenomena between carbide grains, and (6) submicroscopic voids. The electron microstructure of specific samples of commercial carbide tools and its relationship to tool performance is discussed. The replica techniques used in the course of the examinations are also presented.

23. Electron Diffraction Studies of Thin Iron and Chromium Films. LELAND L. ANTES, *The University of Texas, Austin, Texas.*—The formation of air compounds on vacuum-deposited iron and chromium films at room temperature is discussed. When the thickness of the iron films is close to 10A, the conversion of the iron is nearly complete in a few minutes. The reaction of chromium with air is quite similar. The electrical resistance change of thin chromium films is discussed. The talk will be illustrated by slides.

24. Electron Microscopy of Enamel and Dentin. DAVID B. SCOTT AND RALPH W. G. WYCKOFF, *National Institutes of Health, Bethesda, Maryland.*—The fine structure of enamel and dentin has been studied through use of shadowed collodion replicas of etched ground sections of teeth. Of special interest are the fibrous components of the dentin, which include the thin-walled dentinal fibers and their branches, fibers apparently within the dentinal fibers, collagenous fibrils, and ultra-fine fibers in the matrix.

25. Studies of the Action of Sodium Fluoride on Human Enamel by Electron Microscopy and Electron Diffraction. DAVID B. SCOTT AND RALPH W. G. WYCKOFF, *National Institutes of Health, Bethesda, Maryland,* AND ROBERT G. PICARD, *RCA Victor Division, Camden, New Jersey.*—Slabs of enamel, cut parallel to tooth surfaces, were immersed in 2–4 percent NaF solutions for periods ranging from 4 min. to 30 days. Under the electron microscope an inhomogeneous apparently crystalline deposit was observed on replicas taken after 15–30 days; traces were seen after 2–7 days; under 2 days results were negative. Electron diffraction indicated that the deposit is CaF_2; the normal apatite pattern was replaced by that of CaF_2 after treatment as short as 3 min. When treated slabs were washed for prolonged periods in water the deposit was not seen microscopically, and the diffraction pattern reverted to that of the normal apatite. (15 min.)

26. The Molecular Configuration in Seed Globulin Crystals. C. E. HALL, *Massachusetts Institute of Technology, Cambridge, Massachusetts.*—A method for examining the surface structure of small protein crystals will be described. Micrographs have been obtained showing the molecular configuration at the surface of crystalline edestin and certain other seed globulins. It is concluded from the observations that the structure is face-centered cubic with $a=114$A in the dry state. The edestin molecule appears as an approximately spherical particle about 80A in diameter. Small-angle x-ray powder patterns made by Dr. R. S. Bear show spacings consistent with the conclusions drawn from the electron microscope analysis.

Invited Papers on Complementary Methods of Microscopy

Chairman: F. O. SCHMITT

27. Recent Developments in Conventional Microscopic Equipment and Techniques. A. H. BENNETT, *American Optical Company, Stamford, Connecticut* (40 min.)

28. Recent Developments of the Optical Microscope. DAVID S. GREY, *Polaroid Corporation, Cambridge, Massachusetts* (40 min.)

29. An Approach to X-Ray Microscopy. PAUL H. KIRKPATRICK, *Stanford University, Stanford, California* (40 min.)

30. Some Comments on Electron Microscope Research in Europe. E. G. RAMBERG, *RCA Laboratories, Princeton, New Jersey.* (30 min.)

Chairman: C. E. HALL

31. Electron Microscope Study of Isolated Nuclei of Liver Cells from Laboratory Animals. JUAN J. ANGULO, *University of Havana, School of Medicine, Havana, Cuba,* AND JOHN H. L. WATSON,* *Edsel B. Ford Institute for Medical Research, Detroit 2, Michigan.*—Nuclei of liver cells from the Rhesus monkey, guinea pig, rat, mouse and the 16-day chick embryo were isolated by fractional centrifugation and examined without chemical fixation in the electron microscope. Structural details are seen and the identity with nucleoli of certain dense zones in the images is discussed. A relationship is noted between the number of these zones and animal species. Some zones show images which suggest the existence of a nucleolus wall but no evidence is found for the existence of a nucleolus membrane. The absence of a chemical fixation does not distort the nucleus structure and electron microscopy of unfixed, isolated nuclei seems to be superior in some ways to other techniques for electron microscope study of the nucleus.

* To give the paper.

32. An Electron Microscope Study of an Undescribed Orchid Virus. NELSON NEWTON AND DAVID W. ROSBERG, *Battelle Memorial Institute, Columbus, Ohio.*—In connection with phytopathological research on a heretofore unreported virus which produces mottled streak symptoms in orchid plants, electron microscope studies of both diseased and healthy plants have been made. Host range studies have shown the orchid to be the only plant capable of being infected with the virus. Purified and concentrated extracts from raw plant juice were prepared by alternate low (6460 g) and high (19,942 g) speed centrifugation. The material was finally suspended in a 0.05 M phosphate buffer at *p*H 7. Electron microscope examinations of platinum-shadowed specimens prepared from diseased and apparently healthy plants showed both crooked and straight rod-shaped particles present in the diseased material as well as in some of the apparently healthy extracts. Extracts from other apparently healthy plants were free of these rod-shaped particles. The straight rods were approximately 300×24 mμ, while the crooked rods were 400×21 mμ. This suggests that either two viruses or two different phases of the same virus were present. Buffer suspensions of the rod-shaped particles are opalescent and exhibit pronounced Tyndall cone phenomena. When examined with the polarizing microscope, intense streaming birefringence has been observed, comparable to that exhibited by tobacco mosaic virus.

33. Destruction of Bacterial Viruses by Osmotic Shock.* THOMAS F. ANDERSON, *Johnson Foundation, University of Pennsylvania, Philadelphia 4, Pennsylvania.*—The similar viruses, T2, T4, and T6 which appear in the electron microscope to have membranes surrounding the internal structures of the heads can be disintegrated by what might be termed "osmotic shock." If these viruses are incubated with 4M NaCl and the suspension then rapidly diluted with water, the viruses are inactivated, while little inactivation occurs if the suspensions are gradually brought to lower solute concentrations. Electron micrographs of slowly diluted preparations reveal normal virus particles, while micrographs of the former, rapidly diluted preparations reveal virus "ghosts"—empty head membranes with tails attached. Similar destruction of these viruses follows rapid dilution from solutions of ethylene glycol, glycine, glycerol, glucose, or sucrose. These results are compatible with the view that the membranes of the even-numbered viruses, like those of cells, are somewhat permeable to these solutes, but much more permeable to water molecules. Presumably, the virus heads swell when the osmotic pressure is suddenly reduced, and actually burst if the reduction is sufficiently large and sudden. Osmotic shocks which inactivate the even-numbered viruses have no detectible effect on the small viruses T1, T3, and T7 which appear in the electron microscope not to have membranes.

* This work was supported by Contract N6-ori-168 T.O. II between the ONR and the Trustees of the University of Pennsylvania.

34. "Crystalline" Virus-Like Bodies from Human Skin Papillomas. JOSEPH L. MELNICK, MAURICE J. STRAUSS, HENRY BUNTING, AND ERNEST SHAW, *Yale University School of Medicine, New Haven, Connecticut.*—Certain skin papillomas have been shown to be characterized by the presence of intranuclear inclusion bodies. Immediately following removal from patients, such papillomas were fractionated by differential centrifugation and examined in the electron microscope. As control samples, common warts, molluscum contagiosum lesions, and normal skin were studied. From the intranuclear inclusion body papillomas, spherical bodies were readily obtained. These were characterized by their arrangement into crystalline-like clusters or layers in which the average particle diameter was 52 mμ. When these particles were not in crystalline array, they averaged 68 mμ in diameter. In the electron microscope the crystalline arrangement was not unlike that previously noted for certain of the plant viruses. Control preparations of molluscum contagiosum lesions revealed characteristic brick-shaped elementary bodies. The common wart and normal skin preparations revealed no uniform particles, but merely amorphous scattered clumps of matter, collagen fibers, and spherical particles of varying diameter.

35. Plant Virus Growth Curves as Determined by Use of the Electron Microscope. RUSSELL L. STEERE, *University of Michigan Ann Arbor, Michigan.*—Using uniform Dow latex polystyrene particles and applying the spray technique developed by Backus and Williams, we have been able to follow the increase in extractable virus content of plants following inoculation. The procedure involves clarification and dilution of the plant juices, addition of a constant amount of latex and thorough mixing, taking the electron micrographs, and obtaining the ratio of virus particles to latex particles in numerous drop patterns. This procedure is followed for each sample throughout the early development of the virus in the plant host. A comparison of the virus-latex ratio throughout the period results in what might be called a virus growth curve.

36. The Multiplication of Insect Viruses as Organisms. G. H. BERGOLD, *Laboratory of Insect Pathology, Sault Ste. Marie, Ontario.*—Electron micrographs of purified preparations of four different insect viruses indicate the presence of morphologically different forms, which are probably stages of multiplication. The virus first appears as a minute spherical body. This body increases in size and the virus appears as an elongated curved body surrounded by a membrane. Later the virus particle straightens out, ruptures the membrane and appears as a rod-shaped particle characteristic of insect viruses. One may assume that the rod-shaped virus particle contains several smaller sub-units each of which develops into a rod. The complicated nature of multiplication indicates that insect viruses are organisms with a relatively simple morphological structure of the mature rod.

37. The Electron Microscopy of Bacteriophage. RALPH W. G. WYCKOFF, *National Institutes of Health, Bethesda, Maryland.*—Several strains of the bacteriophages against colon bacilli have been under investigation to find out as much as possible about the mechanisms of their growth and multiplication. The electron microscopic results already obtained, to

be illustrated by a series of slides, show how these virus particles attack and destroy susceptible bacteria and make clear many steps in the process whereby they increase at the expense of these bacterial hosts. Reference is made to still incompletely understood aspects of bacteriophage proliferation, and to the bearing of these results on the more general problem of how viruses and other biological particles of macromolecular dimensions are produced in nature. (20 min.)

38. The Adaptation of Cytological Technique to Electron Microscopy. STUART MUDD AND ANDREW G. SMITH, *Medical School, University of Pennsylvania, Philadelphia, Pennsylvania.*—A limiting factor in the electron microscopic study of internal structures such as the nucleus in microbiological specimens has been inadequate contrast. Certain light cytological methods provide contrast but the light microscope has inadequate resolving power for dealing with the structure of the nucleus of bacteria. In the present study techniques of light cytology have been adapted to electron microscopy. The effect on contrast in the electron microscope of each step of the cytological processing has been determined. Technical details and the picture of the bacterial nucleus resulting will be presented.

39. The Effect of Certain Fixatives, Salts and Enzymes on Bacterial Cells with Respect to Chromatinic Structure and Contrast in Electron Microscopy. JON JONSEN AND ANDREW G. SMITH, *Medical School, University of Pennsylvania, Philadelphia, Pennsylvania.*—Bacterial cells which have been suitably fixed, treated with hydrochloric acid and stained show what has been referred to as chromatinic structure of a nuclear apparatus. Similar structures are produced after treatment with ribonuclease. In the present study the same structures were obtained with different salts on air-dried bacteria and bacteria fixed in Chabaud's fixative. Electron micrographs of similarly treated specimens will be shown and the results discussed together with a possible explanation of the salt effect. In addition, bacterial cells treated with osmium tetroxide vapor, Schaudinn's fixative, hydrochloric acid, desoxyribonuclease and trypsin will be presented.

40. A Fibrous Component of the Nerve Axon. FRANCIS O. SCHMITT, *Massachusetts Institute of Technology, Cambridge, Massachusetts.*—In a re-examination of the origin of the dense-edged fibrils (neurotubules) previously described by De-Robertis and Schmitt a study was made of giant fibers of the squid and the marine annelid, *Myxicola infundibulum*. Axons were isolated from the sheaths of formalin-fixed fibers and fragmented with a microblendor. Neurotubules were observed in the sheath of squid nerves from which the axoplasm had been removed before or after fixation; they were observed only occasionally in axon material (sheath contamination?). However, in some preparations no neurotubules could be found. More information is needed before the origin and composition of neurotubules can be stated conclusively. The most prominent feature of formalin-fixed axons is a fibrous component consisting of a reticulum of nodose fibrils 200–400A in width and of indefinite length. The nodes sometimes appear to be regularly spaced though a definitive periodicity has not been demonstrated. Squid axoplasm, extruded from freshly dissected fibers into water, disperses slowly, yielding fibrous structures ranging from relatively thick, rod-like bundles to very thin filaments. This fibrous protein, which may be concentrated by centrifuging at 10,000 g, is probably the chief fibrous component of the axon; its chemical properties are being studied. Even after brief blending, which fragments the fibrous bundles, diluted axoplasm yields nodose fibrils, after formalinization, which resemble closely those obtained from axons isolated from formalin-fixed fibers. The bearing of these results on the structure of the fresh axon will be discussed.

41. Morphologic Characteristics of the Oral Fusiform Bacilli as Revealed by the Electron Microscope. EDWARD G. HAMPP, DAVID B. SCOTT, AND RALPH W. G. WYCKOFF, *National Institutes of Health, Bethesda, Maryland.*—Pure cultures of seven strains of oral fusiform bacilli have been used. Shadowed preparations have been made from cultures of each strain at ages varying from 24 hours to 20 weeks. The morphologic characteristics of the organisms and the changes which occur with age have been studied.

Chairman: R. C. WILLIAMS

42. Use of Polystyrene Latex 580 G, Lot 3584 in Electron Microscopy. CHARLES H. GEROULD, *The Dow Chemical Company, Midland, Michigan.*—A review is presented of size determinations on this latex from 16 different laboratories, 12 of which show an average size of 2593A±40A. The four other determinations range upward to 3200A. Data are presented concerning latex dilution which indicates that particle diameter is not appreciably influenced by degree of dilution, size of drop added to specimen, drying speed, etc. Precautions in handling the latex are reviewed, including freezing, the danger of water evaporation from the undiluted latex, chemical and bacterial contamination, change of pH, over-heating in the electron beam, fusing due to insufficient dilution and contamination under electron bombardment. Electron micrographs are included which illustrate several of these dangers.

43. Particle Size and Density of Dow Latex 580 G—Measurements with the Ultracentrifuge. D. GORDON SHARP, *Duke University, Durham, North Carolina.*—Sedimentation velocity studies of the particles of Dow Latex 580 G suspended in physiological saline solution (0.9 percent NaCl) have been made in order that they may be used as a standard reference material in virus work. They sediment as a monodisperse system; less than 1 percent of the material differs ±2 percent from the mean sedimentation rate. The sedimentation constant is $S_{w20^\circ} = 1960 \times 10^{-13}$ sec.$^{-1}$ extrapolated to infinite dilution. Particle density was measured by observing sedimentation rate in media whose density was increased by addition of D_2O and of bovine serum albumin. Although some boundary instability was encountered near the point of zero sedimentation the particle density is estimated to be 1.054±.001, the same result being given by both albumin and D_2O indicating little or no hydration of the latex particles. This is in sharp contrast to the behavior of the heavily hydrated influenza virus, for example. From these data it is calculated that the particle size of Dow Latex 580 G is 252±2.5 mμ. It is therefore useful as a standard of size in electron microscopy and of sedimentation constant in the ultracentrifuge. It may also be used with the latter instrument to measure viscosity of samples too small to be measured otherwise.

44. The Apparent Size of Small Semi-Opaque Objects. RAYMOND A. KERN AND S. F. KERN, *Lilly Research Laboratories, Indianapolis, Indiana.*—It will be shown that the apparent size of small semi-opaque objects is a function of the conditions under which they are observed. Slides will be shown, demonstrating the apparent size differences of Dow's polystyrene balls 580 G, Lot 3584, as well as other small objects such as bacteriophage. A tentative explanation will be offered for these observed size variations.

45. A Removable Intermediate Lens for the RCA Model EMU. JAMES HILLIER, *RCA Laboratories, Princeton, New Jersey.*—An intermediate lens which can be introduced into the RCA Model EMU electron microscope without modifica-

tion of the column and with only a slight change in the electrical circuits is described. When used in conjunction with the highest power projection lens pole pieces, the new lens provides a full field at ten magnifications in the range 900 to 24,000. In addition, the new lens preserves the easy accessibility of the pole pieces for cleaning and adjustment. The distortion is less than with the single lens for all magnifications except the maximum and is very nearly zero for the lower magnifications. One value of the magnification is essentially independent of the accelerating potential and hence provides the possibility of achieving a permanent magnification calibration.

46. An Optical Method for the Thickness of Thin Films. G. D. SCOTT, *Department of Physics, University of Toronto, Toronto, Ontario.*—Tolansky* has discussed a method of measuring film thickness by multiple beam intereference using fringes of equal chromatic order in reflection. This method has proved very satisfactory for the accurate thickness determinations of films, evaporated metals and others, which are used in electron microscopy. The equipment consists essentially of a white light source and a spectroscope with calibrated wave-length scale. The preparation of the interference plates and the experimental arrangement will be discussed in detail. It has been found that ordinary microscope slides are superior to optically ground flats for the interference plates and their use makes it possible to reduce the fringe order to as low as *one* or *two*. The ease of observation and the accuracy of the measurements are thereby increased. The method can be applied to all types of stable films in thickness from 10A to several microns with areas of film less than one square mm. The measurements give the average metric thickness of the film and an accuracy of within ±5A is readily obtained.

* S. Tolansky, *Multiple Beam Interferometry* (Clarendon Press, New York, 1948).

47. A Technique for Studying the Electron Microstructure of Steel. D. M. TEAGUE AND L. H. ZIMMERMANN, *Chrysler Corporation, Detroit, Michigan.*—A brief history will be presented of the formation of the "Joint Committee on Electron Microstructure of Steel." The aims and scope of this group will be reviewed, together with sample and replica preparation methods. The second portion of the paper will be a discussion of a modified Formvar technique developed in our laboratories for studying the microstructure of steel. The salient features of the procedure are: (1) Deep etching of metal surface. This provides a strong Formvar film with good contrast. (2) Use of a soap monolayer on the metal surface to facilitate stripping. (3) Shadowing at a high angle—approximately 45°. This step improves detail, yet avoids certain difficulties of interpretation. The resultant electron micrographs correlate more readily with the experience of the metallurgist who will utilize the results. (15 min.)

48. Recent Advances in Electron-Microscopical Resinography. M. C. BOTTY, T. G. ROCHOW, AND F. G. ROWE, *Research Laboratories, American Cyanamid Company, Stamford, Connecticut.*—The general resinographic method of manifesting the electron-microscopical structure inside any solidified resin by replicating its fracture-surface was recently described.[1] The present paper will stress the description of the electronmicroscopical techniques and will exhibit micrographs of the *macromolecules* of single and composite resins as well as incorporations of pigments, fillers, and other modifiers.

[1] Anal. Chem. 21, 461–466 (1949).

49. Continuous Observations on the Formation of Metallic Films in the Electron Microscope. R. S. SENNETT AND T. A. MCLAUCHLAN, *University of Toronto, Toronto, Ontario.*—A number of different metals, including silver, gold, cadmium, and zinc, have been evaporated in a special specimen holder designed for the RCA type EMU instrument. Continuous observations have been made on the films during their formation, and micrographs of the same area have been obtained at a number of different stages during the evaporation. In all cases the first indication of a film was the appearance of a number of nuclei, and additional evaporation only increased the size of these aggregates without increasing their number. In zinc and cadmium films, the nuclei which first appeared had a regular crystalline form which was usually distorted during subsequent growth.